Åbo Akademi

Beatriz Vega

Fibre surface engineering
using polysaccharide derivatives

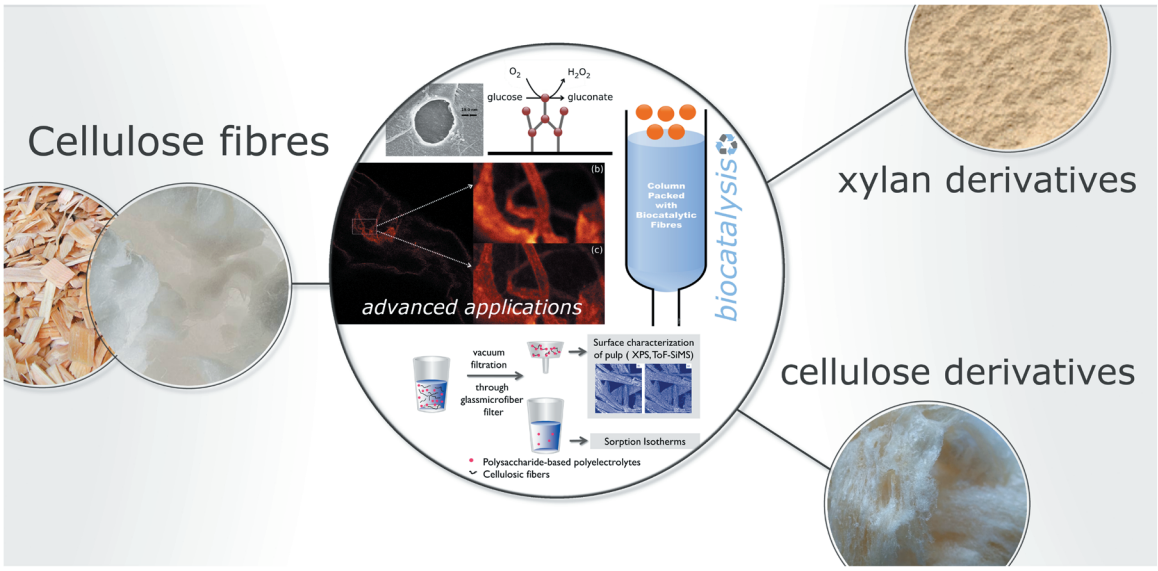

Fibre and Cellulose Technology Laboratory
Faculty of Sciences and Engineering, Chemical Engineering Department
Åbo Akademi University
Åbo/Turku, Finland, 2017

Fibre surface engineering using polysaccharide derivatives

Iris Beatriz Vega Erramuspe

Doctoral dissertation

Laboratory of Fibre and Cellulose Technology
Department of Chemical Engineering
Faculty of Science and Engineering
Åbo Akademi University
Åbo, Finland, 2017

Supervisor
Professor Pedro Fardim
Laboratory of Fibre and Cellulose Technology
Chemical Engineering Department
Faculty of Science and Engineering
Åbo Akademi University, Finland,
Department of Chemical Engineering (CIT)
University of Leuven, Belgium

Co-Supervisor
Professor Thomas Heinze
Organic Chemistry Department
Friedrich Schiller University of Jena (FSU), Germany,
Finland Distinguished Professor (FiDiPro) at Åbo Akademi, Finland
Director of Centre of Excellence for Polysaccharide Chemistry Jena-Rudolstadt
Germany

Opponent
Professor Elisabete Frollini
Centre for Research on Science and Technology of BioResources
Institute of Chemistry of Sao Carlos
University of São Paulo, São Paulo, Brazil

Reviewers

Professor Elisabete Frollini
Centre for Research on Science and Technology of BioResources
Institute of Chemistry of Sao Carlos
University of São Paulo, São Paulo, Brazil

Research Professor Ali Harlin
VTT Technical Research Centre of Finland
Finland

ISBN 978-952-12-3629-7 (print)

ISBN 978-952-12-3630-3 (digital)

Painosalama Oy – Turku, Finland 2017

" I keep the subject constantly before me, and wait 'till the first dawnings open slowly, by little and little, into a full and clear light."

Isaac Newton[129]

Abstract

"Fibre surface engineering using polysaccharide derivatives"

Doctor of Philosophy in Chemical Engineering Thesis
Laboratory of Fibre and Cellulose Technology, Faculty of Science and Engineering, Åbo Akademi University, Turku, Finland.

Keywords: Functional Fibres, Xylan, Polysaccharide Derivatives, Polyelectrolyte complexes, Pressurized Hot-Water Extraction, Biocatalytic Fibres, ToF-SIMS, XPS, Click-Chemistry.

In the search for new materials and innovative solutions, pulp fibres obtained from wood chips have gained attention during the last few decades because they can be converted into a wide variety of pulp-derived products. For example, they can be used for preparing "functional fibres" with potential for advanced applications in important fields such as medicine, biotechnology or packaging. The interfacial modification that is needed to produce functional fibres can be achieved by chemical, enzymatic, or physical treatments.

In the experimental work described in this thesis, the interfacial modification of bleached kraft pulp fibres was achieved by molecular self-assembly of polysaccharide derivatives, under stirring at low temperatures in aqueous media.

To study the interactions between different functional groups and the cellulosic fibres, **three different types of xylan derivatives** (i.e., xylan sulphate, carboxymethyl xylan, and xylan-4-[*N,N,N*-trimethylammonium]butyrate chloride) and **two types of cellulose derivatives** (i.e., cellulose (3-carboxypropyl)-trimethylammonium chloride ester, and (3-carboxypropyl) trimethylammonium chloride ester of 6-deoxyazidocellulose) were used as fibre-modifying agents. The xylan polyelectrolytes were synthesised from a high molar mass xylan (degree of polymerisation DPw <72) previously isolated from birch wood chips by a high-pressure hydrothermal treatment. The two cellulose derivatives were synthesised from microcrystalline cellulose Avicel® PH101 (DPw <350).

The adsorption of polysaccharide derivatives onto fibre surfaces was assessed by sorption isotherms using different detection methods (e.g. polyelectrolyte titration, ultraviolet-visible spectroscopy). In addition, advanced tools such as time-of-flight secondary ion mass spectrometry, X-ray photoelectron spectroscopy, confocal- and stimulated emission depletion-fluorescence microscopy, and field emission scanning electron microscopy were used in the

characterisation of modified fibre surfaces. According to the results, the xylan and cellulose derivatives with cationic charges (either individual polymers, or as polyelectrolyte complexes) were successfully incorporated onto the fibre surfaces. The approach used to introduce different chemical groups onto the surface of cellulose fibres shows many advantages in comparison with existing methods. For example, the modification occurs under very mild conditions, which prevents the degradation of cellulose fibres and helps to maintain the excellent mechanical properties of the original material. Moreover, the challenging step of chemical derivatisation is carried on separately, making the overall process safer, more controlled, and simpler in comparison with those methods where the chemical modification is performed directly on the surface of the cellulose fibres.

In addition to the sorption experiments described above, functional fibres decorated with azido-functional groups were subjected to copper(I)-catalysed alkyne-azide Huisgen cycloaddition (CuAAc) reaction with mono-substituted alkyne molecules, yielding fibres with reactive interfaces (reactive fibres). The possibility of using a multifunctional polysaccharide derivative such as (3-carboxypropyl) trimethylammonium chloride ester of 6-deoxyazidocellulose, offered an additional advantage over the other polysaccharide derivatives described above. As evidenced by the results, the cationic groups in the multifunctional derivative helped with the adsorption of the polymer onto the fibre surfaces, whereas click chemistry reactions were possible thanks to the azide functional groups.

The reactive fibres bearing amino-functional groups were used as efficient templates for the immobilisation of glucose oxidase enzymes, yielding biocatalytic fibres with potential in bioprocess engineering.

Sammanfattning

Designade fiberytor med polysackaridderivat

Doktorsavhandling

Laboratoriet för fiber- och cellulosateknologi, Fakulteten för naturvetenskaper och teknik, Åbo Akademi, 2017

Nyckelord: Funktionella fibrer, xylan, polysackaridderivat, polyelektrolytkomplex, trycksatt hetvattenextraktion (PHWE), biokatalytiska fibrer, ToF-SIMS, XPS, klickkemi

Massafibrer från vedflis har dragit till sig en stor uppmärksamhet under sökandet av nya material och innovativa lösningar eftersom de ha kan konverteras till en bred variation av produkter härstammande från massa. De kan bland annat användas för framställandet av ”funktionella fibrer” med potential för avancerade applikationer i viktiga ämnesområden så som medicin, bioteknologi, och förpackningar. Ytmodifieringar som behövs för att producera nya fibrer har åstadkommits genom kemiska, enzymatiska eller fysiska behandlingar.

Ytmodifieringen av blekta massafibrer har i det experimentella arbetet i denna avhandling gjorts genom molekylär självorganisering (self-assembly) av polysackaridderivat under omrörning vid låga temperaturer i vattenmiljö.

För att studera växelverkan mellan olika funktionella grupper och cellulosafibrer användes tre olika typer av xylanderivat (xylansulfat, karboxymetylxylan och xylan-4-[N,N,N-trimetylammonium]butyratklorid) och två typer av cellulosaderivat (3-karboxypropyl)-trimetylammoniumkloridester och (3-karboxypropyl) trimetylammoniumkloridester av 6-deoxyazidocellulosa) för att modifiera fibrerna. Xylanpolysackariderna (med polymerisationsgrad DPw < 72) syntetiserades från en högmolekylär xylan, vilken isolerats med en trycksatt hydrotermisk behandling av vedflis från björk.. De två cellulosaderivaten syntetiserades från mikrokristallin cellulosa, Avicel® PH101 (DPw <350).

Adsorption av polysackaridderivat på fiberytor utvärderades med adsorptionsisotermer där olika detekteringsmetoder användes, t.ex. polyelektrolyttitrering och UV-VIS spektroskopi. Därtill användes olika avancerade instument så som ToF-SIMS, XPS, konfokal- och STED mikroskopi, samt FE-SEM för att karakterisera de modifierade fiberytorna. Resultaten visade att xylan- och cellulosaderivaten med katjonisk laddning (antingen individuella polymerer eller som polyelektrolytkomplex) framgångsrikt inkorporerats på fiberytan. Detta tillvägagångssätt för att introducera olika kemiska grupper på cellulosafibrers yta visade sig ha många fördelar jämfört med existerande metoder. Bland annat görs modifieringen under väldigt milda förhållanden,

vilket förhindrar att cellulosafibrerna degraderas och därmed bidrar till att bibehålla ursprungsmaterialets utmärkta mekaniska egenskaper. Därtill är det utmanande kemiska derivatiseringssteget gjort separat, vilket gör processhelheten mera säker, kontrollerbar och förenklad jämfört med de metoder där den kemiska modifieringen görs direkt på cellulosafibrernas ytor.

Förutom adsorptionsexperinten beskrivna här ovan blev funktionella fibrer utsatta för kopparkatalyserad alkynazid Huisgencykloadditionsreaktion (CuAAc) med monosubstituerade alkynmolekyler, vilket producerade fibrer med reaktiva ytor (reaktiva fibrer). Möjligheten att använda ett multifunktionellt polysackaridderivat så som (3-karboxypropyl)trimetylammoniumkloridester av 6-deoxyazidocellulosa gav en ytterligare fördel framom de övriga polysackaridderivaten beskrivna här ovan. Resultaten bevisade att de katjoniska grupperna i de multifunktioella derviaten hjälpte att adsorbera polymeren till fibertyan, medan dess funktionella azidgrupper användes i klickkemi reaktioner.

De reaktiva fibrerna, vilka har besitter funktionella aminogrupper användes som effektiva templat för immobilisering av glukosoxidas, vilket gav upphov till biokatalytiska fibrer med potential inom bioprocessteknik.

Preface

The experimental work summarised in this thesis was performed in the Laboratory of Fibre and Cellulose Technology during the period from February 2011 to August 2016, under the supervision of Professor Pedro Fardim and co-supervision of Professor Thomas Heinze. The results are published in peer-reviewed scientific journals and are referred to in the thesis as Papers I-IV, as follows:

I. Vega, B., Petzold-Welcke, K., Fardim, P., and Heinze, T. (2012). Studies on the fibre surfaces modified with xylan polyelectrolytes. *Carbohydrate Polymers, **89 (3)***, 768-776.

II. Vega, B., Wondraczek, H., Salomão Pinto Zarth, C., Heikkilä, E., Fardim, P. and Heinze, T. (2013). Charge-directed fibre surface modification by molecular assemblies of functional polysaccharides. *Langmuir, **29 (44)***, 13388-13395.

III. Vega, B., Wondraczek, H., Bretshneider, L. Näreoja, T, Fardim, P. and Heinze, T. (2015). Preparation of reactive fibre interfaces using multifunctional cellulose derivatives. *Carbohydrate Polymers, **132***, 261-273.

IV. Vega, B., Fazeli, E., Näreoja, T., Trygg, J., Hänninen, P., Heinze, T., and Fardim, P. (2016). Advanced cellulose fibres for efficient immobilisation of enzymes. *Biomacromolecules. **17 (10)**,* 3188-3197.

Author's contribution

Paper I. Beatriz Vega was responsible for the experimental setup, and performed the major part of the measurements, except for the ToF-SIMS and XPS measurements, which were done by Elina Heikkilä (referred to as E. Orblin in the papers). The analysis and discussion of the results, as well as the redaction of the manuscript was undertaken in collaboration with the co-authors. (*)

Paper II. Beatriz Vega was responsible for the experimental setup, and performed the major part of the measurements, except for the CHNO elemental analysis performed by Niklas Vähä-Savo, and the XPS measurements by Elina

Heikkilä. The analysis and discussion of the results, as well as the redaction of the manuscript was undertaken in collaboration with the co-authors. (*)

Paper III. Beatriz Vega was responsible for the experimental setup, and performed the major part of the measurements, except for the XPS measurements conducted by Paulina Saloranta; fluorescence images were taken with the support of Jani Kniivilä, and copper analysis using coupled plasma mass spectrometry (ICP-MS) was performed by Paul Ek. The analysis and discussion of the results, as well as the redaction of the manuscript was undertaken in collaboration with the co-authors. (*)

Paper IV. Beatriz Vega was responsible for the experimental setup, and performed the major part of the measurements, except for the following: (1) manipulation of the STED microscope was the responsibility of Elnaz Fazeli, (2) DSC measurements were performed with the support of Peter Homlund and Mohammad Khajeheian, (3) XPS measurements were performed with the support of Peter Homlund, (4) manipulation of the Zetasizer Nano was the responsibility of Björn Törngren, and (5) manipulation of the FE-SEM microscope was undertaken by Linus Silvander. The analysis and discussion of the results, as well as the redaction of the manuscript was undertaken in collaboration with the co-authors. (*)

(*) The polysaccharide derivatives used as fibre-modifying agents were obtained in collaboration with researchers from the Organic Chemistry Department, Friedrich Schiller University of Jena (FSU), Jena, Germany.

Supporting publications

1. Vega, B., Petzold-Welcke, K., Fardim, P., and Heinze, T. Studies on the cellulose fibre surfaces modified with xylan derivatives. *ABTCP 2012 – 45th International Pulp and Paper Congress and Exhibition*, Brazil, Oct 2012.

2. Reyes, P., Teixeira, R., Rodríguez, J., Fardim, P., and Vega, B. (2013). Characterisation of the hemicellulosic fraction obtained after pre-hydrolysis of *Pinus radiata* wood chips with hot water at different initial pH. *Journal of the Chilean Chemical Society,* ***58 (1),*** 1415-1419.

3. Reyes, P., Texeira, R., Aguayo, M., Rodriguez, J., Vega, B., and Fardim, P. (2013). Extraction and characterisation of hemicelluloses from *Pinus radiata* and its feasibility for bioethanol production. *Revista Árvore*, ***37 (1),*** 175-180.

4. Vega, B., Heikkilä, E., Wondraczek, H., Fardim, P., and Heinze, T. Modification of wood fibre surfaces using functional bio-based Polyelectrolytes as a tool for the production of high-added value materials. *6th International Colloquium on Eucalyptus Pulp*, Uruguay, Nov 2013.

5. Vega, B., Fardim, P., and Heinze, T. Modification of pulp fibre surfaces using multifunctional polysaccharide derivatives. *1st International Workshop on Biorefinery of Lignocellulosic Materials*, Córdoba, Spain, Jun 2015.

6. Vega, B., Grigoray, O., Gustafsson, J., and Fardim, P. (2015). Advances in sugar-based polymers: xylan and its derivatives for surface modification of pulp fibres. In: *Biomass sugars for non-fuel applications*. Dmitry Murzin and Olga Simakova (Eds.). Royal Society of Chemistry, 134-158.

7. Santos, S., Carbajo, J.M., Gómez, N., Vega, B., Ladero, M., Heinze, T., Fardim, P., and Villar, J. Production and characterisation of novel bacterial cellulose-xylan polyelectrolyte composites. *IX Iberoamerican congress on pulp and paper research under the theme "Building bridges in research and innovation for the sustainable bioeconomy" (Ciadicyp2016),* Finland, Sept 2016.

List of abbreviations

SAGs: surface anionic groups

BKEP: bleached kraft eucalyptus pulp fibres

BKPP: bleached kraft pine pulp fibres

CDI: *N,N*-carbonyldiimidazole

CMX$^-$: carboxymethylxylan

CN$^+$: cellulose (3-carboxypropyl)trimethylammonium chloride ester

[CN$^+$CMX$^-$]: system composed of cellulose (3-carboxypropyl) trimethylammonium chloride ester (CN$^+$) and carboxymethylxylan (CMX$^-$)

[CN$^+$XS$^-$]: system composed of cellulose (3-carboxypropyl)trimethylammonium chloride ester (CN$^+$) and xylan sulphate (XS$^-$)

DP: degree of polymerisation

DS: degree of substitution

G and G*: glucose oxidase enzyme and cross-linked glucose oxidase enzyme, respectively

MB: methylene blue

Me-Glc*p*A: 4-*O*-methyl-α-glucuronic acid

MWCO: molecular weight cut-off

N_3-cell$^+$: (3-carboxypropyl)trimethylammonium chloride ester of 6-deoxyazidocellulose

PDI: polydispersity index

PEC: polyelectrolyte complex

S_N: nitrogen detected at the surface of fibres

SAG: surface anionic group

STED: stimulated-emission-depletion microscopy

ToF-SIMS: time-of-flight secondary ion mass spectrometry

TPX: Two-photon excitation fluorescence microscopy

XD: xylan derivative

XPS: X-ray photoelectron spectroscopy

XS^{-}: xylan sulphate

XTMAB^{+}: xylan-4-[*N,N,N*-trimethylammonium]butyrate chloride

Xyl*p*: Xylopyranose

Constants

$\boldsymbol{K_L}$, Langmuir constant (L/μmol)

$\boldsymbol{\varepsilon}$, molar attenuation coefficient ($L.mol^{-1}cm^{-1}$)

Table of contents

Page

1. Introduction

Woody biomass is considered as the very first energy source used by human beings and represents one of the major renewable feedstocks for the next-generation bioproducts, which could substitute many petroleum-derived products. In addition, wood has always played an important role in the production of low molar mass compounds, polymers and fibres. These intermediates might find applications, for example, in food, cosmetics, packaging, films, hydrogels, foams, composites or biomaterials. Unquestionably, biomass has the potential to meet a wide range of human needs. Nevertheless, the efficient use of biomass for the development of new materials, fuels or energy still faces many challenges.

The research work described in the experimental section of this doctoral thesis can be divided into three distinct parts. The first part of the work attempts to shed more light on the recovery of high-molar mass hemicelluloses from hardwood chips, and describes the synthesis of water-soluble polysaccharide derivatives. The second and most important part of the work focused on the utilisation of polysaccharide derivatives as fibre-modifying agents. As will be explained further, the method used for preparing the functional fibres represents a breakthrough over previously reported fibre surface functionalisation methods. The target functional groups are introduced into the backbone of water-soluble polysaccharides, under optimum reaction conditions and prior to their contact with pulp fibres. Subsequently, the polysaccharide-derivative bearing the target functional group is adsorbed onto the fibre surfaces. This process can be carried out in aqueous media, under controlled conditions at room temperature, thus preserving the excellent mechanical properties of the original fibres. In other words, by using this new approach, the challenging step of introducing functional groups onto poorly reactive fibre surfaces is turned into a simple sorption process. The third part of the work described in the thesis is more focused on utilisation of the prepared functional fibres, for example, as a template for the efficient immobilisation of enzymes.

To provide the rationale for the work mentioned above, a brief literature review is presented below, including information about the structure and composition of wood and pulp fibres, different strategies used in the isolation of high-molar mass hemicelluloses from hardwood chips, different uses for

polysaccharide derivatives, and the different methods used in the functionalisation of pulp fibres.

1.1. Wood

Wood is well distributed throughout the world; it is a renewable resource, and is considered as the most important non-food natural feedstock available on our planet. Beyond its use as a building material, in the construction of tools, or as an energy resource, wood has historically been the primary source for the production of pulp and paper.[1] According to the survey 2015-2020 reported by the Food and Agriculture Organisation of the United Nations (FAO), about 160 million metric tons of wood pulp are produced every year around the world (about 65 million metric tons corresponds to bleached sulphate-soda pulp).[2] The integration of different processes into the pulp and paper production chain is converting traditional pulp and paper mills into next-generation bio-product mills.

The term wood refers to the fibrous substance composing most of the stem and branches of the trees, and can be divided into two different types: softwood and hardwood. Although this classification refers only to plant reproduction, the chemical composition and arrangement of the structural elements associated with each type of wood is also distinctive. Independent of the type of wood, three major polymers are always present: cellulose, hemicellulose, and lignin (Table 1).[3] As shown in Table 1, the distribution of these components is different for the different types of wood.

Table 1. Macromolecular components of wood cell wall.[4]

	Content (w/w %)	
	Softwoods	Hardwoods
Cellulose	40-44	40-44
Hemicellulose	30-32	15-35
Lignin	25-32	18-25

Cellulose, which is the major polysaccharide found in wood, is the name given to the linear homopolymer consisting of D-glucopyranose (D-Glc*p*) residues linked by ß-1,4-glycosidic bonds, and its elemental composition was first described by Payen (Figure 1).[5,6] The second most important polysaccharide encountered in wood is referred to as hemicellulose, which is a linear branched polymer comprised of two or more types of sugar monomers (Figure 2).[7] Hardwood hemicelluloses mainly consist of 4-*O*-methylglucuronoxylan (MGX), which is primarily composed of a backbone of (1→4)-linked ß-D-xylopyranose units (Xyl*p*).[8] Unlike hardwood, softwood hemicelluloses mainly consist of glucomannan. These polysaccharides are structural components of woody plants, as well as structural components of non-woody plants, bacteria, fungi, and algae. The third major component encountered in wood is referred to as lignin, which is an aromatic amorphous polymer. Lignin is derived of an apparently random combination of three hydroxycinnamyl alcohol monomers (monolignols): *p*-coumaryl, coniferyl, and sinapyl alcohol (Figure 3). Although many aspects of the biosynthesis of lignin remain a matter of debate, the composition and structure of the different type of lignin is well described in the literature. It is known that the main difference between hardwood and softwood lignin lies in the different ratio between guaiacyl (G), syringyl (S), and p-hydroxyphenyl (H) phenylpropanoid units, which are the structural units of lignin.[9] Coniferous lignin consists mainly of G and S units, (GS-lignin), whereas hardwood lignin also contains H units (GSH-lignin).

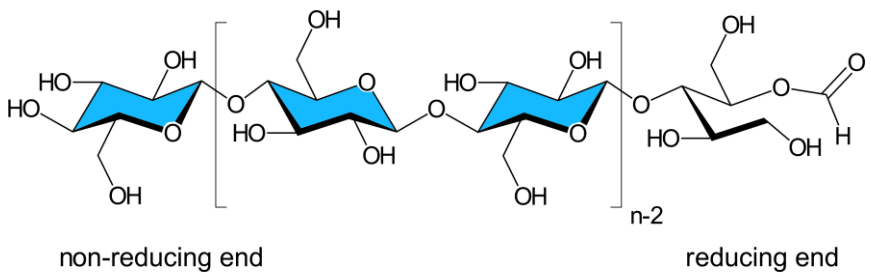

Figure 1. Molecular structure of cellulose with a degree of polymerisation of n

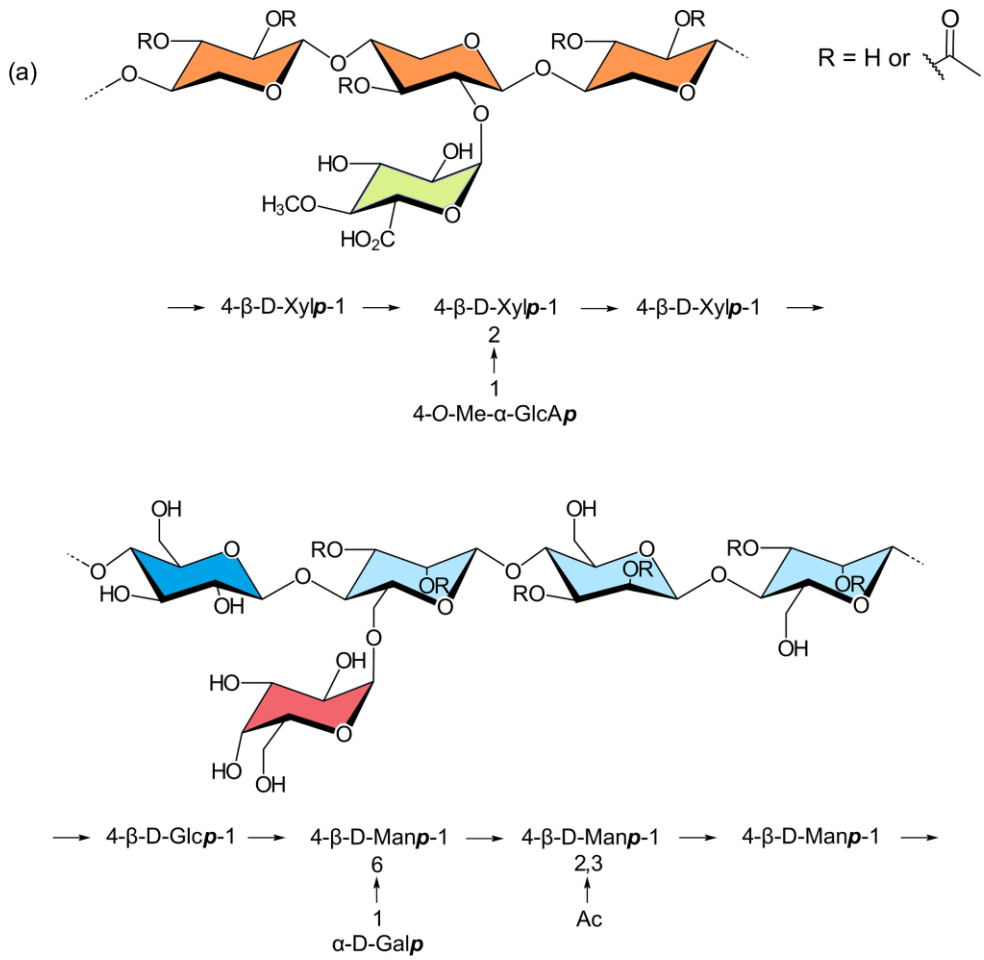

Figure 2. Primary structure of hardwood xylan (a) and softwood glucomannan (b). [Adapted from Laine[10]]. **Xyl*p***, xylopyranose; **Glc*p***, glucopyranose. **Man*p***, mannopyranose. **Me**, methyl.

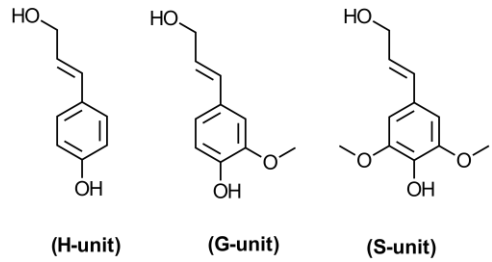

Figure 3. Types of monolignols found as building blocks in lignin. p-coumaryl alcohol (H-unit), coniferyl alcohol (G-unit), sinapyl alcohol (S-unit).[11]

In addition to the major components, wood also contains non-structural components, for example the compounds referred to as extractives, which can be extracted with organic solvents (e.g., terpenes, fats, waxes, and phenols) or liquid hot water (e.g., tannins and inorganic salts). These compounds can be grouped as volatile oils, wood resins, fats and waxes. Wood also contains inorganic compounds (such as metal salts of sulphates, phosphates and silicates). A very simplified schematic illustration of the major wood components among the fibrous material is shown in Figure 4(a). Figure 4(b) illustrates the layered structure of pulp fibres, which will be discussed in more detail below.

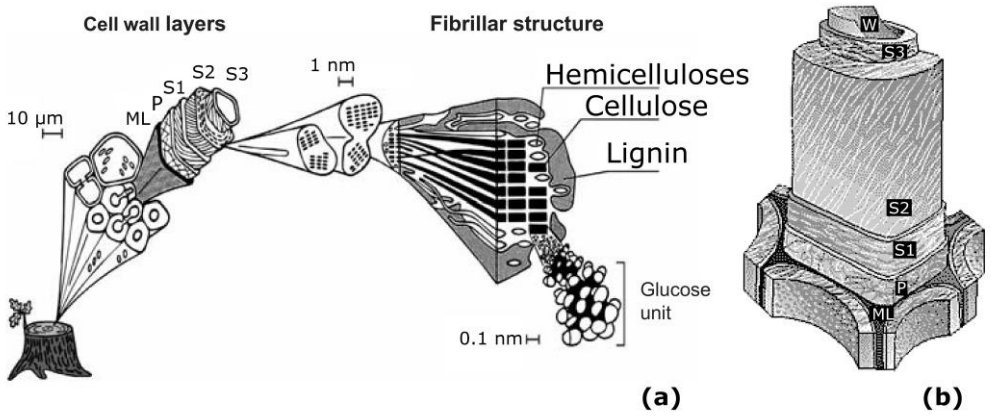

Figure 4. Schematic illustration of the fibrillar structure of the cell wall layers in wood, showing the distribution of the major wood components (a) and the arrangement of a cellulose fibre in different layers (P, S, and W) held together by the middle lamella composed primarily of lignin (b) [Adapted from Koch[4]]

1.2. Pulp fibres

Wood is mainly composed of elongated cells, the structure and composition of which is strongly dependent on the source. In the case of softwoods such as pine, about 90-95% of the elongated cells receive the name of tracheids. The remaining 5-10% consists of ray cells (parenchyma and ray-tracheids), in addition to resin canals.[12] On the other hand, hardwoods such as birch or eucalyptus have elongated cell types like libriform cells and fibre tracheids, and also shorter specialised cells such as hardwood vessels and ray parenchyma cells. Both softwood- and hardwood elongated cells have closed ends, and present different types and amounts of pores, referred to as pits. The presence

of these pits in the elongated fibres is very important, as they control the mass transfer from the outside of the fibres towards the interior, and vice versa.[1] Figure 5 shows a scanning electron microscope image of softwood cut in the transverse section, showing rectangular tracheids connected to one another along their radial walls by bordered pits. The wood cells shown in the picture are interconnected and attached to each other through a lignin-enriched amorphous polymer, known as the middle lamella.

During kraft cooking, the phenolic polymer in the middle lamella is partially removed, and the individual cells are released from the matrix. The resulting fibrous material is usually referred as "pulp".[13] The dark brown colour of the unbleached pulp turns white after pulp bleaching processes, yielding bleached kraft pulp. The individual elongated cells obtained after the kraft cooking are herein referred to as fibres (unbleached or bleached (pulp) fibres) for simplicity.

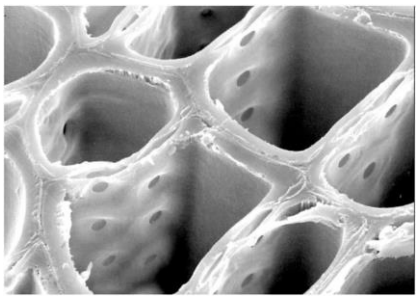

Figure 5. Scanning electron microscope image of conifer wood cut in the transverse section, showing rectangular tracheids connected to one another along their radial walls by circular pits [Reprinted from Mustoe et al.[14]]

In the context of modern pulp and paper production, bleached fibres are a very attractive material, with great potential for the development of advanced applications. The material is produced from a renewable source; it is biocompatible and already available on the large scale at a convenient price. Moreover, pulp fibres possess large surface area, and are highly hydrophilic but insoluble in water, showing poor reactive surface and excellent mechanical properties. Although the original water-swollen state is not fully regained after drying, the irreversible changes that take place might not be significant for most of the applications related to functional fibres.[15,16] This implies that the dry fibres can be transported and/or stored until further use, which is not only very practical but also convenient from an economic point of view.

1.3. Structure and composition of pulp fibres

A thorough understanding of the structure and chemical composition of cellulose fibres might be critical for the successful development of novel materials and bio-products made of them. It is therefore worth mentioning their main characteristics. Independent of the type of wood (i.e., softwood of hardwood), the diameter of the fibres becomes smaller and cell walls become thicker when evolving from earlywood (spring) to latewood (summer). Typical softwood fibres are 2-4 mm long, with a thickness of 2-8 μm and a width of 20-40 μm, whereas typical hardwood fibres such as *Eucalyptus* fibres are 0.6-1.1 mm long, 3-5 μm thick, and 15-20 μm wide.[17] Evidently, the dimensions of hardwood fibres are smaller than those of softwoods, and the variation in length, wall thickness and diameter is more pronounced in the case of softwoods.

Fibres are built up of concentric layers (also named interlayers) with different chemical compositions and different orientations between structural elements, such as the fibril agglomerates (also known as microfibrils).[18] These interlayers are distinguished as the primary layer (P), secondary layer (S), and tertiary layer (T). They show different thicknesses depending on the natural origin. The secondary layer (S) is often split into S1 and S2, and in the case of parenchyma cells, a third interlayer S3 is also distinguished. Of the sub-layers of the secondary wall, S2 has been shown to be the thicker one, whereas S1 seems to be the thinner one in most cases.[1] These interlayers, in turn, consist of a scaffold of cellulose fibril agglomerates embedded in a complex matrix, which is mainly composed of lignin, non-cellulosic polysaccharides (e.g., hemicelluloses and pectic-polysaccharides). To a lesser extent, the matrix also contains minor compounds (e.g. inorganic matter, terpenes, and phenolic compounds such as tannins).[1,19]

As mentioned before, during kraft pulping and bleaching processes, the soluble lignin from the middle lamella is removed almost completely. According to Stone et al.,[13] at the beginning of kraft cooking, the lignin in the interior of the cell wall is also partially dissolved; therefore, small pores (nanopores) merge, yielding larger pores. While the amount of lignin is progressively reduced, the space between the interlayers decreases, and the cell wall shrinks.[13] Doubtless, important changes take place during the kraft cooking, affecting the structure and chemical composition of the fibres. One remarkable change is the increment of anionic groups on the fibres after kraft pulping.

According to the literature, this increment originates from hemicelluloses, due to the formation of new carboxylic groups within their polymeric chain (e.g. alkali-catalysed formation of hexenuronic acids from 4-O-methyl-D-glucuronoxylan). Unlike the aforementioned, elementary fibrils composed of crystalline and amorphous cellulose do not change significantly.[12,20] An illustration of a cellulose fibre with its main components is shown in Figure 6.

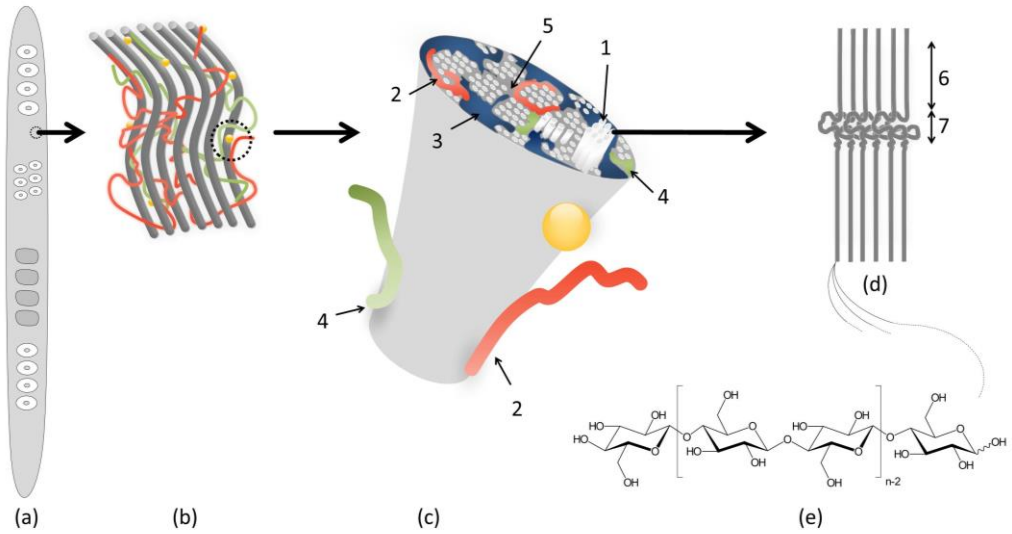

Figure 6. Illustration of:

(a) An individual softwood fibre showing different type of micropores (pits)

(b) A cellulose fibril aggregates (grey), which are embedded in a lignin matrix (not shown), ringed by minor components such as extractives (yellow and green), and hemicelluloses (orange)

(c) A fragment of a fibril aggregates composed of elementary fibrils bundles *(1)* hemicelluloses *(2)*, lignin *(3)*, minor compounds *(4)* with nanopores *(5)*

(d) A bundle of elementary fibrils, which are composed of pure cellulose chains arranged in crystalline *(6)* and amorphous (7) regions

(e) A cellulose chain

1.4. **Isolation of xylan from birch wood chips**

In the particular case of birch wood, xylan represents about 26% of the total wood (Figure 7).[21] The degree of polymerisation (DP) of the native xylan is estimated to be about 30-150 sugar units.[22] The xylopyranose units of birch xylan are partially substituted by 4-*O*-methyl-α-glucuronic acid moieties (Me-Glc*p*A) at the O2 position, showing a molar ratio for Me-Glc*p*A:Xyl*p* of ca. 1:10.[1,7]

In addition, C2 and C3 positions of the Xyl*p* units are partially acetylated (substitution rate of ca. 70%). According to Johansson et al., the unit next to the reducing xylose end-group in Me-Glc*p*A is D-galacturonic acid, linked to an L-rhamnose unit.[23]

Thanks to advanced techniques such as microscopic sample manipulation, it has become possible to study the distribution of xylan in the different cell-wall layers of hardwood fibres. According to Meier,[24] the native xylan is not evenly distributed in cell wall layers. For example, in the case of young wood fibres from birch (*Betula verrucosa*), the xylan content reaches its maximum weight percentage in the middle layer of the secondary wall (S2), as illustrated in Figure 8.

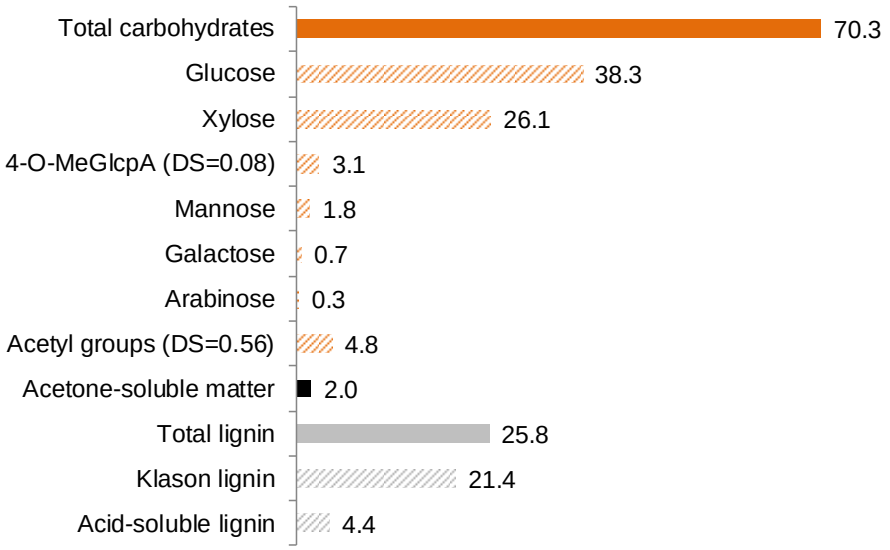

Figure 7. Chemical composition of birch wood chips (in %, and based on oven-dry-matter).[21] The acetone-soluble matter was measured, but was not considered in the mass balance. The carbohydrate composition is expressed as anhydro-sugars. **DS**, Degree of substitution. Values next to colour-filled columns refer to subtotal of individual values reported right-below and next each pattern-filled column.

Xylan has drawn much interest during the last decades because it is available from renewable sources, especially from wood, and because it shows potential for a wide variety of interesting applications.[25,26,27,28,29,30,31,32,33] For example, xylan-type polymers might find application in important fields such as medicine,

cosmetic or packaging. It could be also an excellent intermediate to produce non-petroleum based plastics (e.g., xylan as additive, adhesive, or thickener). The biocompatibility of pure xylan (i.e., its ability to be in contact with living system without producing an adverse effect) makes the polymer suitable for the development of biomaterials such as hydrogels, nanocapsules or other drug delivery systems.[34,35,36]

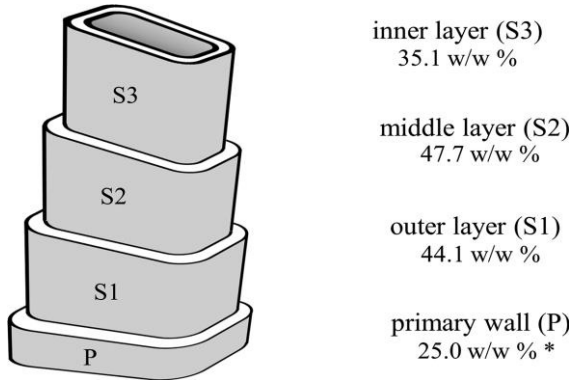

Figure 8. Schematic illustration of the fibre cell wall layers of young fibres of birch (*Betula verrucosa*), with the xylan content as a weight percentage of the corresponding layer/wall primary wall (P) and the three layers of the secondary wall (S1–S3).[24] *As a weight percentage of the primary layer and middle lamella [Reproduced from Vega et al.[25]]

Unfortunately, the utilisation of xylan in many of the above-mentioned applications is not as straightforward as one would think. This is attributable to the fact that the properties of the different types of xylan greatly depend on their exact chemical structure, which depends heavily on the natural origin and method of extraction. In addition, other factors such as the sample preparation methods and pre-treatments might also have a significant impact on the final composition of the isolated xylan. For example, a pre-impregnation step contributes to enhanced liquor penetration and air removal, therefore, it prevents oxidation reactions during the process and increases the extraction yield.[25,37,38,39] Storage conditions, wood moisture content, and wood particle size might not be so important in terms of the resulting chemical composition of the extracted xylan; nevertheless, these parameters play a significant role in liquor penetration, thereby influencing the mass transfer which ultimately determines the final yield.[40,41] In summary, the selection of the natural origin, sample storage conditions, pre-treatment, and method of extraction, together with an extensive

characterisation of the isolated xylan, are essential for the success of many applications.

In the experimental work described in this thesis, the efforts were focused on addressing the extraction of high molar mass xylan. Solid-liquid extraction is the most useful technique to separate high-molar mass xylan from wood chips.[22,25,26,42] In this context, different liquids have been tested as extraction media for extracting xylan from wood (e.g. acidic, neutral or alkaline aqueous solutions, or dimethyl sulphoxide). According to Cornel et al.,[43] the removal of xylan from wood seems to occur in two different phases: an initial fast phase, followed by a slower second phase. The two different rates of xylan removal are attributed to the differences in accessibility, rather than any variability in the polymeric structure of the xylan being removed.

One of the most common methods for the extraction of xylan is the so-called pressurised hot water extraction (PHWE) method, which can be carried out in both flow-through and static batch modes. The term PHWE refers to the processes of extraction that use liquid water at higher than ambient boiling temperature (i.e., T_b = 100°C, P_b = 1 atm) and below supercritical conditions (T_c = 374°C, P_c = 22.1 MPa, ρ_c = 320 kg/m^3).[44] From ambient to supercritical conditions, the properties of water change significantly. For example, as the ion-product constant value for water (K_w) increases with the increase in temperature, the pH of subcritical water is lower than the corresponding pH of water at 25°C.[45,46] One of the consequences of this drop in pH value at elevated temperatures and high pressure is that the acetyl groups originally bound to the hemicelluloses are released into the aqueous medium, ergo acetic acid is formed. The ionisation of acetic acid further catalyses the hydrolysis of glycosidic bonds in polysaccharides, and autohydrolysis takes place.[47,48,49] At the same time, degradation products such as furfural, uronic acids, and methanol might be released to the extraction liquor, due to the degradation reactions which occurred during the PHWE processes, especially at elevated temperatures.[1,20,50,51] For these reasons, it is recommended to avoid drastic extraction conditions. On the other hand, too weak extraction conditions would be not sufficient to breakdown the chemical bonds between side groups in the xylan polymeric chain and other cell wall constituents such as lignin (e.g., low yield).[50] Moreover, since starch is solubilised at lower temperatures, very mild conditions might facilitate contamination with this non-cellulosic polysaccharide.[46] High molar mass xylan has been recovered from hardwood using short-time solid-liquid extractions

under mild conditions (i.e., extraction time less than 30 min, initial pH ca. 7, final pH ca. 3.5, and temperature range from 160-180°C).[22,43,52,53]

After PHWE, the water soluble xylan needs to be separated from other components dissolved in the extraction liquor. Ethanol has shown to be a very effective anti-solvent for the precipitation of enriched hemicellulose fractions from the aqueous media. The ethanol:liquor ratio is critical because it determines the molar mass fraction of the hemicellulose that is precipitated, and lower ethanol:liquor ratio only precipitates higher average molar mass polysaccharides.[54,55] Membrane filtration of wood hydrolysates has also been useful for the recovery of hemicelluloses from the aqueous liquor.[56]

1.5. **Polysaccharide derivatives**

In addition to the large variety of naturally occurring polysaccharides with different chemical composition and distinct properties, polysaccharides can be derivatised, yielding new compounds.[57] This results in a wide variety of novel polysaccharide derivatives with tuned functionalities, and opens the way to novel materials and applications. The chemical derivatisation is carried out under heterogeneous reaction conditions or in the homogeneous phase.

In the case of cellulose, with polymeric chains arranged in crystalline and amorphous regions, the hydroxyl groups can partially or fully react with different reagents, either by esterification or etherification. Alternatively, less conventional or complex processes might involve nucleophilic displacement reactions, “click-chemistry”, or controlled oxidation reactions.[58] The commercial production of cellulose ethers, such as carboxymethyl cellulose, is exclusively carried out under heterogeneous conditions. Likewise, the commercial esterification of cellulose is conducted only under heterogeneous reaction conditions. Control over the even or uneven distribution of functional groups along the cellulose chain also remains a challenge, especially under heterogeneous conditions. This is because solid cellulose chains are arranged in amorphous and highly packed crystalline regions, and most of the hydroxyl groups on the crystalline region of cellulose do not react during the heterogeneous reactions.

The chemical structure of a polysaccharide derivative and its intrinsic properties are strongly connected. The degree of polymerisation (DP), degree of substitution (DS), and functionalisation patterns are key parameters as they determine the physical and chemical properties of the polymer. Thus, the

homogeneous phase chemistry is the most important tool in the design of cellulose derivatives, because it enables fine-control over the reaction progress. Unfortunately, homogeneous reaction conditions are not easy to achieve because cellulose does not melt, and it is difficult to dissolve.

The regioselective functionalisation of cellulose might be conditioned by the different reactivity of the hydroxyl groups depending of the solvent and upon different reaction conditions. Nevertheless, the regioselective derivatisation of protected cellulose leading to 3-O, 2,3-O, and 6-O cellulose derivatives is possible, and the obtained products have shown remarkable differences in properties with common cellulose derivatives.[58] These synthesis pathways described above are also applicable for the synthesis of non-cellulosic polysaccharide derivatives, such as hemicellulose derivatives. However, additional challenges appear in these cases due to the more complex structures of the non-cellulosic polysaccharides. At the same time, more opportunities arise because not only hydroxyl groups react, but also amine-, carboxylic-functional groups, etc.

Some examples of xylan and cellulose derivatives are mentioned in Tables 2 and 3, respectively. As shown, the properties and applications might be very different.

1.6. **Functionalisation of pulp fibres**

Pulp and paper industries have been able to increase their production volumes by several orders of magnitude during recent decades. This successful scale-up has also increased opportunities for the development of new lines of production, which aim to produce new bio-products from pulp fibres. In this context, several strategies for converting fibres into value and solutions have been tested (e.g., the introduction of target functionalities onto the fibre surfaces to produce functional fibres).

Functional fibres bearing specially designed functionalities, while preserving the excellent mechanical properties of the traditional pulp fibres, can be obtained by different methods.[59,60,61,62,63] For example, since (bleached) pulp fibres are primarily composed of cellulose, many of the conventional heterogeneous-phase routes used in functionalisation of cellulose have also been considered for fibre modification. However, the modification of the fibre surfaces by using conventional cellulose chemistry is not an attractive solution because the it usually requests harsh conditions, with detrimental effect on the mechanical properties due to degradation of the cellulose chains.[64,65,66] In addition, the

extreme conditions always raise concerns in terms of safety, and the characterisation of the resulting materials require strong expertise and sophisticated techniques. Unlike conventional chemical treatments, enzymatic treatments carried out under mild conditions may be an alternative. Nevertheless, the implementation of enzymatic treatments has also been constrained because of important drawbacks such as the limited availability of the specific enzyme and/or its high cost and poor stability, the large volume of solvent that is usually required, or difficulties with the purification of the final product. Alternatively, the self-assembly of polyelectrolytes on the surface of cellulose fibres can take place, mainly due to electrostatic interactions of the surface anionic groups (SAGs) on the fibre surfaces and the cationic charge of the polyelectrolytes. The method is very simple, reproducible, and safe. In the latest forty years, different polyelectrolytes have been tested and used in pulp and paper as dry- or wet-strength additives, and as retention and fixing aids. More recently, functional fibres with the potential for advanced applications have been developed, using tailored polymers as modifying agents. The target properties of the functional fibres can be easily tuned with high precision by adjusting the doses of the functional polymer and/or modifying its chemical structure, making this approach even more attractive.[67,68,69,70,71,72] Table 3 shows some examples of functional fibres prepared by the self-assembly of polyelectrolytes onto pulp fibre surfaces.

Table 2. Examples of polysaccharide derivatives prepared from cellulose and xylan.

Name	Functional group	Potential application	Ref.
Xylan furoate	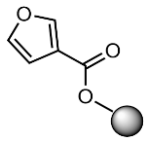	Film formation	30
Xylan ibuprofen	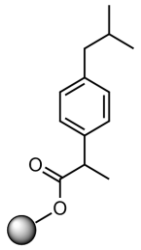	Biologically active component in drugs	35
HPMAX	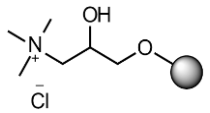	Antimicrobial agent, flocculation aid (paper additive)	28,73
FTIC[a] xylan	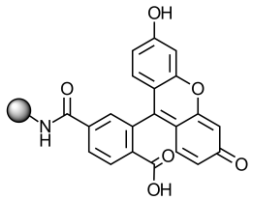	Mapping	74
6-deoxy-6-azido cellulose		CuAAc reaction	75

HPMAX, Hydroxypropyltrimethylammonium chloride xylan. **FTIC**, fluorescein isothiocyanate.

Table 3. Examples of functional fibres prepared by the self-assembly of functional polymers

Type of pulp	Polymer	Added function	Potential application	Ref.
Birch kraft	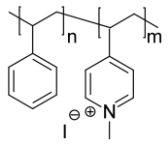	Hydrophobicity	Water-repellent coatings, microfluidics, self-cleaning surfaces	68
Birch kraft	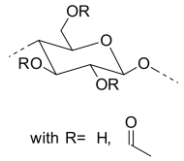	Improved mechanical properties	Pulp and paper	67
Spruce sulphite	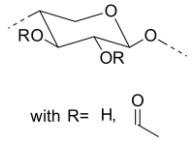	Improved mechanical properties	Pulp and paper	72
Eucalyptus kraft	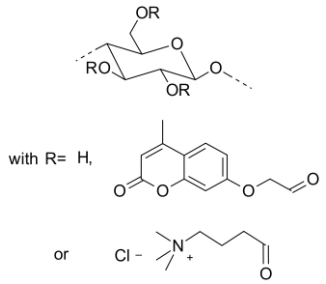	Light response	Counterfeit-detection fibres and papers	69,70
Cellulosic fibres#	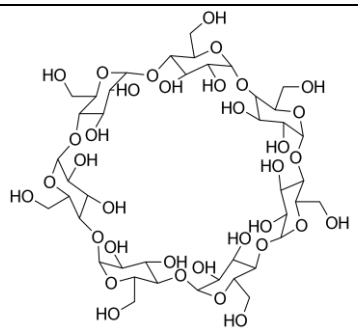	Metal and organic dye sequestration	Industrial sewage treatment	76

non-pulp cellulosic fibres

1.7. **Advanced techniques used in the characterisation of pulp fibres**

- *Field emission scanning electron microscopy (FE-SEM)*. This technique provides topographic information about the samples. Briefly, a field-emission (FE) cathode in the electron gun of a scanning electron microscope (SEM) provides a narrow beam probe at broad electron energy. The electron beam is scanned across the surface of the sample, generating secondary electrons which are collected by the detector, and the detected signals are converted into images. FE-SEM images with ultra-high magnification (10x to 300,000x) allow small areas on the sample to be examined, with small contamination features. High spatial resolution is achieved, with minimised sample charging and damage.

- *X-ray photoelectron spectroscopy (XPS).* High resolution XPS spectra can be obtained by irradiating the samples with *X*-rays while simultaneously measuring the kinetic energy of the photoelectrons emitted from the surface (sampling depth of about 5 to 10 nm). The X-rays are generated in the instrument by bombarding a target anode with high energy electrons from a heated filament. In the case of aluminium anode bombarded with 15 keV, the energy of the characteristic emitted line ($K\alpha_{1,2}$) is 1486.6 eV. In a nutshell, spectra are collected by counting the ejected core electrons over a range of electron kinetic energies (hence, binding energy), with high resolving power. XPS is a high-sensitivity technique for the accurate quantitative analysis of the surface chemical composition of analysed samples at ultra-high vacuum (see illustration in Figure 9).

The XPS technique has proved to be applicable for monitoring the changes on a broad range of sample surfaces, including the surface of polymer materials such as lignocellulosic biomass.[77,78,79,80] In the case of the latter, the measurements require additional care, as sample contamination and experimental artefacts can significantly affect C 1s signal, which is one of the most important signals from that type of sample. The role of sample handling, light exposure, radiation dose, charging and data analysis on the XPS of air-exposed paper specimens has been reported by Johansson et al.[81]

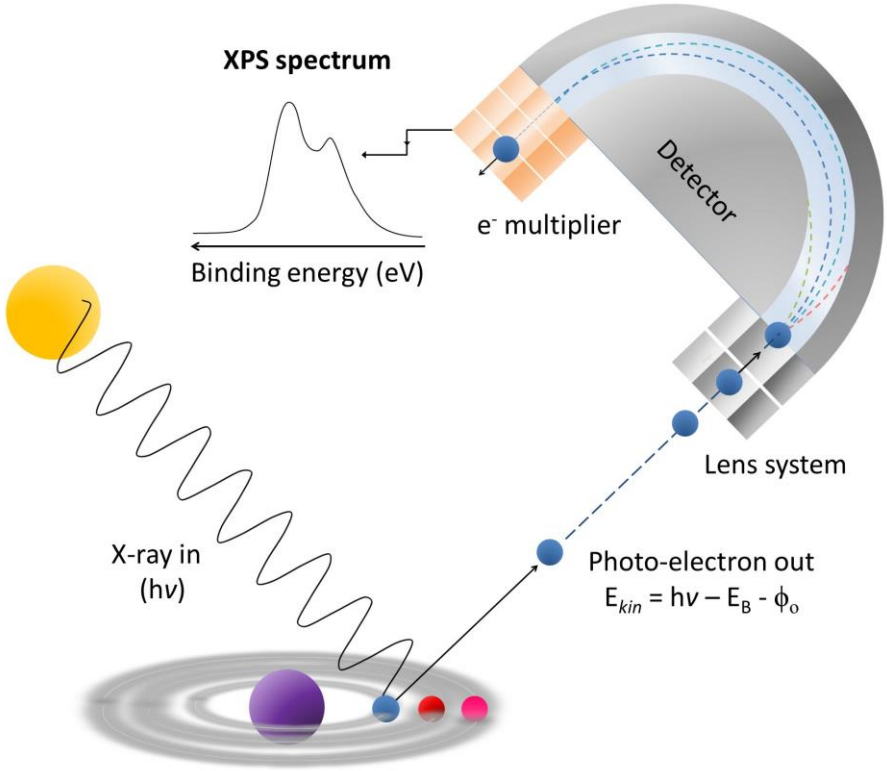

Figure 9. Schematic illustration of X-ray photoelectron spectroscopy analysis (XPS). $\mathbf{E_{kin}}$, measured kinetic energy of the emitted electron e^- (J). **h**, Planck constant (6.626×10^{-34} J.s). $\boldsymbol{\nu}$, frequency of the exciting X-ray photon (Hz). $\mathbf{E_B}$, electron binding energy (J). $\mathbf{\Phi_o}$, work function of the spectrometer (~ 5 eV). The equation shown in the figure exclusively refers to the elastic photoemission process.

- *Time-of-flight secondary ion mass spectrometry (ToF-SIMS).* Time-of-flight secondary-ion mass spectrometry (ToF-SIMS) is a powerful technique to study the chemical composition of the extreme surface of solid samples (sampling depth of about 1-2 nm). Briefly, a finely focused primary ion beam is pulsed and rastered towards a solid sample under high vacuum. Thus, various atoms and molecules are "sputtered" from the uppermost layers of the bombarded sample, and only a small percentage of those possess net electric charge (i.e., are secondary ions). The secondary ions are separated in the high-resolution mass spectrometer according to their different mass to charge ratio (m/z). As a result,

a mass spectrum representing the relative abundance of each secondary ion (in counts) versus their m/z values is obtained.

Frequently, charging compensation techniques are used during measurements to ensure static conditions during the measurements. For example, charge compensation is obtained with an electron flood gun pulsed out-of-phase with respect to the ion gun.

In addition to the mass spectrum obtained for each sample, which allows target moieties to be identified based on their characteristic peaks with specific m/z values, ToF-SIMS spectral images brings valuable additional information. As each image pixel contains a complete mass spectrum, it is possible to use ToF-SIMS imaging to accurately determine the distribution of the moieties of interest on the sample surface. This is possible because in each pixel of a ToF-SIMS image, a colour value can be assigned to the relative abundance (in counts) of each secondary ions of interest, leading to m/z resolved images. A schematic illustration of the ToF-SIMS analysis is shown in Figure 10.

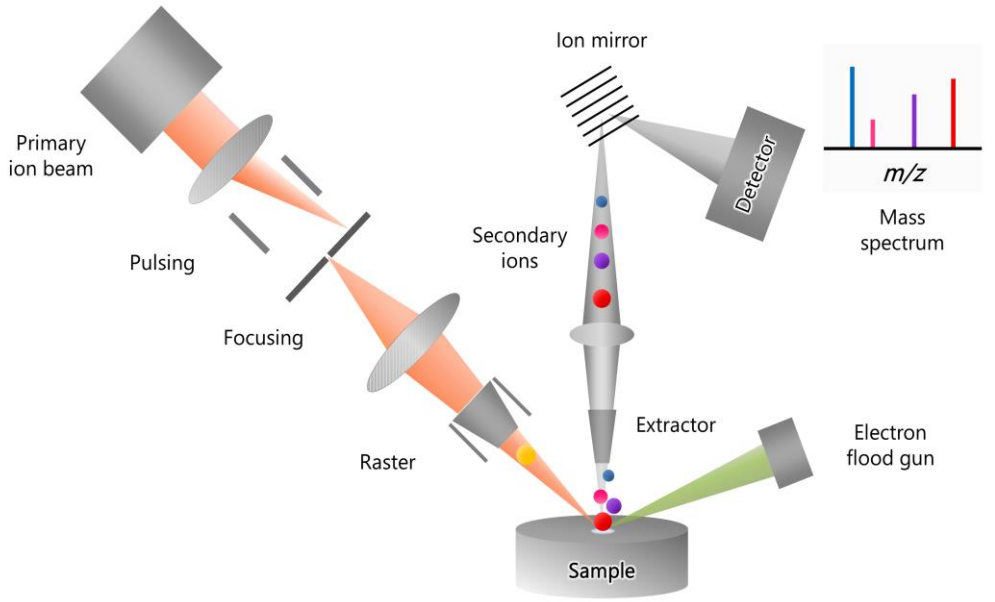

Figure 10. Schematic illustration of ToF-SIMS analysis. **m/z**, mass to charge ratio [adapted from Hofmann et al.[82]]

2. Experimental

2.1. **Materials**

Wood chips:

Birch chips were collected from UPM pulp mill (Lappeenranta, Finland), air-dried, screened using vibrating screen bars, and stored in a dark place until further use (accepted size between 2-8 mm, dry content ≥92%). Determination of the non-cellulosic polysaccharides content of the wood chips according to Bertaud et al.[83] yielded a mass fraction of: 25.4% xylose, 2.5% glucose, 2.0% galacturonic acid, 1.1% mannose, 1.1% galactose, 0.6% rhamnose, 0.5% arabinose, and 0.5% glucuronic acid.

Pulp fibres:

Never dried bleached kraft pulp from pine (*Pinus sylvestris L.,* kraft cooking process followed by bleaching sequence DO-EOP-D1-P; brightness of 86) was obtained from a Metsä Fibre mill (Rauma, Finland) and used in experiments described in Papers I-IV. The pulp bleached kraft pine pulp (BKPP) was aliquoted and stored in plastic bags at -20°C. After thawing, and after dewatering to a dry matter content of ca. 25%, each sample batch with pulp was kept at +4°C until shortly before the experiments.

Bleached chemical sulphate pulp from eucalyptus (*Eucalyptus grandis*, kraft cooking process followed by bleaching sequence A/D-EOP-D-P; brightness of 91) was obtained from UPM (Fray Bentos Mill, Uruguay), macerated in water to re-swell before used in the experiments.

List of chemicals:

2,2'-Azino-bis(3-ethylbenzothiazoline-6-sulfonic acid) diammonium salt (≥98%), Bradford reagent, (3-carboxypropyl)trimethyl ammonium chloride (technical grade), dimethyl sulphoxide (DMSO, ACS reagent grade), glucose oxidase (type VII prepared from *Aspergillus niger*, ≥100 $U.mg^{-1}$), glucose oxidase activity assay kit MAK097, glutaraldehyde (grade II, 25% in H_2O, ACS reagent grade), HRP peroxidase (type II prepared from horseradish, 150−250 $U.mg^{-1}$), methanol (anhydrous, 99.8%), mowiol 4−88 (ACS reagent grade), *N*,*N*-carbonyldiimidazole (CDI), *N*,*N*-dimethylformamide (DMF), sodium chloride (bioXtra, ≥99.5%), sodium

onochloroacetate, sodium phosphate dibasic heptahydrate (ACS reagent), sodium phosphate monobasic dihydrate (puriss p.a., crystallised ≥99%, ACS reagent grade), sulphur trioxide pyridine complex, tris[(1-benzyl-1H-*1,2,3*-triazol-4-yl)methyl]amine (97%), 2-propanol and paraformaldehyde (PFA, ACS reagent grade) were purchased from Sigma-Aldrich. ACS grade sodium hydrogen carbonate and acetone were purchased from J. T. Baker. ACS reagent phosphate buffered saline was purchased from Gibco (Thermo Fisher Scientific). Abberior STAR 365 (NHS ester) was purchased from Abberior GmbH. Lithium chloride was purchased from VWR. Ethanol (>99.5%) was purchased from Altia Oyj. Microcrystalline cellulose Avicel PH101 was purchased from Fluka, 1-ethynylpyrene was purchased from Lumiprobe, and propargylamine was purchased from Acros Organics. Unless specified otherwise in this paper, the chemicals were used as received and the results from weight measurements related to wood and wood pulp fibres are expressed on an oven-dry basis.

2.2. **Extraction and characterisation of xylan from birch chips**

High molar mass xylan was extracted from screened birch wood chips by the pressurised hot water extraction method (PHWE). Batch extractions were performed using a 5 L rocking digester provided with electrical heating controlled by an Eurotherm 3504 Process Controller, under a rotational speed of about 1 rpm through an arc of 360 degrees. For every batch, 1 kg of wood chips and distilled water (liquor to wood ratio 5:1) were loaded in a preheated digester at 110°C, and the mixture was warmed up using a 2°C.min^{-1} ramp rate, until a temperature of 160°C was reached. After 10 min dwell time at this temperature, the liquor with pH of 3.8 (measured at rt) was discharged and concentrated to 1 L under vacuum (42 mbar) at 42°C. Subsequently, 4 L of ethanol (≥99.5%) was added to the concentrated liquor under vigorous stirring for 20 min, and the resulting mixture was stored at 8°C in the refrigerator, overnight. After that, the supernatant solution was separated from the precipitate by vacuum filtration through a MN 640 w filter paper (Macherey-Nagel GmbH and Co. KG, Düren, Germany). Finally, the recovered solid was thoroughly washed with ethanol, dried in an oven desiccator at 40°C, freeze-dried, and stored in a dark place until further use. Following this procedure, 10.5 g of xylan was recovered from each kg of wood chips (average value). Characteristics of the extracted xylan are provided in Paper I and Table 4.

2.3. **Synthesis and characterisation of xylan derivatives**

Xylan sulphate (XS^-), carboxymethyl xylan (CMX^-) and xylan-4-[*N,N,N* trimethylammonium]butyrate chloride ($XTMAB^+$) were synthesised from the xylan isolated from birch chips, using PHWE conditions described above. Scheme 1 illustrates the paths followed for the synthesis of each derivative. More details about the synthesis and characteristics of those derivatives are provided in Paper I and Table 4.

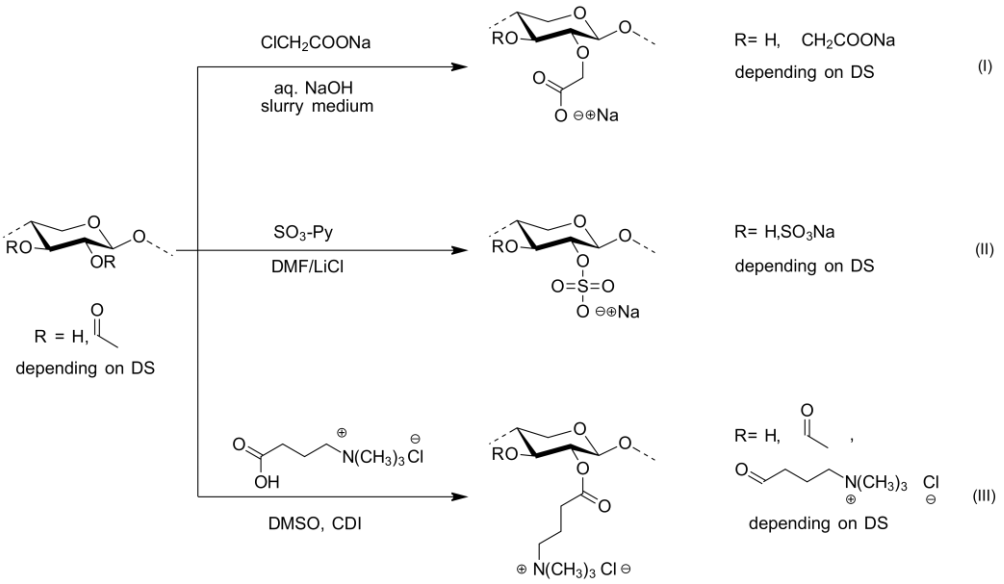

Scheme 1. Paths for the synthesis of xylan derivatives CMX^- (I), XS^- (II) and $XTMAB^+$ (III), from acetylated idealized xylan. **XS^-**, xylan sulphate. **CMX^-**, carboxymethyl xylan. **$XTMAB^+$**, xylan-4-[*N,N,N* trimethylammonium]butyrate chloride. [Adapted from Vega et al.[84]]

2.4. **Synthesis and characterisation of cellulose derivatives**

2.4.1. Synthesis of CN^+

The synthesis of cellulose (3-carboxypropyl)trimethylammonium chloride ester (CN^+) is illustrated in Scheme 2. More details about the synthesis and characterisation of the derivative are described in detail in Paper II. The main characteristics of the polymer are summarised in Table 5.

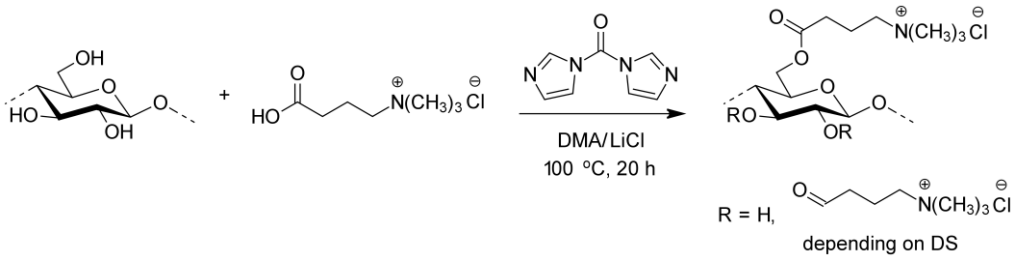

Scheme 2. Synthesis of cellulose (3-carboxypropyl)trimethylammonium chloride ester (CN^+) via in situ activation of (3-carboxpropyl)trimethylammonium chloride with *N,N*-carbonyldiimidazole in *N,N*-dimethylacetamide/LiCl (DMA/LiCl). [Adapted from Vega et al.[85]]

2.4.2. Synthesis of N_3-cell$^+$

The poly-functional cellulose derivative (3-carboxypropyl)trimethylammonium chloride ester of 6-deoxyazidocellulose (N_3-cell$^+$) was synthesised in a three-step synthesis route, as illustrated in Scheme 3. More details about the synthesis and characteristics of this polymer are found in Paper III and Table 5.

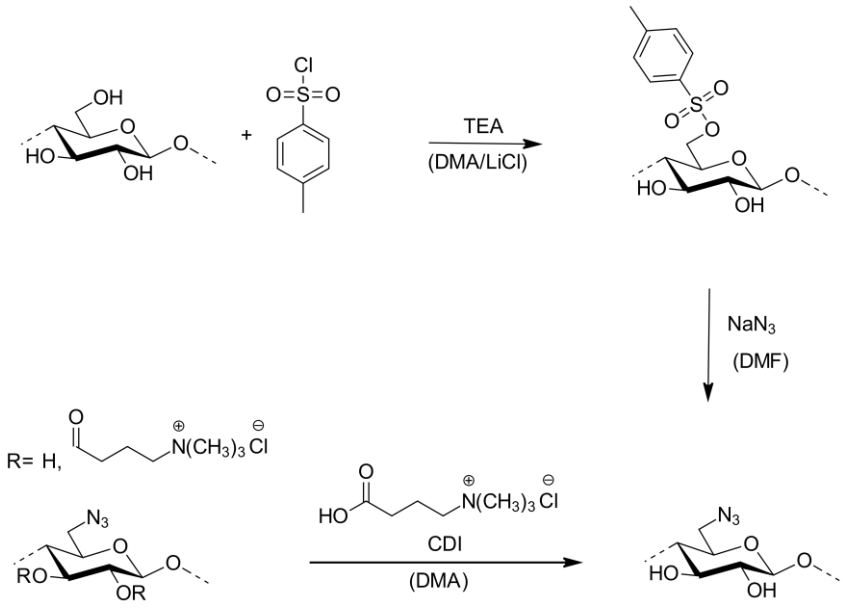

Scheme 3. Synthesis scheme for the preparation of (3-carboxypropyl)trimethylammonium chloride ester of 6-deoxyazidocellulose (N_3-cell$^+$) [Adapted Vega et al.[85]]

2.4.3. Synthesis of amino-cell

N_3-cell$^+$ was subjected to copper(I)-catalysed alkyne-azide Huisgen cycloaddition (CuAAc) with propargylamine (Scheme 4). Briefly, an N_3-cell$^+$ (150 mg, 636.9 μmol) dissolved in 150 mL of deionised water was mixed with propargylamine aqueous solution (10 mM, 610 μmol) and 10 mL of triethylammonium acetate buffer (2 M in water, pH 7). After that, the solution was purged with nitrogen gas in order to remove the reactive gases such as oxygen, and 10 mL of copper(II)-tris[(1-benzyl-1H-1,2,3-triazol-4-yl)methyl]amine complex solution (1.0 mM in 55% aqueous DMSO) and 10.0 mL of fresh ascorbic acid solution (5 mM in water) were added to the reaction media. The reaction vessel was closed, and the system maintained for 24 h with shaking (200 rpm, rt). Further purification was carried out using a dialysis membrane (Spectra/Por® 4, MWCO=12-14 kDa) against distilled water.

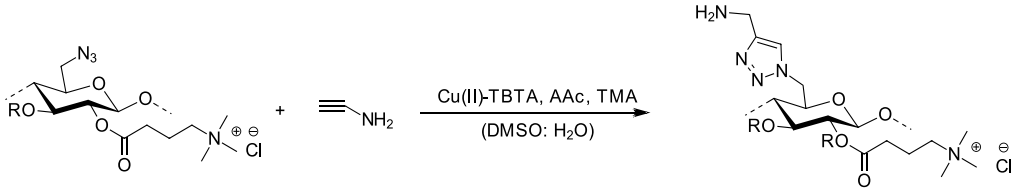

Scheme 4. Synthesis scheme for the preparation of amino-cell from (3-carboxypropyl)trimethylammonium chloride ester of 6-deoxyazidocellulose (N_3-cell$^+$) and propargylamine. Cu(II)-TBTA, Cu(II)-tris[(1-benzyl-1H-1,2,3-triazol-4-yl)methyl]amine complex solution. **AAc**, ascorbic acid. **TMA**, trimethylammonium acetate buffer. [Adapted from Vega et al.[85]]

2.4.4. Synthesis of photo-cell

The N_3-cell$^+$ was subjected to copper (I)-catalysed alkyne-azide Huisgen cycloaddition (CuAAc) with 1-ethynylpyrene (Scheme 5). Briefly, an N_3-cell$^+$ (50 mg, 212 μmol) dissolved in 50 mL of deionised water was mixed with 1-ethynylpyrene (46 mg, 203 μmol) dissolved in 90.0 mL DMSO, and 4.0 mL of triethylammonium acetate buffer (2 M in water, pH 7). After that, the solution was purged with nitrogen gas, and 4.0 mL of copper(I)-tris[(1-benzyl-1H-1,2,3-triazol-4-yl)methyl]amine complex solution (1.0 mM in 55% aqueous DMSO) together with 4.0 mL of fresh ascorbic solution (5 mM in water) were added to the reaction media. Subsequently, the stream of nitrogen was stopped, the

reaction vessel was closed, and the system was maintained for 24 h with shaking (200 rpm, rt). Further purification was carried out using a dialysis membrane (Spectra/Por® 4, MWCO=12-14 kDa) against distilled water.

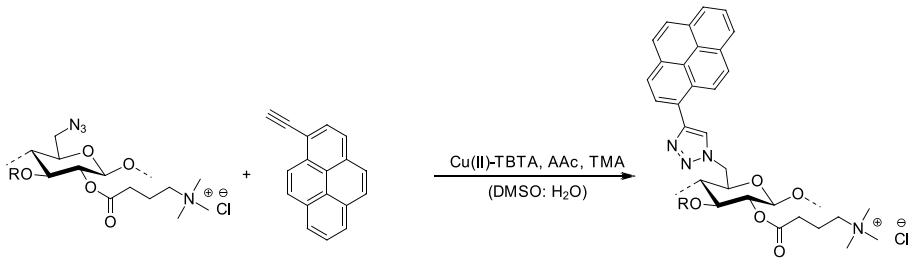

Scheme 5. Synthesis scheme for the preparation of photo-cell from (3-carboxypropyl)trimethylammonium chloride ester of 6-deoxyazidocellulose (N_3-cell$^+$) and 1-ethynylpyrene. Cu(II)-TBTA, Cu(II)-tris[(1-benzyl-1H-1,2,3-triazol-4-yl)methyl]amine complex solution. **AAc**, ascorbic acid. **TMA**, trimethylammonium acetate buffer. [Adapted from Vega et al.[85]]

2.5. **Bio-based polyelectrolyte complexes (PECs)**

Solutions of CMX^- and XS^- (0.8 mg/mL) and CN^+ (1.20 mg/mL) in 10 μM aqueous $NaHCO_3$ solution were prepared. Subsequently, the polyelectrolyte complexes [CN^+CMX^-] and [CN^+XS^-] were obtained by the one-shot addition of 80 mL solution of the corresponding negatively charged xylan derivative to 100 mL solution of the positively charged cellulose derivative. By diluting the resulting mixture to 200 mL with 10 μM aqueous $NaHCO_3$ solution, the amount of positive charges was adjusted to 0.65 mmol/l in the case of [CN^+CMX^-] and 1.23 mmol/L for [CN^+XS^-]. Thus, the ratios of the ionic groups $-N(CH_3)_3^+/COO^-$ in the case of [CN^+CMX^-] and $-N(CH_3)_3^+/SO_3^-$ in the case of [CN^+XS^-]) equalled 1.7 and 4.6, respectively.

Table 4. Characteristics of xylan derivatives used in charge-directed self-assembly experiments.

Sample	Functional groups	DS	M_{RU} (g/mol)	M_w (g/mol)	DP_w	PDI	Structure†	Paper
Xylan	$-COCH_3$	0.39	148	11×10^3	72	2.1	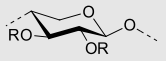	I
XS^-	$-SO_3Na$	0.16	148	16×10^3	110	1.5		I, II
CMX^-	$-CH_2COOH$	0.52	174	16×10^3	94	2.0		I, II
$XTMAB^+$	$-CO(CH_2)_3N(CH_3)_3Cl$	0.32	201	55×10^3 (#)	276	1.7		I
	$-COCH_3$	0.16						

DS, degree of substitution. $\mathbf{M_{RU}}$, molar mass of the repeating unit. $\mathbf{M_w}$, weight average molar mass. $\mathbf{DP_w}$, degree of polymerisation**. PDI,** polydispersity index. M_w, DP and PDI values were determined by size exclusion. The calculations were done with software WinGPC (Polymerstandardservice, PSS Mainz, Germany) with pullulan standards.

Xylan (M_w measured in DMSO/LiBr)

XS^-, xylan sulphate (M_w was measured in 0.1 M Na_2HPO_4/NaN_3)

CMX^-, carboxymethyl xylan (M_w was measured in 0.1 M Na_2HPO_4/NaN_3)

$XTMAB^+$, xylan-4-[*N*,*N*,*N*-trimethylammonium]butyrate chloride (M_w was measured in 0.1 M trifluoroacetic acid/ 0.05 N NaCl).

***** in aqueous solution at neutral pH

† R = H or functional group described in second column of the table

The large Mw observed in the case of $XTMAB^+$ might be attributed to the presence of aggregates

Table 5. Characteristics of cellulose derivatives used in charge-directed self-assembly experiments.

Sample	net charge*	Functional groups	DS	M_{RU} (g/mol)	M_w (g/mol)	DP_w	PDI	Structure†	Paper
CN^+	cationic	$-CO(CH_2)_3N(CH_3)_3Cl$	0.75	285	20 x 10^3	72	3.9	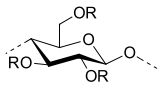	II
N_3-cell$^+$	cationic	$-N_3$ $-CO(CH_2)_3N(CH_3)_3Cl$	0.87# 0.23	222	-	-	-		III-IV

***** in aqueous solution at neutral pH
† R = H or functional group described in third column of the table
# at the C_6 position in the pyranose ring
DS, degree of substitution. $\mathbf{M_{RU}}$, molar mass of the repeating unit. $\mathbf{M_w}$, weight average molar mass. $\mathbf{DP_w}$, degree of polymerisation**. PDI,** polydispersity index. M_w, DP and PDI values were determined by size exclusion.
CN^+, (3-carboxypropyl)trimethylammonium chloride ester (M_w was measured in 0.1 M Na_2HPO_4/NaN_3).
N_3-cell$^+$, (3-carboxypropyl)trimethylammonium chloride ester of 6-deoxyazidocellulose.

2.6. **Charge-directed self-assembly of polyelectrolytes**

As illustrated in Figure 11, adsorption experiments of different polysaccharide derivatives (i.e., XS^-, CMX^-, $XTMAB^+$, CN^+, PECs or N_3-$cell^+$) on cellulose pulp were conducted in aqueous media, at rt, using the batch technique. Briefly, a set of polyelectrolyte solutions having different concentrations of the target polyelectrolyte (or PEC) in 10 µM $NaHCO_3$ solution of pH 6.8 was prepared. In each individual experiment, an equal amount of pulp was mixed and stirred in an equal volume of polyelectrolyte solution, under the same experimental conditions, over an equal period of time. Sample blanks were also prepared by adding only polyelectrolyte solution to the Schott glass bottles (without pulp), so that the adsorption of the polyelectrolyte in the glass surface is estimated. Once the reaction time has elapsed, the supernatant was recovered by filtration under vacuum and through a Whatman® Glass microfiber filter GF/A-grade. The fibres were kept at ca. +4°C until further use and the supernatant was analysed. The main parameters for each set of experiments are mentioned in Table 6.

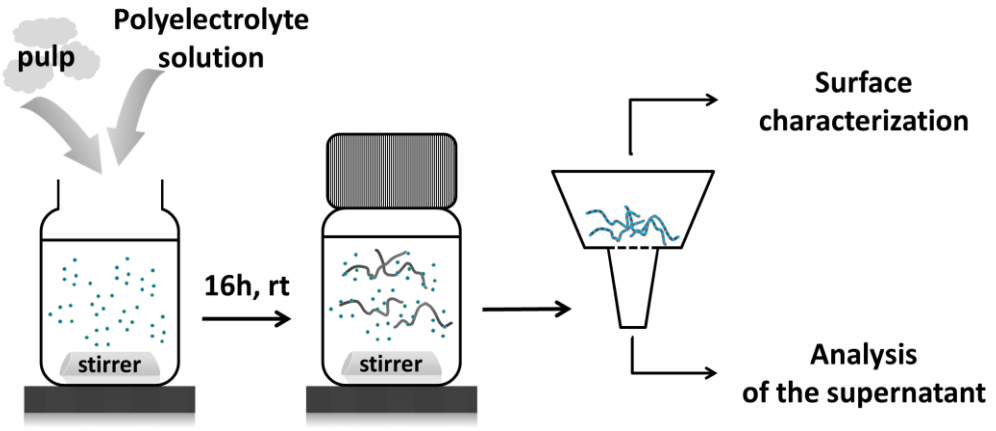

Figure 11. Schematic illustration of charge directed self-assembly of polyelectrolytes on pulp fibres.

Table 6. Polyelectrolytes and quantitative methods used in sorption experiments.

Polysaccharide derivative or PEC			Quantitative method	Paper
name	**net charge**	**Stock sol. (mmol/L) [#]**		
XS^-	anionic	0.86		
CMX^-	anionic	1.27	Titration[§]	I
$XTMAB^+$	cationic	2.39		
CN^+	cationic	1.23		
$[CN^+XS^-]$	cationic	1.23	Titration[§]	II
$[CN^+CMX^-]$	cationic	0.65		
N_3-$cell^+$	cationic	0.16	UV-vis[†1]	III

[#] maximum concentration of the polyelectrolyte solution in contact with fibres during sorption experiments, expressed as amount of net charge per litre (mmol/L)

[§] polyelectrolyte titration using polybrene and KPVS for cationic and anionic polymers, respectively

[†1] the absorbance of the solution was measured at λ= 227 nm

[*] non-quantitative method, fluorescence spectroscopy, $\lambda_{excitation}$= 351 nm, $\lambda_{emission}$= 390 nm

2.7. **CuAAc reaction**

Fibres decorated with azido functional groups (i.e., reactive fibres) were subjected to copper (I)-catalysed alkyne-azide cycloaddition (CuAAc) reaction with 1-ethynylpyrene and propargyl amine, respectively. Therefore, two different types of fibres were prepared and named photo-fibres, and amino-fibres. (Figure 12)

2.7.1. Photo-fibres

Here, 2.0 mL of triethylammonium acetate buffer (2 M in water, pH 7) was added to 5.4 mL of 1-ethynylpyrene solution (1.0 mM in DMSO). After the addition of 100 mg of reactive fibres, the system was purged with nitrogen gas in order to remove the reactive gases such as oxygen. Then, 2.0 mL of copper(II)-tris[(1-benzyl-1H-1,2,3-triazol-4-yl)methyl]amine complex solution (1.0 mM in 55% aqueous DMSO) and 2.0 mL of fresh ascorbic acid (5 mM in water) were added to the system. The stream of nitrogen was stopped, the reaction vessel was closed, and the system was maintained for 24 h with shaking (200 rpm, rt). After that, the fibres were separated from the supernatant by filtration under vacuum and

through a Whatman GF/A glass microfiber filter. Subsequently, the fibres were washed twice with 20 mL of DMSO, 2x20 mL of DMSO:water (1:1, v/v), and then with 2x50 mL of deionised water. Finally, the samples were dried between two unpolluted cellulose filter papers, and stored until further analysis. Three different reference samples were prepared by making the following modifications to the above-described procedure: **PF-B1,** with no addition of 1-ethynylpyrene; **PF-B2**, using BKPP fibres instead of reactive fibres; and **PF-B3**, using BKPP fibres instead of reactive fibres, and with no-addition of 1-ethynylpyrene to the reaction medium. In addition, 200 mg BKPP fibres and 2.0 mL of 1-ethynylpyrene solution (2.0 mM in hexane) were mixed, then rinsed 5 times with 20 mL of hexane, and dried at 40°C, overnight (**PF-B4**). All samples were protected from light before analysis.

2.7.2. Amino-fibres

Here, 40 mL of triethylammonium acetate buffer (2 M in water, pH 7) was added to 33 mL of propargylamine solution (20 mM in water). After the addition of 2.0 g of reactive fibres, the system was purged with nitrogen gas. Then, 40 mL of copper(II)-tris[(1-benzyl-1H-1,2,3-triazol-4-yl)methyl]amine and 40 mL of fresh ascorbic acid (5 mM in water) were added to the system. The stream of nitrogen was stopped, the reaction vessel closed, and the system was maintained for 24 h with shaking (200 rpm, rt). After that, the fibres were separated from the supernatant by filtration under vacuum and through Whatman GF/A glass microfiber filter, and then thoroughly washed with water. Finally, the amino-fibres were dried between two unpolluted cellulose filter papers, and stored until further use.

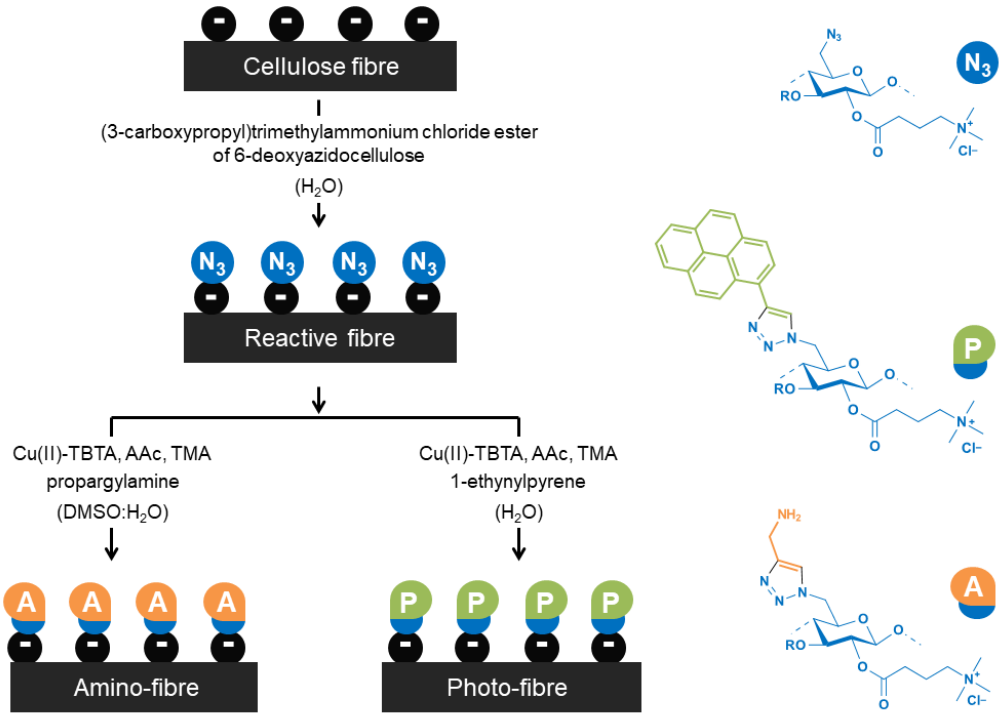

Figure 12. Illustration of the steps followed in the development of fibres decorated with amino functional groups (amino-fibres) and with photo-active moieties (photo-fibres), respectively, from cellulose fibres. **Cu(II)-TBTA**, Cu(II)-tris[(1-benzyl-1H-1,2,3-triazol-4-yl) methyl]amine complex solution. **AAc**, ascorbic acid. **TMA**, triethylammonium acetate buffer. The negative charges on the surface of fibres represent surface ionic groups. [Reproduced from Vega et al.[85]]

2.8. **Experiments using enzymes**

2.8.1. Synthesis of cross-linked glucose oxidase enzymes

A similar procedure to that described by Solomon et al.[86] was used in the preparation of cross-linked glucose oxidase enzymes (G*) from glucose oxidase enzyme (G). Briefly, 500 µL of GA solution (25% in water) was slowly added to a 5.0 mg/mL solution of G in 0.1 M PBS solution of pH 6.2, and the mixture was stirred at 200 rpm on an orbital shaker (SKF2050, Lab. Companion), at rt. After 12 h of reaction, the solution was dialyzed against 5 L of 0.1 M PBS pH 6.2 twice, and then four times against 5 L of deionised water. After dialysis, the sample was aliquoted and stored in a freezer at -20°C, until further use.

2.8.2. Bio-catalytic fibres

A 2.0 mL of 1.6 mg/mL solution S1, consisting of G* in 0.1 M PBS pH 6.2, was mixed with 100 mg of amino functional groups-containing fibres F in a 15 mL Falcon test tube (17 mm × 120 mm, propylene). After 2 h of stirring (170 rpm, rt), the supernatant S2 was removed. Then, 10 mL of the same buffer and 1.0 mL of GA (25% in water) were added to the Falcon tube. After 5 min of stirring (170 rpm, rt), the supernatant S3 was removed and the fibres were thoroughly washed with the buffer yielding the named biocatalytic fibres (Scheme 6).

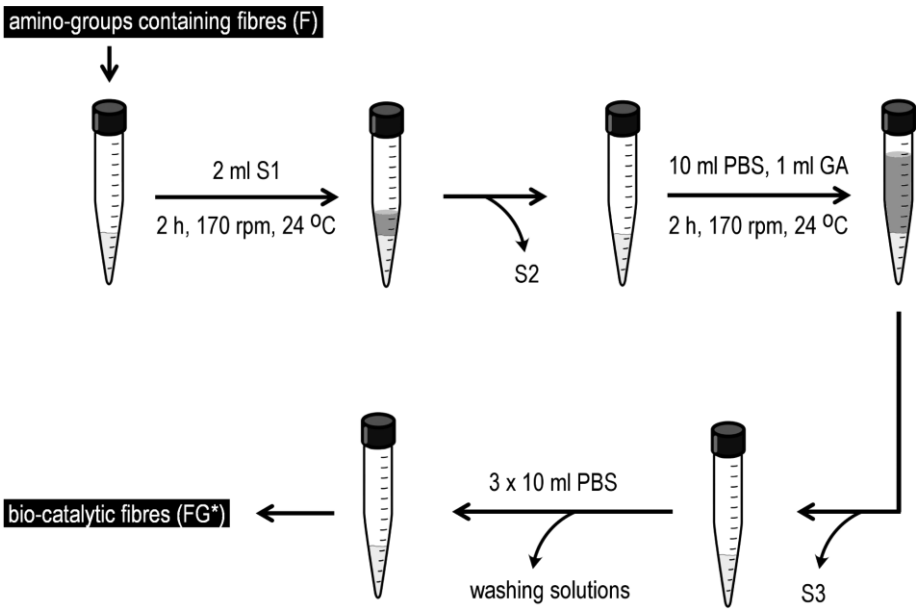

Scheme 6. Schematic illustration of the steps followed in the of bio-catalytic fibres development. [Reproduced from Vega et al.[87]]

2.8.3. Characterisation of G and G*

- *Differential scanning calorimetry (DSC).* Thermal analysis of G and G* was assessed by differential scanning calorimetry measurements performed with a TA Instruments' Q1000 Tzero DSC. The measurements were carried out using nitrogen gas as sweep fluid at a flow rate of 50 L/min. The following temperatures were used: 20°C (initial), 80°C (upper), and 0°C (lower).

- *Dynamic light scattering (DLS).* The hydrodynamic particle size and poly-dispersive index of G and G*, in 0.1 M PBS solution of pH 6.2, were

measured using dynamic light scattering (Zetasizer Nano ZS, Malvern Instruments, Malvern, UK).

- *X-ray spectroscopy (XPS).* The measurements were performed using a Physical Electronics PHI Quantum 2000 ESCA instrument equipped with Al Kα X-ray monochromatic radiation source (hν of 1486.6 eV) operated at 25.0 W, and using a take-off angle of 45° in relation to the sample surface. Additionally, a combination of electron flood gun and ion bombarding was used for charge compensation. MultiPak data reduction ULVAC-PHI, Inc. software was used for data treatment. In the case of G and G*, XPS spectra of solid samples were recorded, and at least 10 spots were analysed on each sample with a beam diameter of 100 µm with fixed analyser transmission (FAT) mode. The wide-scan was measured using 117.40 eV pass energy in 5.5 min (sampling depth up to 10 nm). The chemical state of each different element found in the sample was examined with the high-resolution spectra collected under pass energy of 46.95 eV and the following times: 10.77 min (C 1s), 5.39 min (O 1s), and 10.77 min (N 1s).

- *Attenuated total reflectance Fourier transform infrared spectroscopy (ATR-FTIR).* Attenuated total reflection sampling technique in conjunction with infrared spectroscopy was used for studying the chemical composition of the enzymes G and G*. FT-IR spectra were collected using a Thermo Scientific Nicolet iS50 FTIR spectrometer equipped with a deuterated tri glycine sulphate (DTGS) detector and a built-in Thermo Scientific Nicolet iS50 Nicolet iS50 ATR module equipped with diamond crystal. All spectra were recorded over the spectral range from 4000 to 400 cm^{-1} at room temperature (rt), with 4 cm^{-1} resolution. Sixty-four scans were recorded for each spectrum, using autogain function and an aperture of 100.

- *Determination of the enzyme activity of G and G* in solution.* For the determination of the activity of the cross-linked glucose oxidase G* in 0.1 M PBS of pH 6.2 solution, at 37 °C, a 1.7 µg/mL solution of G* in 0.1 M PBS of PH 6.2 was prepared, and the same was done in the case of G. Then, 20 µL if the diluted enzyme solution was mixed with the two components ABTS-Peroxidase substrate system (**400 µL of component A**: 0.16 M glucose and horseradish peroxidase enzyme HRP in O_2-saturated 0.1 M PBS of pH 6.2; **400 µL of component B**: 0.9 $\mu g.mL^{-1}$ of ABTS in O_2-saturated 0.1 M PBS of pH 6.2). After exactly 6 min of reaction, the reaction was stopped with 800 µL of concentrated sulfuric acid, then cooled down and the absorbance of the resulting solution at 415 nm ($\mathbf{A_{415}}$) was measured. The measurements were done by triplicate, and

each individual value A_{415} was corrected by the absorbance of the sample blank (sample without enzyme). The mean value $\mathbf{A'_{415}}$ was obtained with the individual corrected values, for each sample. The amount of hydrogen peroxide, which is generated together with D-glucono-δ-lactone during the enzymatic conversion of glucose,[88] was calculated using the calibration curve A'_{415} vs nmol of H_2O_2 in 0.1 M PBS of pH 6.2, and the two components ABTS-Peroxidase system using the same procedure described avove for the enzyme solutions with unknown activity.

2.8.4. Enzyme labelling

Enzyme labelling with Abberior STAR 635 (NHS ester) fluorescent dye was carried out in three steps as described in the Abberior protocol.[89] Briefly: *Step 1: preparation of dye solution*. A concentrated dye solution was prepared by dissolving less than 1 mg of dye in 50 µL of dry DMSO. The concentration of dye in the prepared solution was determined by indirect measurement using UV-vis spectroscopy, as described in paper IV. *Step 2: Preparation of the enzyme solution*. One milligram of solid free enzyme G (or G*) was dissolved in 50 µL of 100 mM $NaHCO_3$ buffer solution of pH 8.0-8.5. *Step 3: Enzyme labelling*. The exact volume of concentrated dye solution that is necessary for a 10-fold molar excess of dye over the free enzyme G (or 6-fold molar excess of dye over G*) was added slowly to the corresponding stirred enzyme solution. The mixture was gently stirred in the dark at rt, and after 2 h, 1 mL of 10 mM Tris buffered saline (TBS) of pH 7.4 was added to the system to stop the reaction. The unbound dye was removed, and the dye-labelled enzymes were washed three times with 1X phosphate-buffered saline solution, using 30 kDa Amicon Ultra4 centrifugal filters (Merck Millipore Ltd. Ireland) at 3000 rpm for 12 min. Thus, the dye-labelled enzymes were suspended in 100 µL of 1X phosphate-buffered saline solution, and transferred into safe-lock micro-centrifugal tubes. The solutions were named LG and LG*, in the case of free enzyme G and G*, respectively. The dye/enzyme ratio (D/E ratio) in LG (or LG*) was determined by measuring the absorbance of the solution at 635 nm (A_{635}) and 280 nm (A_{280}), after diluting 1 µL of LG (or LG*) with 1X phosphate-buffered saline solution (dilution factor 500).

2.8.5. Immobilisation of dye-labelled enzymes

Dye-labelled enzymes were immobilised on amino-functional groups containing fibres. Briefly, 2 µL of dye-labelled enzyme solution LG (or LG*) and few wet amino functional groups-containing fibres F were mixed and incubated in the

dark for 2 h. Then, 100 µL of 3-4% PFA was added to the system, and after 15 min the supernatant was removed by centrifugation at 10,000 rpm for 3 min. The resulting pellet was washed twice with 1X phosphate-buffered saline and once with Milli-Q water, with 3 min under the same centrifugal force. The fibres bearing LG or LG* enzymes were named FLG and FLG*, respectively. A set of each type of fibres was mounted on clean glass microscope slides, embedded in Mowiol mounting medium, and stored at +4°C until further measurements. A reference sample BKPP-LG* was prepared from BKPP and LG* enzymes using the same procedure.

2.9. **Characterisation of the functional fibres**

2.9.1. Analysis of entire fibres

- *Polyelectrolyte titrations.* The concentration of the polysaccharide-based polyelectrolytes in solution was measured by polyelectrolyte titrations (Papers I, II). The measurements were performed using a particle charge detector Mütek PCD 03 (Mütek Analytic GmbH, Herrsching) with a separate automatic dispenser (736GP Titrino, Metrohm). As a titrant of cationic polyelectrolytes in solution, a 0.001 N potassium poly(vinyl alcohol)sulphate solution was used, 0.0005 N polybrene solution was used as a titrant of anionic polyelectrolytes (Figure 13). The amount of polyelectrolyte that is adsorbed on the fibres was calculated indirectly from the difference in the results of the titration of the polyelectrolyte solutions before and after contact with the pulp. Each measurement was taken at least in triplicate. Sorption isotherms were prepared with the collected data after the titrations.

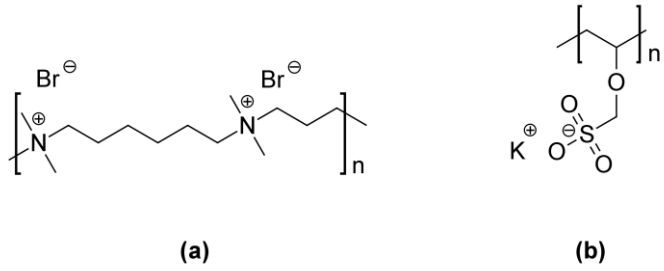

Figure 13. Chemical structures of polybrene (a) and potassium poly(vinyl alcohol) sulphate, KPVS (b).

- *Elemental analysis.* Elemental analysis of modified fibres with the cellulose derivative CN^+ (Paper II), as well as the elemental analysis of the original fibres, were performed on Vario ELIII instrument (Elementaranalysensysteme, Hanau, Germany), and the halogen content was determined by the procedure described by Schöniger.[90]

- *Inductively coupled plasma spectrometry (ICP-MS).* The copper content in the fibres after CuAAc reaction (Paper III) was determined using inductively coupled plasma mass spectrometry. For that purpose, the modified fibres were digested using microwave digestion system from Anton Paar, Multiwave 3000. The sample amount was balanced in a range of 0.1 g to which 5 cm^3 of HNO_3 65% Suprapur® have been added. The temperature in the microwave oven was up to 200°C. The analysis was performed using an ICP-MS from Perkin Elmer Sciex Elan 6100 DRC+. The instrument was calibrated with a multi-standard solution from Ultra Scientific IMS-102, using the following parameters: sweeps (11), replicates (7), dwell time (100), and Rh (10 ppb) as an internal standard solution.

- *Ultraviolet and visible (UV-Vis) spectroscopy.* The concentration of N_3-$cell^+$ in 10 µM sodium bicarbonate solution can be determined by measuring the absorbance of the solution at 227 nm, using UV-Vis spectroscopy. The amount of N_3-$cell^+$ that is adsorbed on the fibres developed in Paper III was calculated indirectly from the difference in the concentration of polyelectrolyte solution before and after contact with the pulp. Sorption isotherms were prepared with the collected data in the UV-Vis spectrophotometer. Thus, the maximum amount of N_3-$cell^+$ was estimated from the plateau of the curve.

UV-Vis spectroscopy was utilised in the quantification of amino groups in amino-fibres described in Paper III, also. The amount of amino functional groups in these fibres was determined using the acid orange 7 ("AO7") method.[91,92] For that purpose, 100 mg of amino-fibres were mixed with 20 mL of AO7 solution (0.17 mM, in water) for 14 h, at rt. Subsequently, the samples were washed thoroughly with deionised water followed by 5.0 mL of HCl solution (0.1 mM, in water). After no dye-molecules could be detected by UV–vis measurements in the washing solution, the dye-ion complexes formed were desorbed by treating the film with NaOH (1.0 M, in water). The pH of the resulting supernatant was adjusted to pH 3 with HCl solution (1.0 M, in water). Then, the concentration of

amino groups in the amino-fibres (C_{NH2}, μmol/g of fibres) was calculated according to Eq. 1:

$$C_{NH2} = [(A_{485}.V)/(\varepsilon.b.m)].(1 \times 10^6) \quad \text{(Eq. 1)}$$

where $\mathbf{A_{485}}$ is the absorbance of the pH 3–supernatant at 485 nm (arbitrary units), **ε** ($L.mol^{-1}.cm^{-1}$) is the molar absorptivity of AO7 at 485 nm, **b** is the path length (cm) of the cuvette in which the sample was contained, **V** (L) is the total volume of the supernatant with pH 3, and **m** (g) is the mass of amino-fibres. In Equation 1, the factor 10^6 was used to convert mol of amino groups per gram of amino-fibres in μmol/g.

- *Fluorescence spectroscopy.* Fluorescence emission spectra were recorded on a Perkin-Elmer LS50B fluorescence spectrometer (excitation wavelength of 351 nm, emission wavelength of 390 nm, excitation and emission slit widths of 0 nm and 10 nm, respectively). Excitation spectra were monitored at 390 nm and 488 nm for monomer and excimer spectra, respectively. (Paper III)

- *Attenuated total reflection-Fourier transform infrared spectroscopy (ATR-FTIR).* The FTIR spectra were obtained using a Thermo Scientific Nicolet iS50 FTIR spectrometer equipped with deuterated triglycine sulphate (DTGS) detector and a built in Thermo Scientific Nicolet iS50 ATR module (diamond crystal). All spectra were recorded over the spectral range from 4000 to 400 cm^{-1} at rt, with 4 cm^{-1} resolution. Sixty-four scans were collected for each spectrum, using autogain function, and an aperture of 100. (Paper IV)

- *Raman spectroscopy.* The Raman spectra were acquired in the range of 4000-400 cm^{-1} using the iS50 Raman module mounted in the Thermo Scientific Nicolet iS50 FT-IR spectrometer equipped with a 1064 nm laser-exciting radiation and provided with the InGaAs detector. The laser power was of 0.45 W. To improve the signal-to-noise ratio of the Raman spectra, the solid samples were compressed with a force of 1 tonne using a laboratory hydraulic press before the analysis. For each sample, 64,000 scans with a resolution of 8 cm^{-1} were taken. (Paper III)

- *Fluorescence imaging.* Fluorescence microscopy was used to assess the distribution of target fluorophores on the surface of pulp fibres modified with photo-active moieties. (Paper III and IV)

- *Epifluorescence microscopy*. The functional fibres were mechanically separated in aqueous suspension, and smeared to a coverslip. After being left overnight in a

dust free container, the dry fibres were imaged with an Olympus BX60 epifluorescence microscope equipped with a high-pressure mercury burner at 40× magnification. The images were acquired with mirror unit turret at "WU" position (excitation filter, 330–385 nm; dichroic mirror, 400 nm; barrier filter, >420 nm), and captured with a NiKonDS-Fi2 digital camera using 200 ms as exposure time. (Paper III)

- *Two-photon microscopy.* The photo-fibres developed in Paper III were mechanically separated in aqueous suspension and smeared onto a coverslip. In order to provide an optimal refractive index, the fibres were embedded into Mowiol mounting medium after drying in a dust free container overnight. Then, fibres were imaged with Leica TCSSP5 STED/MP Laser scanning microscope (Leica Microsystems GmbH, Germany) with Spectra-Physics Mai Tai® Ti: Sapphire laser (Newport, Santa Clara, CA) adjusted to 780 nm for excitation at 6% power. Measurements were taken under 100x oil objective (Leica) using GaAs-hybrid detector (Leica) set to band pass of 440-510 nm. The image analysis, quantification and 3D rendering were performed with ImageJ software-standard Fiji plug in collection and 3D viewer.[93]

- *Stimulated emission depletion (STED) and confocal microscopy.* The images from fibres described in Paper IV were acquired using Leica SP5 STED microscope, also. Fluorophores in analysed samples were excited with 635 nm pulsed light and fluorescence was collected with an avalanche photo diode (APD) detector at 665-705 nm range. During STED, imaging excited sample was depleted at 760 nm. Images were collected using an oil immersion objective (N.A.1.4 100x oil, Leica) while confocal pinhole was set to 151.6 µm equal to one airy unit, with a line-scan speed of 600 Hz and line averaging of 8. Pixel-size was set according to the Nyquist sampling requirement, about 25 nm for STED, and 100 nm for confocal microscopy.

- *Enzymatic assays*. Bradford assay was used to estimate the concentration of enzyme in solution.[94] The difference between the amount of enzyme in a solution, before and after the enzyme immobilisation experiments described in Paper IV was taken as an indirect estimation of the amount of enzyme that was immobilised in a known amount of fibres.

The enzyme activity is expressed in enzyme units (U), which are defined as the amount of enzyme that produces a certain enzymatic activity. In the case of glucose oxidase, 1 U corresponds to the amount of enzyme that generates 1 µmol of H_2O_2 per minute at 37°C (1 U corresponds to 16.67 nkat).[95,96] Thus, the enzyme

activity of biocatalytic fibres (in mU/g of fibre) was measured with the glucose oxidase activity assay kit MAK097. Briefly, the measurements were performed as follows: (I) *Preparation of the standard solutions:* 150 µL of H_2O_2 standard solutions containing 0, 2, 4, 6, 8, and 10 nmol of H_2O_2 solution were prepared by diluting the 0.88 M H_2O_2 solution with glucose oxidase buffer provided in the kit. S*ample preparation*: 150 µL of glucose oxidase buffer was added to a 1.5 mL polypropylene Eppendorf containing c.a. 0.2 mg of wet biocatalytic fibres and kept at room temperature for one hour before the assay. (II) *Preparation of reaction mixture for samples and standards:* Each 50 µL of reaction mixture contained 36 µL of glucose oxidase assay buffer, 2 µL of glucose oxidase developer, 2 µL of fluorescent peroxidase substrate, and 10 µL of glucose oxidase substrate. *Preparation of reaction mixture for blank samples*: Each 50 µL of reaction mixture for the blank sample contained 46 µL of glucose oxidase assay buffer, 2 µL of glucose oxidase developer, and 2 µL of fluorescent peroxidase substrate. (III) *Standard curve*: 50 µL of reaction mixture was added to 150 µL of H_2O_2 standard solutions. (IV) *Enzymatic assay*: 50 µL of the reaction mixture described above was added to the suspension containing the wet fibres. The mixture was shaken and incubated at different time intervals (each 2 min, max. 10 min) at 37°C. Once the reaction time was completed, the suspension was removed from the incubator, and 150 µL of PBS was added. The system was quickly filtered through 0.2 µm nylon membrane (13 mm Acrodisc® syringe filter) and the enzyme activity was quantified using UV-vis spectroscopy (λ=570 nm). The final measurement of the absorbance at 570 nm (A_{570}) was obtained using a UV-vis 2600 spectrophotometer from Shimadzu.

The dependence of enzyme activity on pH and temperature is very well known and needs to be studied to select the experimental conditions which ensures the optimal performance of a system. The performance of biocatalytic fibres was studied at four different pH values (3.5, 5.5, 6.2, and 7.5), and three different temperatures (32°C, 37°C, and 52°C). The control of pH was achieved using 0.1 M sodium formate buffer pH 3.5, 0.1 M sodium acetate buffer pH 5.5, 0.1 M potassium phosphate buffer pH 6.2, or 0.1 M sodium phosphate buffer pH 7.5. About 5 mg of biocatalytic fibres FG* were mixed with 5 mL of 0.16 M glucose in the selected buffer solution, and incubated under stirring, over a period of time. After that, the samples were filtered through a 0.2 µm nylon membrane (13 mm Acrodisc® syringe filter). The amount of H_2O_2 in solution that is produced during the incubation time was measured with the two components ABTS-HRP system, similarly to the method described for the determination of enzyme activity of G

and G* in solution. Two parallel samples were incubated for each condition of pH and T, and the amount of hydrogen peroxide produced in each sample was determined by triplicate. The average of individual values was calculated for each case.

2.9.2. Analysis of fibre surfaces

- *X-ray photoelectron spectroscopy (XPS).* X-ray photoelectron spectroscopy was a powerful tool used in the characterisation of fibres developed in the context of the present thesis (papers I-IV). In all samples, the elemental survey scanning (low resolution XPS spectra) was performed with the pass energy of 187 eV in 3 minutes, as an overview of the sample composition. Table 7 shows experimental settings used in the different measurements (more details were provided above in the section describing the experiments conducted for the characterisation of G and G*).

Table 7. X-ray photoelectron spectroscopy (XPS) experimental settings.

			LR-spectra		***HR-spectra***			
Angle* (°)	**Sample area**	**Energy#** (W)	**PE** (eV)	**time** (min)	**Element 1s level**	**PE** (eV)	**time** (min)	**Paper**
70	1[a]	200	93.6	20	-	-	-	I[c]
45	100[b]	25	93.6	19	-	-	-	II
45	200[b]	48	117.4	5.5	N 1s	46.95	8.08	III

* take-off-angle in relation to the sample surface

Energy applied to the X-ray source.

a, area (mm^2). **b**, diameter (μm). **LR,** low resolution spectra used to analysing the surface atomic composition (%). **HR**, high resolution spectra subjected to curve fitting to analysing the chemical states distribution of each element that is mentioned in the column "element 1s level". **PE,** Pass energy. **c**, measurements performed with a Physical Electronics PHI 5500 ESCA instrument, instead of a Physical Electronics PHI Quantum 2000 ESCA instrument.

- *Time-of-flight secondary ion mass spectrometry (ToF-SIMS).* In the work described in this thesis, secondary ion mass spectra were collected using a physical electronics ToF-SIMS TRIFT II spectrometer. A primary ion beam of $^{69}Ga^+$ liquid metal ion source (LIMS) at 15 kV was applied, either in positive or

negative modes. The distribution of the different polysaccharide derivatives on the fibre surfaces was analysed with the best spatial resolution using the ion gun operating at 25 kV. Secondary positive ions were detected with a TRIFT time-of-flight analyser, a multi-channel plate (MCP) and a time-to-digital converter (TDC). Peak intensities were measured as the Poisson-corrected area of the peak, normalised to the total counts. Positive mass spectra were calibrated by using the m/z values of the following reference ions: CH_3^+ (m/z=15.023), $C_2H_3^+$ (m/z=27.023) and $C_3H_5^+$ (m/z=41.039). Further information regarding each experimental setting used in the measurements is shown in Table 8.

Table 8. Description of ToF-SIMS measurements.

Paper	Raster size (μm^2)	Time (min)	Comments
I	200x200	8	BKPP and fibres treated with XTMAB were studied. The samples with xylan and XTMAB were prepared as follows: a solution of polymer (0.8 mg/mL in deionised water) was dropped on a MN 640w filter paper (Macherey-Nagel GmbH and Co. KG, Düren, Germany) and air-dried, avoiding any type of contamination.
II	200x200	8	BKPP, and fibres treated with $[CN^+CMX^-]$, $[CN^+XS^-]$ or CN^+, respectively, were studied. In addition, a sample with CN^+ was prepared by dropping a solution of the polymer on an ash-free filter paper and air-dried, in the same way as described in paper I
III	100x100	5	BKPP, reactive fibres, and photo-fibres were studied. Thin films of photo-cell were prepared by drying aqueous solution of the polymer on top of clean glass surfaces and the measurements were performed with an acquisition time of 300 s, at a TDC time resolution of 138 ps.

ToF-SIMS, Time-of-flight secondary ion spectrometry.

- *Field emission scanning electron microscopy (FE-SEM).* The samples studied with FE-SEM (Paper III-IV) were sputtered with carbon in a Tamcarb TB500 sputter carbon equipped with a rotating base. SEM images of magnification orders of 500×, 1000× and 2500× were obtained in an FE-SEM LEO 1530 Gemini. The dimensions of selected elements from the acquired FE-SEM images were assigned with ImageJ software.[97]

3. Results and discussion

3.1. **Paper I. Studies on the fibre surfaces modified with xylan polyelectrolytes**

3.1.1. Composition of the modified fibres

Charge-directed self-assembly of xylan derivatives (i.e. $XTMAB^+$, XS^-, CMX^-) onto bleached kraft pine pulp (BKPP) was studied by conducting a set of adsorption experiments in aqueous media at rt (equilibrium time, 16 h; amount of pulp in each individual experiment, 100 mg; polyelectrolyte concentration, 0 to 2.55 mM; volume of polyelectrolyte solution, 20 mL). Polyelectrolyte titration offered the possibility to measure the concentration of the target polyelectrolyte in solution. Thus, the amount of polyelectrolyte that is adsorbed onto the surface of a known amount of BKPP was estimated indirectly from the difference in concentration of polyelectrolyte in the supernatant (i.e., the concentration of the solution before and after its contact with pulp). The amount of xylan derivative that is adsorbed onto the glass vessels used in the sorption experiments was estimated in the same way by using a sample blank (without pulp), and the obtained value was taken into the account in the foregoing calculation. In this way, an adsorption isotherm was prepared with the collected results from a set of adsorption experiments. Figure 14 shows the sorption isotherm plot, representing the amount of $XTMAB^+$ that is adsorbed onto BKPP fibres (μmol/g) versus the amount of $XTMAB^+$ that remains in solution under equilibrium conditions, at room temperature (mmol/L). Langmuir's adsorption model was used to describe the adsorption process. The model is based on the following assumptions: (a) the molecules only bind to specific sites on the solid surface, (b) there are no interactions between the adsorbed molecules, (c) all the adsorption sites have equal energy, and (d) only a monolayer is formed at the maximum adsorption plateau. According to Langmuir's model fitting, the maximum adsorption capacity of BKPP fibres was ca. 73 μmol of $XTMAB^+$ per gram of BKPP (sorption isotherm plateau). In agreement with this value, the XPS results also showed that the sample contained ca. 73 μmol of surface anionic groups SAGs (sampling depth for XPS analysis is less than 10 nm). Although it would be necessary to conduct additional studies to explain the mechanism of adsorption, the consistency between the SAG values and the maximum amount of $XTMAB^+$

that is adsorbed onto BKPP fibres evidenced the strong contribution of electrostatic interactions in the self-assembly of $XTMAB^+$ onto the pulp fibre surfaces.

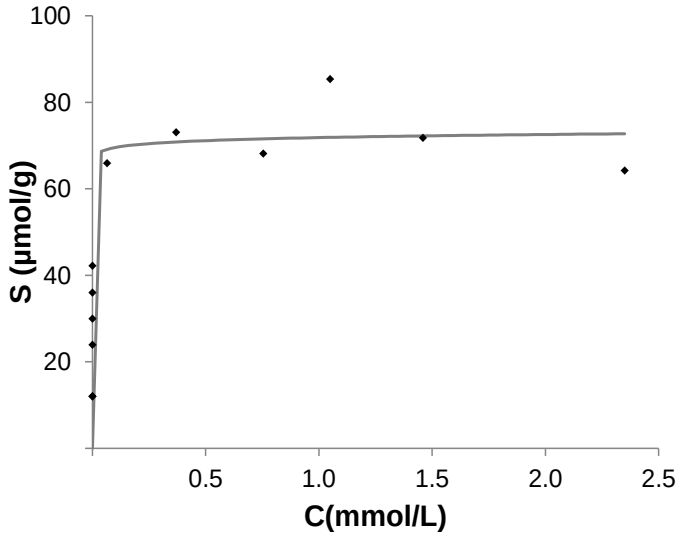

Figure 14. Sorption isotherm of xylan-4-[*N,N,N*-trimethylammonium]butyrate chloride ($XTMAB^+$) onto bleached kraft pine pulp (BKPP) obtained from polyelectrolyte titrations. **S**, amount of adsorbed charge (µmol/g). **C**, equilibrium concentration of $XTMAB^+$ in the supernatant solution (mmol/L). Trend line (grey colour) was built up with Origin 7.5® using Langmuir EXT2 non-linear extrapolation model fitting.

As expected, the amount of anionic xylan derivatives (i.e., CMX^- and XS^-) adsorbed onto the fibre surfaces was not significant as no difference was observed between the concentration of the polyelectrolyte solution before and after its contact with pulp. An alternative route for the adsorption of anionic polyelectrolytes onto the cellulose surfaces was tested and the results will be discussed later in this thesis (Section 3.2).

3.1.2. Distribution of the polyelectrolytes onto the fibres surfaces

ToF-SIMS spectrometry provided valuable information about the novel xylan polyelectrolyte $XTMAB^+$. Two intense signals originating from the fragmentation of $XTMAB^+$ into characteristic secondary ions were identified in the corresponding ToF-SIMS spectrum. Thus, the peaks with m/z values of 58 and

146 assigned to $[H_2C=N^+(CH_3)_2]$ and $[HOOC(CH_2)_3N^+(CH_3)_3]$, respectively, were selected for the subsequent analysis of fibres modified with the same polymer. ToF-SIMS spectra of the original BKPP fibres (Figure 15) and the fibres treated with $XTMAB^+$ (Figure 16) are shown below. A typical fragmentation pattern for cellulose is observed in Figure 15, whereas Figure 16 also shows the characteristic peaks with m/z=58 and m/z=146. The differences between the spectra evidence a successful modification of BKPP with $XTMAB^+$ as modifying agent. In addition, ToF-SIMS imaging helped to accurately determine the distribution of $XTMAB^+$ on the surface of treated BKPP fibres. The Figure 17a shows a ToF-SIMS image with the distribution of total secondary ions, whereas Figure 17b shows the ToF-SIMS image of selected secondary ions with m/z=58 and m/z=146. The comparison between these two ToF-SIMS images reveals the same pattern, which suggests an even distribution of $XTMAB^+$ on the sample surface.

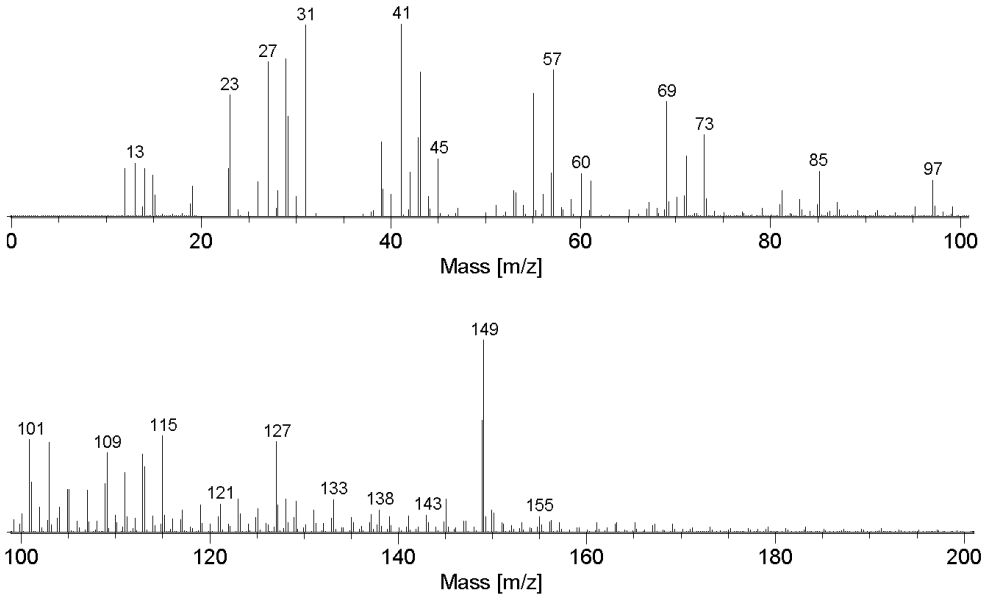

Figure 15. Time-of-flight secondary ion mass spectrum of the non-modified bleached kraft pulp pine fibres. [Reproduced from Vega et al.[98]]

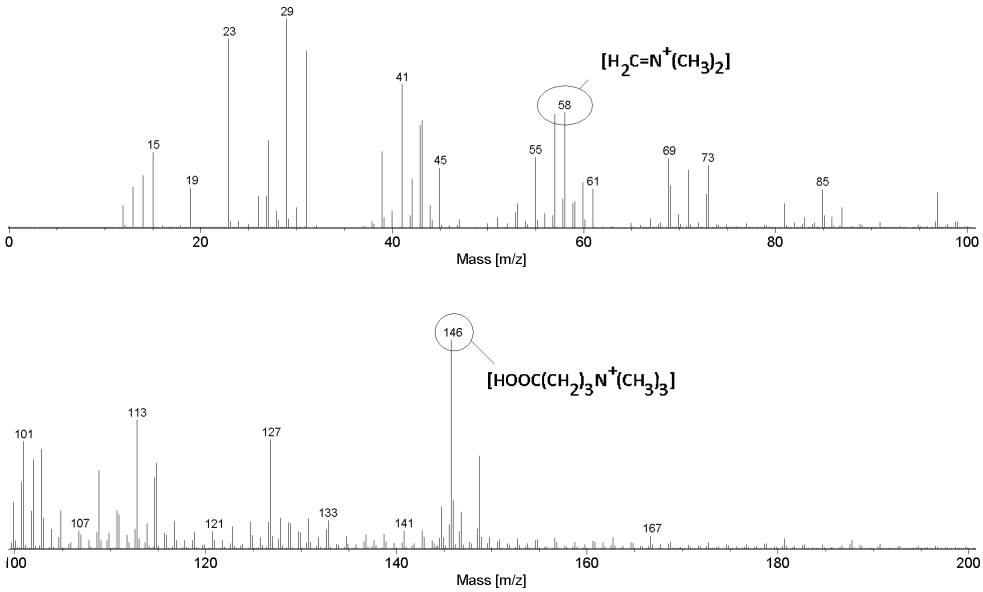

Figure 16. Time-of-flight secondary ion mass spectrum of the bleached kraft pulp pine fibres (BKPP) modified with xylan-4-[*N,N,N*-trimethylammonium]butyrate chloride (XTMAB$^+$), pointing out two characteristic peaks with m/z values of 146, and 58, respectively. [Reproduced from Vega et al.[98]]

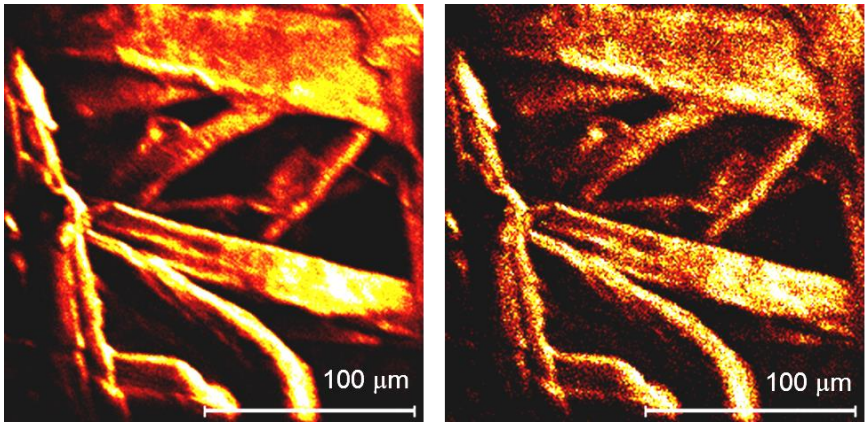

Figure 17. ToF-SIMS images of the bleached kraft pulp fibres treated with XTMAB$^+$, showing the distribution of total ions (a) and secondary ions with m/z=58 and m/z=146 (b), respectively. XTMAB$^+$, xylan-4-[*N,N,N*-trimethylammonium]butyrate chloride. From black to white, white represents the maximal number of counts for the specified m/z. [Reproduced from Vega et al.[98]]

3.2. **Paper II. Charge-directed fibre surface modification by molecular self-assembly of functional polysaccharides**

3.2.1. Characterisation of CN^+ using ToF-SIMS

ToF-SIMS measurements (spectrum not shown) from the sample that was prepared by dropping an aqueous solution of CN^+ on an ash-free filter paper and air-drying showed a strong signal from a secondary ion with m/z=58. This signal was assigned to the ion $H_2C=N^+(CH_3)_2$ arising from the fragmentation of CN^+, and it was further used as a reference peak to assess the distribution of the adsorbed $[CN^+CMX^-]$, $[CN^+XS^-]$, and CN^+ on the fibre surfaces by ToF-SIMS imaging.

3.2.2. Composition of the modified fibres

Two different types of soluble PECs were prepared by mixing of CN^+ either with carboxymethylxylan (CMX^-) or xylan sulphate (XS^-) in 10 μM $NaHCO_3$ solution of pH 6.8. The resulting PECs have a positive net charge and were applicable for the surface modification of bleached pine kraft pulp fibres by adsorption. For this purpose, equal amounts of pulp were suspended in solutions with different PEC concentrations. Similar adsorption experiments were carried out using CN^+ as a modifying agent (equilibrium time, 16 h; amount of pulp in each individual experiment, 100 mg; volume of polyelectrolyte solution, 20 mL). Polyelectrolyte titration of the modifying agent solutions -before and after their contact with pulp fibres- was carried out as an indirect measurement of the total amount of PECs or CN^+ adsorbed. Figure 18 shows the sorption isotherms obtained by plotting S (μmol/g) versus C (μmol/L), where S is the amount of net charge adsorbed per gram of pulp and C is the equilibrium concentration of the net charge originating from the adsorbate. According to the isotherms obtained, the saturation of the fibres treated with $[CN^+CMX^-]$, $[CN^+XS^-]$, and with CN^+ was reached when approximately 70 μmol of positive charge per gram of pulp was adsorbed, in all cases. Based on the data collected from polyelectrolyte titration, different sorption models were tested. The Langmuir model, assuming equal binding sites, only adsorbate–adsorbent interactions, and an adsorption process limited to a monolayer, was found to best describe the obtained sorption isotherms, as in the case of fibres treated with $XTMAB^+$ (described in Section 3.2.1).

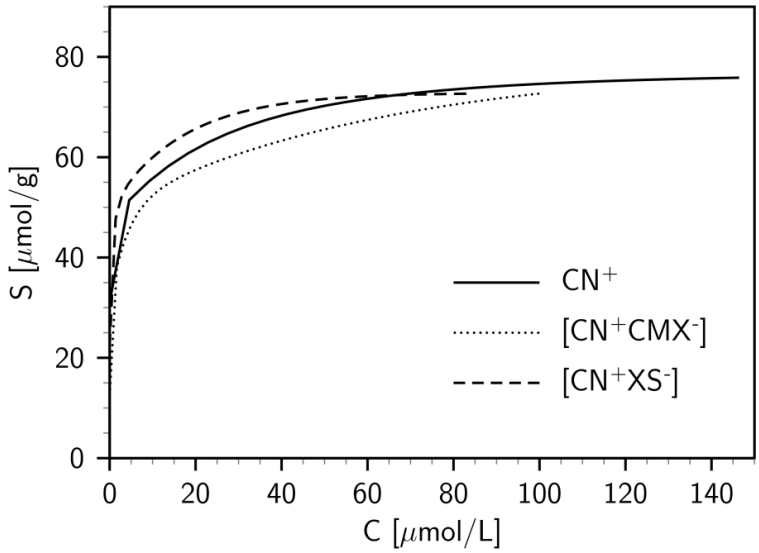

Figure 18. Sorption isotherms of polyelectrolyte onto BKPP fibres, obtained from polyelectrolyte titrations of [CN^+CMX^-] (system composed of carboxymethylxylan (CMX^-) and cellulose (3 carboxypropyl)trimethylammonium chloride ester (CN^+)), [CN^+XS^-] (system composed of xylan sulphate (XS^-)), and CN^+. **S**, amount of adsorbed charge (μmol/g). **C**, equilibrium concentration in the solution (μmol/L). [Reproduced from Vega et al.[99]]

For the three systems studied, the experimental data can be fitted well by the linear Langmuir equation (Eq. 2).

$$\frac{C}{S} = \frac{C}{n_s} + \frac{1}{K_L . n_s} \qquad \text{(Eq. 2)}$$

where n_s represents the maximum amount of adsorbed net charge (μmol/g), and K_L is the Langmuir constant (L/μmol) frequently named the intensity of adsorption.[80] The slope and y-intercept values from the linear Langmuir equation are equal to $1/n_s$ and $1/K_L.n_s$, respectively. As shown in Table 9, the n_s value estimated from the Langmuir model is like the corresponding value of saturation level that can be noticed from the sorption isotherms in Figure 18. The value of K_L can be correlated with the enthalpy of adsorption ΔH by Eq. 3:

$$K_L = K_L^0 . e^{-\Delta H/RT} \quad \text{(Eq. 3)}$$

Where $K_L°$ is a constant, R is the universal gas constant, and T is the absolute temperature. At least two different K_L values obtained at different temperature would be needed to calculate the exact value of the enthalpy of adsorption. However, in the present case, it did not seem reasonable to compare the adsorption isotherms obtained at different temperatures and the parameters of the linear Langmuir equation thereof, since the morphology of pulp fibres is strongly influenced by temperature.[1] Thus, it might be difficult to distinguish between the temperature effects on K_L and the changes of fibre morphology (e.g., the area suitable for adsorption) on the adsorption process. Nevertheless, a qualitative comparison of the adsorption is possible, since the higher the K_L value, the stronger the interaction between the adsorbate and the surface is. In the case of the fibres treated with [CN^+CMX^-], [CN^+XS^-], and CN^+ the obtained K_L values indicate an enhanced interaction when polyelectrolyte complexes were used.

Table 9. Parameters of the linearized Langmuir equations fitted from the data obtained from polyelectrolyte titration.[a]

	Linearized Langmuir equation $C/S = C/n_s + 1/(K_L.n_s)$			***Estimated values***	
Modifying agent	**slope**	***y*-intercept**	R^2	n_s **[µmol/g]**	K_L **[L/µmol]**
[CN^+CMX^-]	0.0138	0.0134	0.996	72.5	1.030
[CN^+XS^-]	0.0136	0.0185	0.999	73.5	0.735
CN^+	0.0142	0.0882	0.977	70.4	0.160

[a] **S**, amount of charge adsorbed per gram of pulp. **C**, equilibrium concentration of the adsorbate. n_s, the maximum amount of adsorbed charge (µmol/g). K_L, Langmuir constant (L/µmol). **[CN^+CMX^-]**, system composed of carboxymethylxylan (CMX^-) and cellulose (3-carboxypropyl) trimethylammonium chloride ester (CN^+). **[CN^+XS^-]**, system composed of xylan sulphate (XS^-) and CN^+.

The results from direct measurements of the C, H, N, S and O content in fibres by elemental analysis are summarised in Table 10 (the S content is not shown in the table, since it was below the limit of detection of the device in all cases). It can be noticed that the fibres treated with CN^+ contained 46 µmol of nitrogen per gram of modified pulp. This value corresponds to 46 µmol/g of adsorbed charge in the saturation level since all nitrogen arises from the cationic substituents of CN^+ and

there is no charge compensation as in the PECs. The fibres treated with [CN^+CMX^-] and [CN^+XS^-] contain 95 µmol and 57 µmol of total nitrogen per g of modified pulp, respectively.

Table 10. Elemental composition (in % w/w) of the modified bleached kraft pine pulp fibres treated with different modifying agents, and bulk nitrogen content (B_N) in µmol/g.[a]

Modifying agent	% (w/w)				B_N
	O	C	H	N	[µmol/g][b]
[CN^+CMX^-]	47.6 (0.9)	41.5 (1.8)	6.00(0.26)	0.132(0.007)	95(5)
[CN^+XS^-]	48.7 (0.3)	43.0 (0.1)	6.24(0.02)	0.080(0.005)	57(4)
CN^+	47.4 (1.0)	41.3 (0.4)	6.06(0.05)	0.065(0.003)	46(2)
none	47.8 (0.5)	40.6 (1.3)	5.96(0.21)	0.015(0.002)	10(2)

[a] **[CN^+CMX^-]**, modifying agent composed of carboxymethylxylan (CMX^-) and cellulose (3-carboxypropyl) trimethylammonium chloride ester (CN^+). **[CN^+XS^-]**, modifying agent composed of xylan sulphate (XS^-) and CN^+. **None**, no modifying agent was applied to this sample. [b] Calculated as B_N = (N%/100)(10^6/14), were the factors 10^6 and 14 were used to convert grams of N per gram of modified pulp into micromoles of N per gram of modified pulp. Standard deviation of each result is showed in parentheses.

If the polyelectrolyte complexes stay intact during the adsorption, the ratio of the ionic groups ($N(CH_3)_3^+/COO^-$ or $N(CH_3)_3^+/SO_3^-$) in [CN^+CMX^-] and [CN^+ XS^-] that were adjusted to 1.7 and 4.6 should stay constant as well. Considering these values, the amount of adsorbed charge should be 40.8% and 78.2% of the total nitrogen. This corresponds to approximately 39 µmol and 44 µmol of adsorbed charge per gram of modified pulp in the saturation level. On the one hand, it can be noticed that the values of adsorbed charge calculated on the basis of elemental analysis are almost equal for CN^+ and both PECs, considering the experimental error. This is in agreement with the findings of polyelectrolyte titration, as all three modifying agents have a similar saturation level in terms of charge. On the other hand, there seems to be a significant difference between the exact numbers of the saturation values determined by polyelectrolyte titration and calculated from elemental analysis. However, this difference can be explained as follows: first, polyelectrolyte titration refers to oven dry and unmodified pulp while

elemental analysis refers air-dry and modified pulp. This basically means that the increase in the mass of the modified fibres by the modifying agents itself and some inevitable water uptake lead to an underestimation of the nitrogen content by elemental analysis and thus to lower values of adsorbed charge. Second, polyelectrolyte titration may lead to a slight overestimation of the real values since the removal of some amount of non-bounded modifying agents during the washing of the samples could not be considered due to the limit of detection of the method.

Figure 19 shows the direct comparison of the ToF-SIMS spectra of the untreated fibres and fibres treated with [CN^+CMX^-], [CN^+XS^-], and CN^+, respectively. It can be noticed that an intense signal from the secondary ion with m/z = 58 appears in the spectra of the treated samples but not in the spectrum of the unmodified pulp fibres. As described above, this ion arises exclusively from the fragmentation of the (3-carboxypropyl)trimethylammonium chloride ester moieties of CN^+ (fragment $H_2C=N^+(CH_3)_2$). Therefore, this signal proves that the modification of the fibre surfaces by [CN^+CMX^-], [CN^+XS^-], and CN^+ took place. Moreover, the ratio of the counts for the peak with m/z = 58 and the total ion counts allow a semi-quantitative estimation of the amounts of CN^+. As can be seen from Table 11, the ratio of m/z = 58 to total ions increases in the order CN^+ < [CN^+XS^-] < [CN^+CMX^-] and is zero in case of the unmodified fibres. The percentage increase of this ratio is roughly the same as that for of the values of the total nitrogen content in µmol/g determined by elemental analysis and thus supports the conclusions drawn before.

In addition to the information from the spectra, ToF-SIMS imaging provided information about the surface distribution of the modifying agents.[77,100] The mapping of the total secondary ions (a,c,e) yields qualitatively the same pattern as the mapping of the characteristic ion with m/z = 58 (b,d,f), which show a homogeneous distribution of the polyelectrolytes on the surface of the fibres (Figure 20).

For an additional analysis of the chemical composition of the surface of the cellulosic fibres, XPS was applied. The oxygen, carbon, nitrogen, and sulphur atomic percentages are summarised in Table 11, as previously mentioned. The results confirm the presence of sulphur at the surface of the [CN^+XS^-] treated fibres. Moreover, it can be noticed that the values found for the atomic percentages of nitrogen are in the same order as the values obtained from analysing the bulk.

Table 11. Results from XPS (elemental composition expressed as atomic percentage of the total amount of detected O, C, N, and S, and surface nitrogen content (*S_N*) expressed in µmol/g) and results from Time-of-flight secondary ion mass spectrometry, obtained from the analysis of the different fibres.[a]

Modifying agent	XPS					ToF-SIMS
	Atomic %					
	O	C	N	S	*S_N* [µmol/g]	ratio[†]
[CN^+CMX^-]	39.1(0.2)	60.3(0.2)	0.6(0.1)	n.d.	467(43)	0.19(0.02)
[CN^+XS^-]	41.5(0.5)	58.0(0.5)	0.4(0.1)	0.20(0)	269(85)	0.13(0.01)
CN^+	43.3(0.3)	56.6(0.4)	<0.1(0.1)	n.d.	24(42)	0.08(0.02)
none	43.8(0.6)	56.2(0.6)	n.d.	n.d.	n.d.	0.00(0.00)

[a] **[CN^+CMX^-]**, modifying agent composed of carboxymethylxylan (CMX^-) and cellulose (3-carboxypropyl) trimethylammonium chloride ester (CN^+). **[CN^+XS^-]**, modifying agent composed of xylan sulphate (XS^-) and CN^+. **None**, no modifying agent was applied to this sample. [†]ratio between peak with m/z =58 and total counts. Standard deviation of each result is showed in parentheses

The fact that the exact numbers of the surface nitrogen (S_N, calculated from the N atomic percentage) are much higher than in elemental analysis can be explained by the conformation and size of the PECs as well as by the low sampling depth of XPS (3–10 nm). Basically, it can be assumed that the PECs have a hydrodynamic radius higher than 3–10 nm and tend to be more rigid than CN^+. If the PECs stay intact, XPS will measure predominately the chemical composition of their surface. In the case of CN^+ modified fibres, the polymer and up to 10 cellulose layers of fibres might be measured.

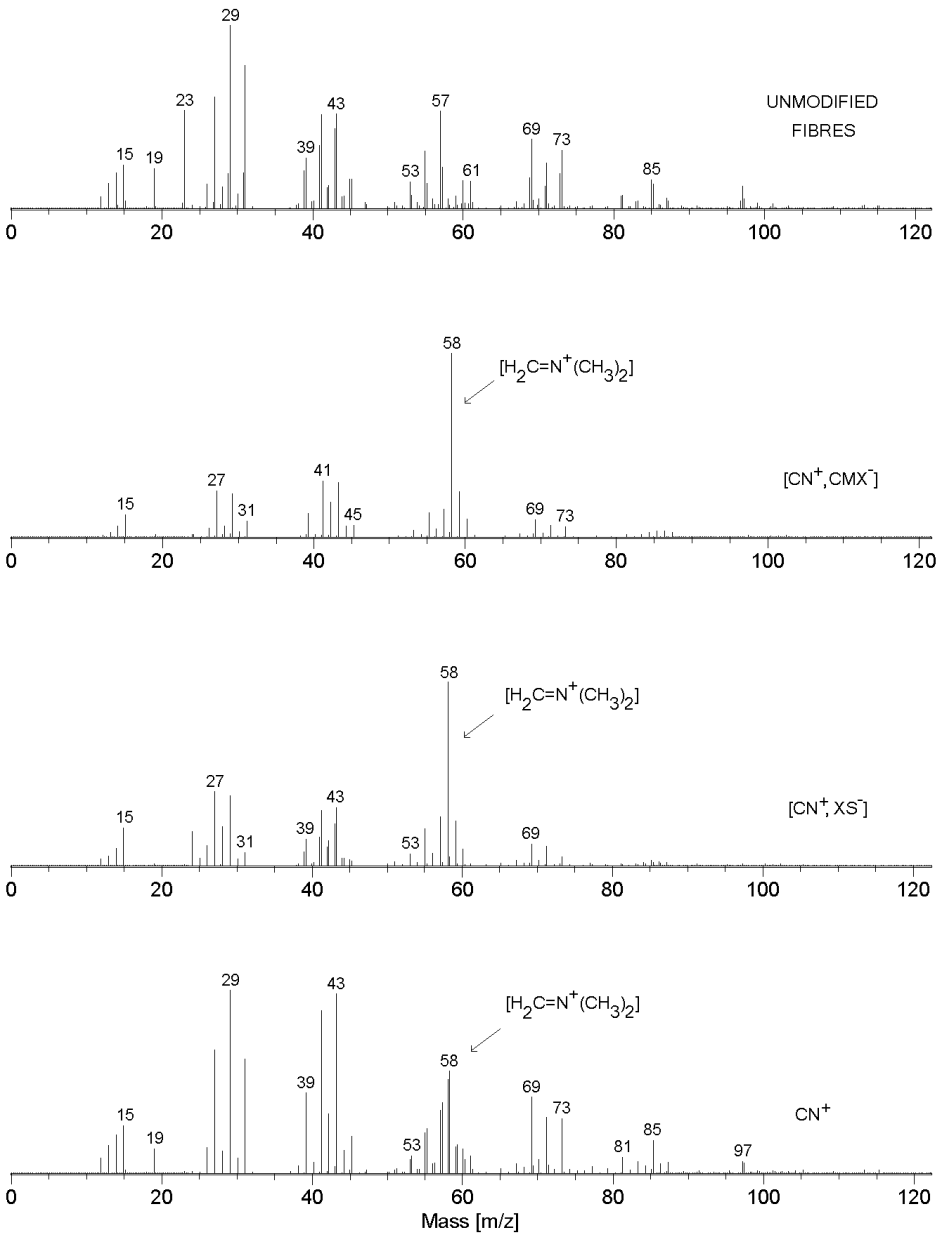

Figure 19. Time-of-flight secondary ion mass spectra of the unmodified pulp, and pulps modified with [CN^+CMX^-] (system composed of carboxymethylxylan (CMX^-) and cellulose (3-carboxypropyl)trimethylammonium chloride ester (CN^+)), [CN^+XS^-] (system composed of xylan sulphate (XS^-), and CN^+. The peak with m/z=58 is assigned to [$H_2C=N^+(CH_3)_2$] [Reproduced from Vega et al.[99]]

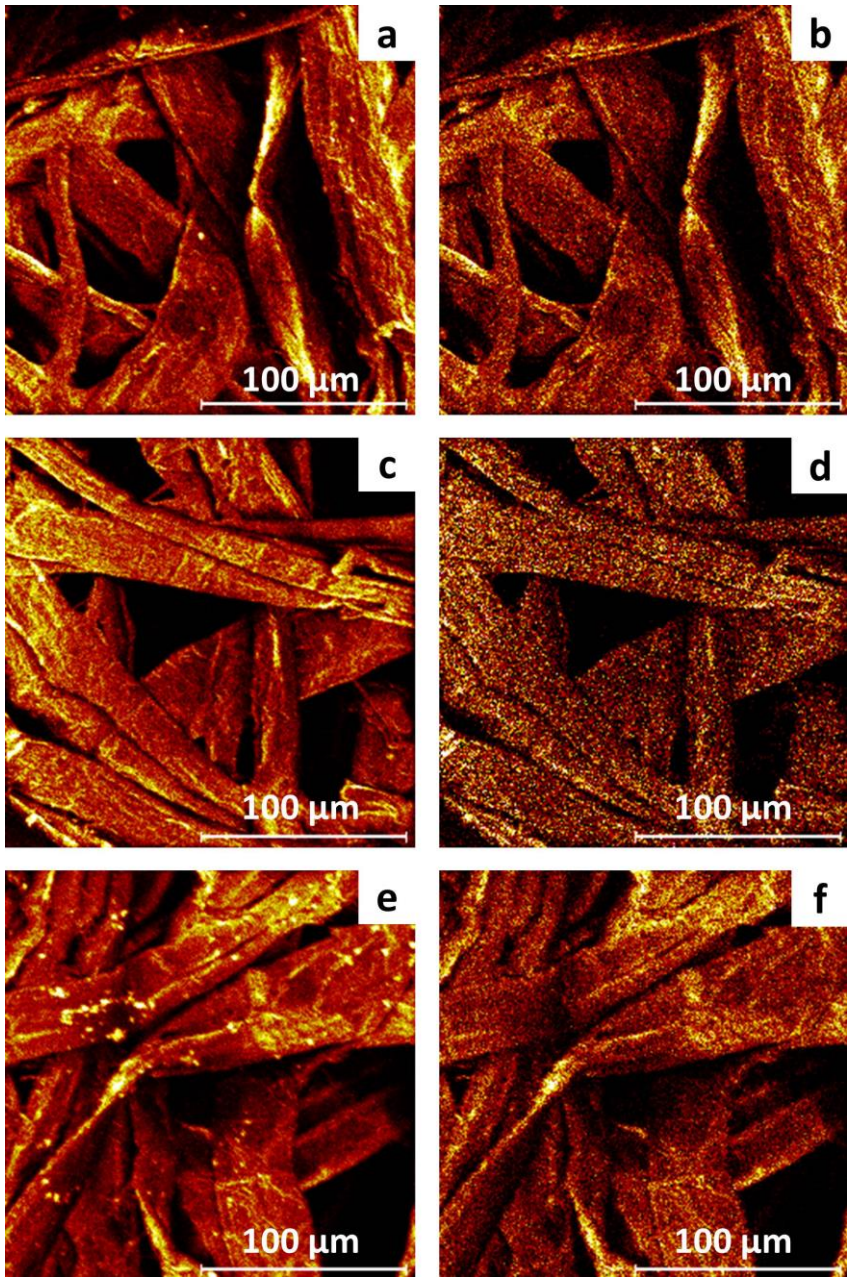

Figure 20. Time-of-flight secondary ion mass spectrometry (ToF-SIMS) images in positive mode of total secondary ions for a transverse section of bleached kraft pulp treated with the polyelectrolyte complexes [CN^+CMX^-], [CN^+XS^-], and CN^+ (**a, c**, and **e**, respectively), and the characteristic secondary ion with signal at m/z = 58 for the corresponding samples (**b**, **d**, and **f**, respectively). [CN^+CMX^-], system composed of cellulose (3-carboxypropyl)-trimethylammonium chloride ester (CN^+) and carboxymethylxylan (CMX^-); [CN^+XS^-], system composed of CN^+ and xylan sulphate (XS^-). [Reproduced from Vega et al.[99]]

It is worth mentioning that similar studies using bleached kraft eucalyptus pulp (BKEP) were conducted using the same group of polyelectrolytes described in paper III (Supporting publications, Vega et al.[101]). According to the results of these studies, the values corresponding to the maximum amount of the polyelectrolytes adsorbed on the surface of BKEP are about 1.5 times larger than the values observed for BKPP (Figure 21). As it is well reported in the literature, the surface anionic groups in BKEPs are also larger than in BKPPs. The concordance with these observations contribute to the evidences of the importance of the electrostatic interactions "adsorbate-adsorbent" on the adsorption of the polyelectrolytes at issue on the kraft pulp fibres.

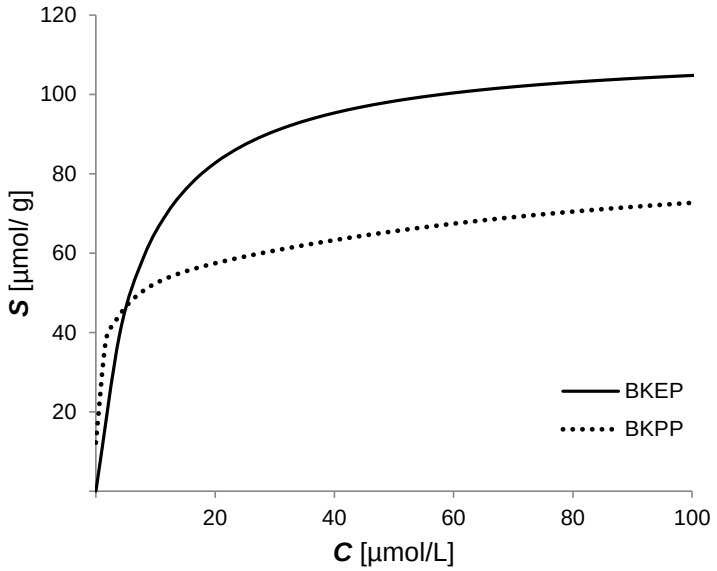

Figure 21. Sorption isotherms of [CN^+CMX^-] onto pulp fibres, obtained from polyelectrolyte titrations of [CN^+CMX^-] (system composed of carboxymethylxylan (CMX^-) and cellulose (3-carboxypropyl) trimethylammonium chloride ester (CN^+)). **S**, amount of adsorbed charge [µmol/L]. **BKEP**, bleached kraft eucalyptus pulp. **BKPP**, bleached kraft pine pulp.

3.3. **Paper III. Preparation of reactive fibre interfaces using multifunctional cellulose derivative**

3.3.1. Chemical composition of the reactive fibres

A multi-functional cellulose derivative (3-carboxypropyl)trimethylammonium chloride ester of 6-deoxyazidocellulose (N_3-cell$^+$) was synthesised and characterised as described in Paper III. N_3-cell$^+$ with molar mass of the repeating unit (MRU) of 221.58 g/mol, degree of substitution of the quaternary ammonium functional groups (DS_{N+}) of 0.23, and degree of substitution of azido functional groups (DS_{N3}) of 0.87, was used as a fibre modifying agent for bleached kraft pine pulp (BKPP). Briefly, a stock solution of N_3-cell$^+$ (150 mg/L, 0.68 mM) in 10 µM aqueous $NaHCO_3$ of pH 6.8 was prepared. According to DS values, 1 L of the stock solution contained 0.59 mmol of azido functional groups and 0.16 mmol of cationic functional groups. Then, sorption experiments were conducted using BKPP and N_3-cell$^+$ diluted solutions, which were prepared by dilution of the stock solution in 10 µM aqueous $NaHCO_3$ with pH of 6.8. In each individual experiment, the same volume of polymer solution was mixed with a known amount of pulp, and stirred with a magnetic stirring bar at rt (equilibrium time, 16 h; amount of pulp, 100 mg; volume of polyelectrolyte solution, 20 mL; concentration of polyelectrolyte solution, 0 to 0.68 mM).

The concentration of N_3-cell$^+$ in the supernatant was assessed using UV-Vis spectroscopy (absorption maximum at λ = 227 nm, $\varepsilon = 5.37\times10^3$ Lmol^{-1}cm^{-1}). Thus, the amount of N_3-cell$^+$ that is adsorbed on BKPP (S, in µmol/g) was estimated from the difference in concentration of the polymer before and after the solution took contact with pulp. The amount of polymer that was adsorbed on the glass vessel during the sorption experiments was estimated with a sample blank and considered in the foregoing calculation. Figure 22 shows the sorption isotherm obtained by plotting the amount of adsorbed cationic charge per gram of pulp at equilibrium conditions (S) versus the equilibrium concentration of the N_3-cell$^+$ (C).

The sorption isotherm shown in Figure 22 indicates that the saturation of the BKPP fibres treated with N_3-cell$^+$ was reached when approximately 43 µmol of the quaternary ammonium groups was adsorbed in each gram of pulp. Considering the ratio DS_{N+}:DS_{azido} (0.23:0.87), 43 µmol of the cationic groups corresponds to approximately 163 µmol of azido functional groups in the same polymer chain. As described earlier in Section 3.1,[98] the BKPP fibres contain approximately 73 µmol of surface anionic groups (SAGs) per gram of pulp. The

difference between the maximum number of cationic groups adsorbed on the fibres and the SAG value indicates that the negative charge on the surface of the fibres was not entirely neutralised by the cationic charge of the N_3-cell$^+$. Apparently, the nucleophilic character of the terminal nitrogen of the azido functional group plays a significant role in the adsorption process.[102]

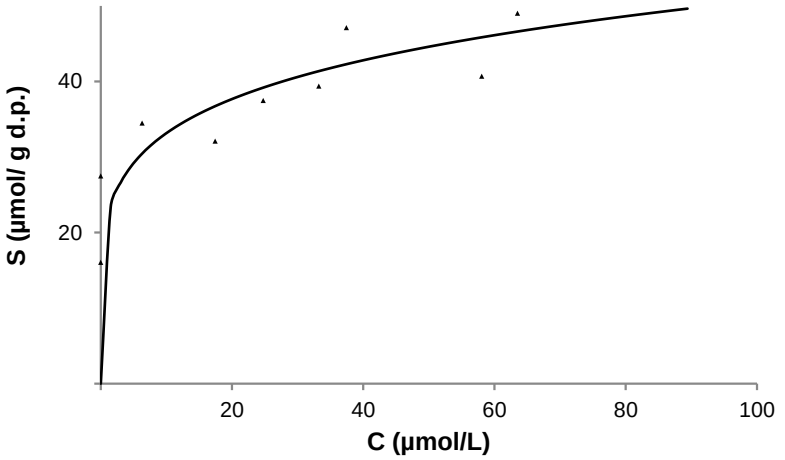

Figure 22. Sorption isotherm of N_3-cell$^+$ on BKPP fibres obtained from UV–Vis absorption radiation measurements. **S**, amount of adsorbed (3-carboxypropyl)trimethylammonium chloride ester of 6-deoxyazidocellulose (N_3-cell$^+$) on basis of positive charge per unit weight of solid at equilibrium [µmol/g]. **C**, equilibrium concentration of N_3-cell$^+$ remaining in aqueous solution [µmol/L]. [Reproduced from Vega et al.[85]]

3.3.2. Chemical composition of the photo-fibres

Reactive fibres with a maximum amount of 163 µmol of azido functional groups per gram of pulp –a value estimated from the sorption isotherm shown in Figure 22– were subjected to CuAAc reaction with 1-ethynylpyrene. As described in the experimental section, the reaction was conducted in the absence of oxygen under heterogeneous conditions for 16 h, at rt. Tris-[(1-benzyl-1H-1,2,3-triazol-4-yl)methyl]amine (TBTA) was used as a chelating agent for copper sulphate. In parallel, three sample blanks were prepared by introducing the following variations on the original protocol briefly described above: **PF-B1**, with no addition of 1-ethynylpyrene, **PF-B2**, using BKPP fibres instead of reactive fibres, and **PF-B3**, using BKPP fibres instead of reactive fibres, but with no addition of 1-

ethynylpyrene to the reaction medium. The UV-Vis spectra shown in Figure 23, which were recorded in the wavelength range of 250-450 nm, highlight the differences in light absorption between photo-fibres and the sample blanks. At the same time, it is evident that the control samples and BKPP fibres showed similar spectra in the same wavelength range. Despite the poor resolution of the spectra shown in Figure 23, it is clear the increment of the relative absorption of photo-fibres in the wavelength range of 300-400 nm. This range is the same range where light absorption of chromophore groups from 1-ethynylpyrene in solution have been reported.[103] Therefore, the results plotted in Figure 23 support the hypothesis that pyrene moieties were successfully incorporated onto the photo-fibres. In addition, the fluorescence emission spectrum of photo-fibres also showed a broad emission peak, with a maximum intensity at approximately 470 nm. In contrast, no emission was detected at this wavelength in the case of control samples (Figure 24). The observed peak at 470 nm might be attributed to the fluorescence emission of the pyrene excited-state dimers (shortly, excimers), which are formed when the intermolecular distance between pyrene moieties is shorter than 1 nm.[104]

The formation of pyrene excimers can take place either at a high concentration of pyrene in solution, or by controlling the arrangement of the pyrene fluorophores belonging to the same molecule.[105,106] Thus, in the case of photo-fibres, the formation of pyrene excimers might take place not only because of high concentration, but due to the proximity between nearby pyrene residues on the polymeric chain , after CuAAc reaction (discussed more in detail in Paper III).

The distribution of the fluorophores on photo-fibres was studied using two-photon microscopy (TPM) and epi-fluorescence microscopy. Figure 25 shows a section (XY plane) of the scanned XYZ-volume of photo-fibres obtained with TPM, and the 3D rendering of a cross-section of an individual fibre at the position marked “ROI2” on the left figure. The images clearly show a dense and uniform distribution on fluorophore groups in the fibres, as well as the preserved 3D shape during the activation and labelling processes (a video showing a set of section images of the same group of fibres is available online as the supplemental information in Paper III). Figure 26 shows the 2D images obtained with the epi-fluorescence microscope at 10× and 40× magnifications. These images show that fluorophores are evenly distributed on the photo-fibres. In the same conditions, none of the blank samples showed significant fluorescence in TPM or using an epi-fluorescence microscope (images not shown).

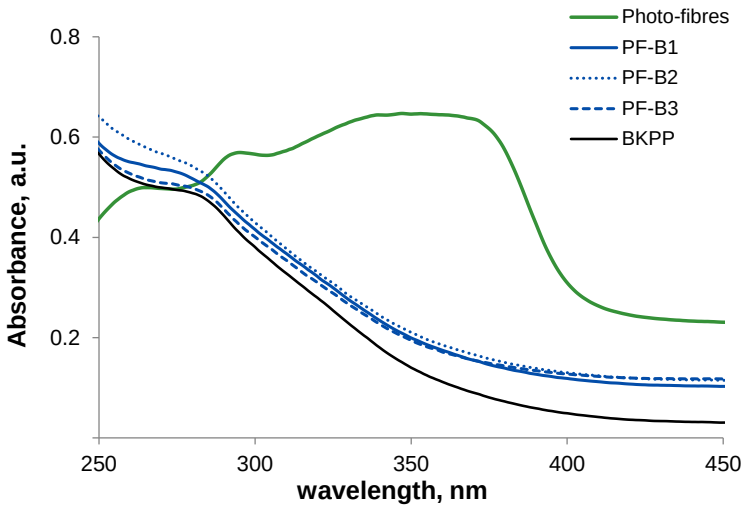

Figure 23. UV–Vis absorption radiation spectra of Photo-fibres, BKPP and bland samples PF-B_x. **BKPP,** bleached kraft pine pulp. **PF-B_x**, blank samples prepared with the following change with respect to Photo-fibres preparation protocol: **PF-B1**, no addition of 1-ethynylpyrene; **PF-B2**, BKPP instead of reactive fibres; **PF-B3**, BKPP instead of reactive fibres, and no addition of 1-ethynylpyrene. [Adapted from Vega et al.[85]]

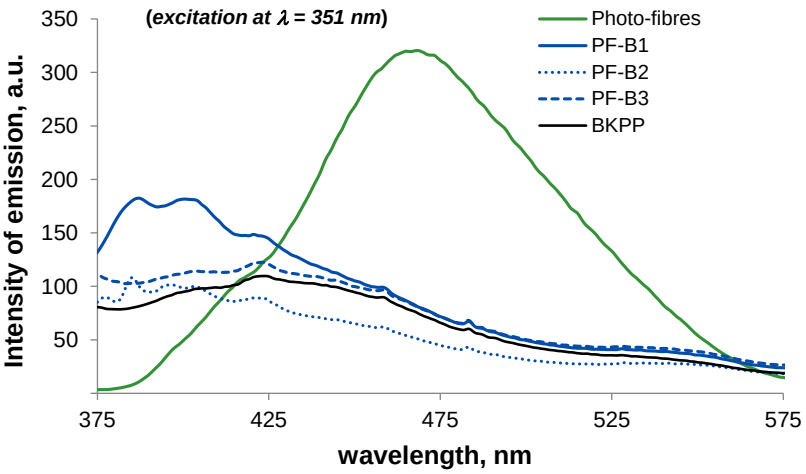

Figure 24. Fluorescence emission spectra of photo-fibres, BKPP, and blank samples PF-Bx. **BKPP**, bleached kraft pine pulp. **PF-Bx**, blank samples prepared with the following change with respect to Photo-fibres preparation protocol: **PF-B1**, no addition of 1-ethynylpyrene; **PF-B2**, BKPP instead of reactive fibres; **PF-B3**, BKPP instead of reactive fibres, and no addition of 1-ethynylpyrene. [Adapted from Vega et al.[85]]

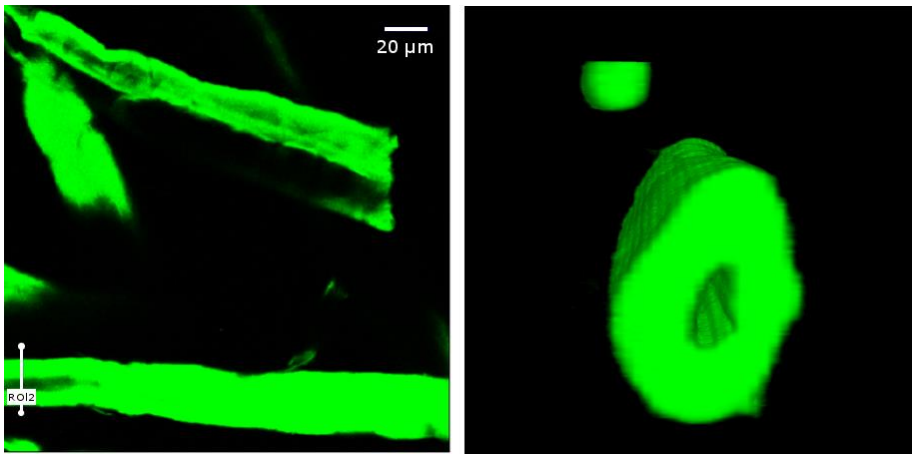

Figure 25. A section (xy-plane) of scanned xyz-volume of photo-fibres obtained with Two-photon excitation microscopy (left). A 3D-rendering of a cross-section of an individual fibre at the position marked "ROI2" on the left figure (right). The figures illustrate the dense labelling of the fibres and the preserved 3D shape during the activation and labelling. [Reproduced from Vega et al.[85]]

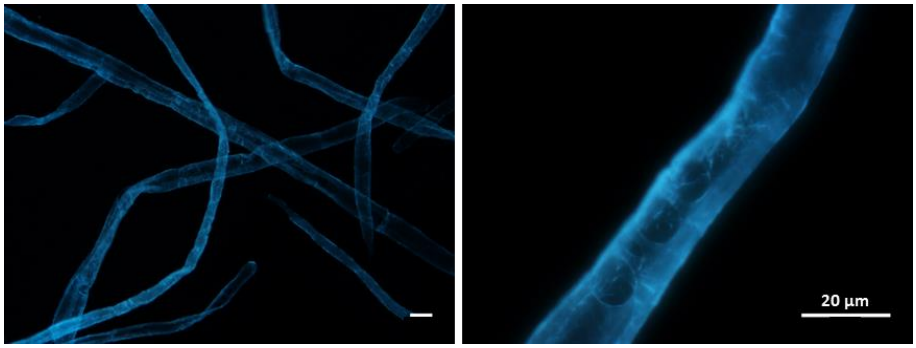

Figure 26. Image of photo-fibres observed with Olympus BX60 epi-fluorescence microscope at 10× magnification (left) and 40× magnification (right). Excitation filter, 330-385 nm; dichroic mirror, 400 nm; barrier filter, > 420 nm. [Adapted from Vega et al.[85]]

The top of Figure 27 shows the Raman spectra normalised to the intensity of 1095 cm^{-1} band from the same group of samples described before in this section. As expected, the Raman spectrum of blank samples exhibits the characteristic bands of cellulose. For example, numerous bands between 1460 and 1200 cm^{-1} originated from CH_2, C-H and O-H deformation vibration bands are observed, as well as C-O-C and C-OH str. vibrations (1120–1095 cm^{-1}), and asymmetric ring

vibration band (898 cm^{-1}). In addition to these bands, several Raman bands between 1630 and 1540 cm^{-1}, as well as in the 1230 and 1315 cm^{-1} region, are observed in the case of photo-fibres. The Raman bands in the 1640–1540 cm^{-1} region usually involve the C=C str. and/or C=N str. vibrations for aromatic compounds, whereas the band observed at 1240 cm^{-1} is attributed to aromatic in-plane C-H def. vibration for the pyrene moieties.[107,108]

The results discussed so far in Section 3.3 are the only indication that the pyrene residues were successfully incorporated onto the azido functional group-containing fibres; however, they are not sufficient proof that the CuAAc reaction took place. Additional measurements using Raman spectroscopy helped to prove that. A new sample named **PF-B4**, which was prepared by evaporating the solvent from a mixture of BKPP fibres and a solution of 1-ethynylpyrene in hexane, was analysed. The Raman spectrum of the sample PF-B4 and the spectrum of photo-fibres are compared at the bottom of Figure 27. Evidently, the spectra differ at the regions highlighted in grey. The differences between the spectra bring enough proof that the CuAAc reaction took place in the case of photo-fibres. This affirmation is based on the following observations: (i) a group of bands in the 1630–1540 cm^{-1} and 1315–1230 cm^{-1} regions are observed in the spectrum of the sample PF-B4; however, they are not distinguished in the spectrum of the hexane-washed PF-B4 sample, meaning that the pyrene residues were washed away from PF-B4. On the contrary, the pyrene residues are not washed away from photo-fibres, as the characteristic Raman peaks are also observed in the hexane-washed photo-fibres. The strong covalent bonds formed after of the CuAAc reaction would explain this observation. (ii) Although the spectra shown at the bottom of Figure 27 show bands with very similar Raman intensity in the frequency region where the vibrational bands for aromatic compounds are observed (e.g., 1627-1554 cm^{-1}), only the spectrum for PF-B4 shows one band at 2094 cm^{-1} which is usually associated with the C≡C str. vibrations for the C-C≡C-H functional groups.[107,108] The lack of that band in the spectrum of photo-fibres indicates might be justified by the absence of the alkyne groups in that sample. In the context of the present discussion, the presence of bands at 1627-1554 cm^{-1} in the absence of the band at 2095 cm^{-1} could only happen if the alkyne groups reacted chemically with functional groups from reactive fibres. Therefore, the results also support the hypothesis that the CuAAc took place. (iii) The spectrum of pure 1-ethynylpyrene (not shown) shows two bands at 1624 cm^{-1} and 1596 cm^{-1}, and two bands at 1240 cm^{-1} and 1230 cm^{-1}. The presence of these bands can be attributed to C=C str. vibration for the

aromatic ring system in the first case, and associated with aromatic in-plane C-H bending vibrations in the second case.[107,109]

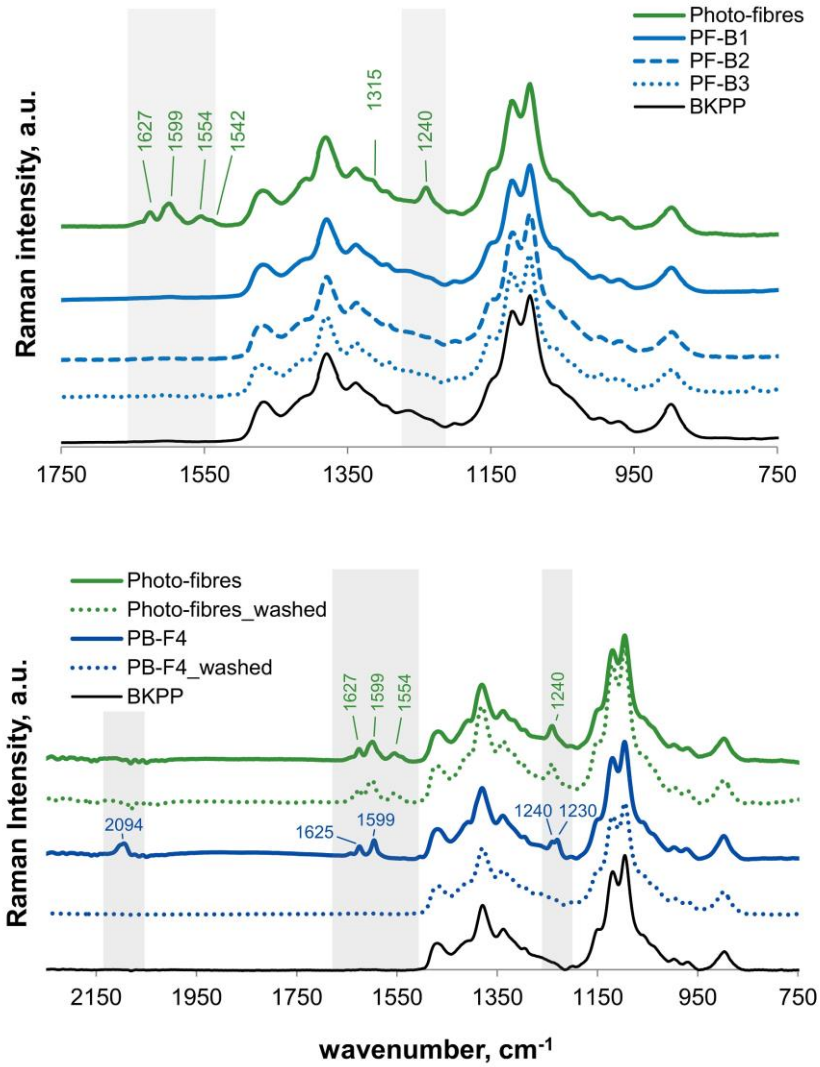

Figure 27. Raman spectra and blank samples (top) Raman spectra of photo-fibres, the original BKPP fibres, and the blank fibres PF-B4, before and after thorough washing with hexane (bottom). **BKPP**, bleached kraft pine pulp. Blank samples prepared with the following variation in the original protocol described used for the preparation of Photo-fibres: **PF-B1**, the CuAAc reaction was performed with no addition of 1-ethynylpyrene; **PF-B2**, using BKPP fibres instead of reactive fibres; **PF-B3**, using BKPP fibres instead of reactive fibres, with no addition of 1-ethynylpyrene to the reaction medium. **PF B4**, mixture of reactive fibres and 1-ethynylpyrene. [Reproduced from Vega et al.[85]]

Evidently, the spectrum of PF-B4 shows these bands. However, the spectrum from photo-fibres shows four bands at the 1624–1540 cm^{-1} region and one single band at 1240 cm^{-1}. The differences in the group frequencies again show the chemical changes after CuAAc reaction. ToF-SIMS analysis provided additional information in the same direction and the results are discussed in detail in Paper III).

3.3.3. Chemical composition of the amino-fibres

Reactive fibres with a maximum amount of 163 μmol of azido functional groups per gram of pulp –a value estimated from the sorption isotherm shown in Figure 22– were subjected to CuAAc reaction with propargyl amine under heterogeneous conditions, yielding cellulosic fibres decorated with amino functional groups (amino-fibres). The Acid Orange7 dye ("AO7") colorimetric method was used to quantify the amino functional groups from amino-fibres.[110] The method relies on the formation of ion pairs from the negatively charged sulphonate groups from AO7 with the protonated primary amino functional groups. The protonation of amino functional groups is expected to occur at pH values below 10.[111] In excess of AO7 dye, it is reasonable to assume that each amino functional group forms one ion pair with the corresponding sulphonate moiety of AO7. Therefore, the total amount of amino groups can be estimated indirectly by measuring the amount of AO7 molecules used in the formation of the ion pairs. The concentration of AO7 in solution was estimated by UV-Vis absorption spectroscopy (absorption maximum at λ = 485 nm, with ε = 1.719×10^4 $L.mol^{-1}cm^{-1}$). According to the results, the amino-fibres contained 6.4 μmol of amino functional groups per gram of fibres.

XPS spectroscopy measurements confirmed the occurrence of the CuAAc reaction between propargyl amine and the azido functional groups originating from the N_3-$cell^+$. Figure 28 shows the comparison of XPS high resolution spectra from the N_3-$cell^+$ and amino-cell (at the right) and the comparison of XPS high resolution spectra of reactive fibres and amino-fibres (at the left), in the same binding range. The polymer amino-cell, the synthesis of which is described in the experimental part (Scheme 4), and reactive fibres showed two characteristic peaks, at ca. 402 eV and 404 eV. The N1s bands with binding energy below 402 eV are commonly associated with the presence of nitrogen from triazole ring, R-NH^2, or quaternary ammonium groups.[111,112,113,114,115,116] On the other

hand, the N1s band with binding energy at 404 eV, is usually attributed to the presence of azide functions.[117,118] The absence of the peak at 404 eV in the N1s spectra of amino-fibres and amino-cell is consistent with the hypothesis that azide functions from reactive fibres and N_3-cell$^+$ were converted into triazole rings after the CuAAc reaction.

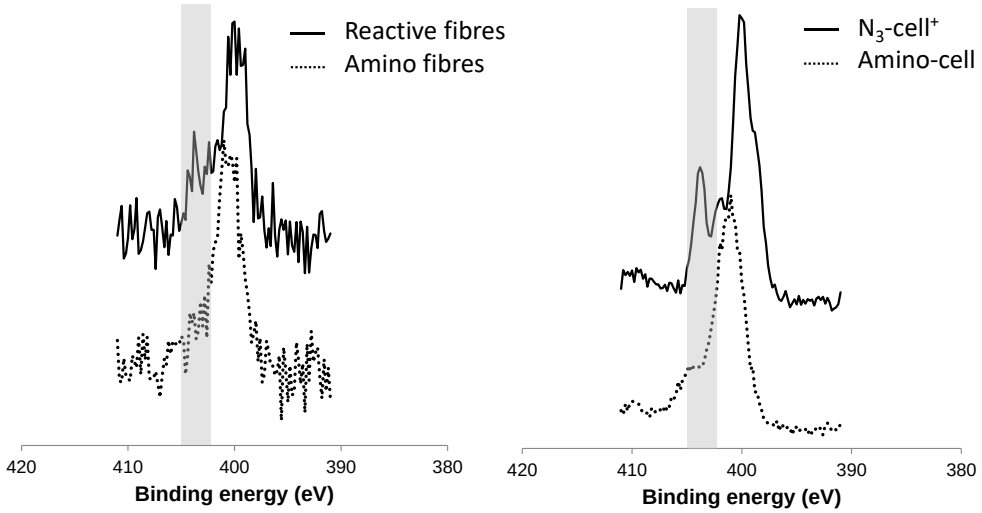

Figure 28. X-ray photoelectron high resolution spectra, showing N1s peaks from reactive fibres, amino-fibres, N_3-cell$^+$ and amino-cell. [Reproduced from Vega et al.[85]]

3.3.4. Residual copper in photo- and amino-fibres.

Triazole products obtained from CuAAc reaction are usually isolated in high yield and without the need for purification.[119] However, in the present case, the elemental analysis using ICP-MS revealed that photo-fibres contained (53.9±0.4) ppm and amino-fibres contained (436±2) ppm of the remaining copper, respectively. In contrast, the original BKPP fibres contained (0.14±0.1) ppm. As shown by the results, the catalyst was not successfully removed from the treated fibres despite the intense washing. Despite the evident copper contamination on the produced fibres, some remarkable advantages in using this catalyst can still be pointed out to justify its use. For example, the use of copper in the azide-alkyne Huisgen cycloaddition (CuAAc) avoids the use of high temperatures, which can significantly affect the mechanical properties of

the cellulosic fibres. The possibility of using mild conditions may extend the range of alkyne molecules that can be linked to the reactive fibres (e.g., heat-labile alkyne-containing molecules).[102] Additionally, the use of Cu(I) as catalyst facilitates the regiospecific 1,3-dipolar cycloaddition yielding1,4-di substituted 1,2,3-triazoles.[120,121]An additional purification step was not carried out in the present work; however, it might be necessary depending on the type of application. As reported in the literature, Cu has successfully removed the remaining copper with ion-exchange resins, or using solid-phase extraction techniques.[98,122]

3.3.5. Morphology of the functional fibres after click reaction

In addition to the studies on the chemical composition of photo-fibres, the morphology of photo-fibres was investigated using field emission scanning electron microscopy (FE-SEM). For that purpose, SEM images from BKPP fibres and photo-fibres were compared. The images shown in Figure 29 do not exhibit changes in the morphology of the fibre surfaces after treatment.

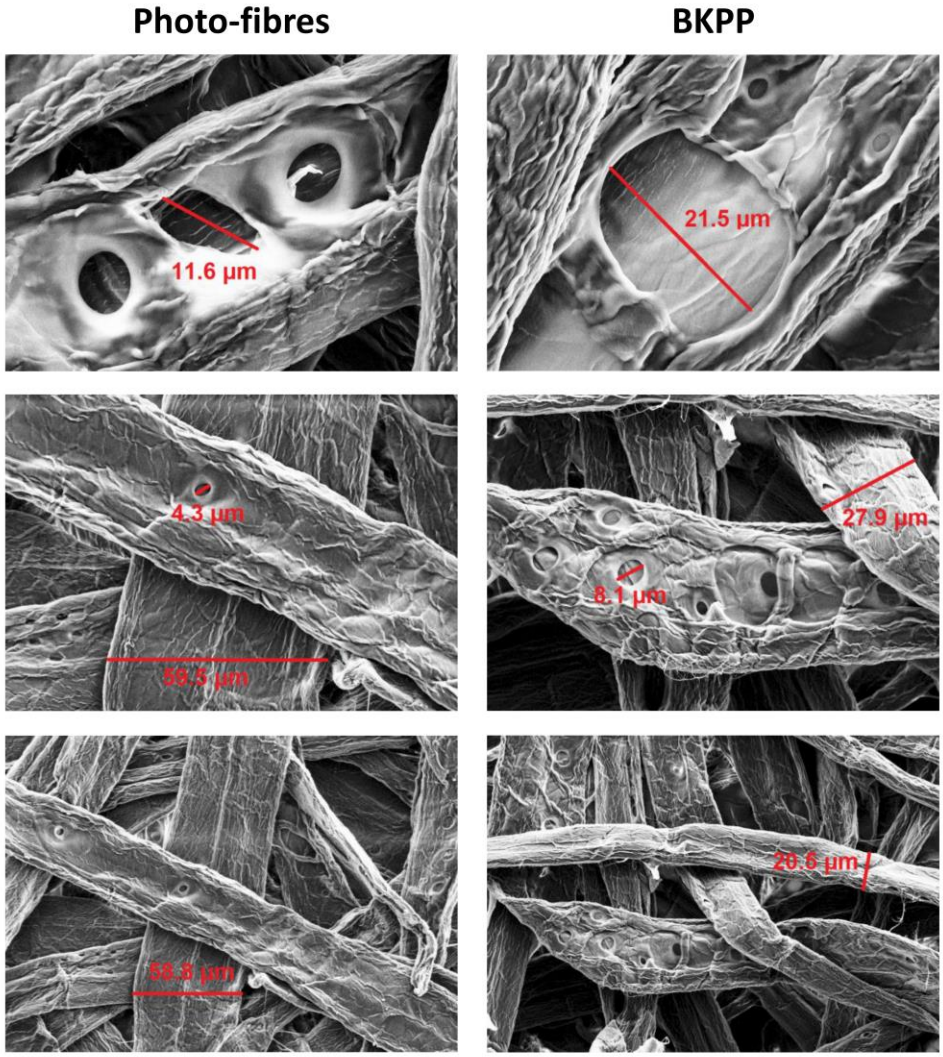

Figure 29. Field-emission-Scanning Electron Microscope (FE-SEM) pictures from photo-fibres and bleached kraft pine pulp (BKPP) shown with different orders of magnification (the dimensions of the elements showed on the pictures were assigned using ImageJ software). [Reproduced from Vega et al.[85]]

3.4. **Paper IV. Advanced Cellulose Fibres for the Efficient Immobilisation of Enzymes**

3.4.1. Characterisation of the enzymes G and G*

Differential Scanning Calorimetry (DSC) was used as a method to assess the differences between the thermodynamic properties of the commercial glucose oxidase G, and the cross-linked glucose oxidase enzyme G* obtained after the chemical reaction between G and glutaraldehyde GA. Due to the covalent bonds created after the chemical reaction between GA and G, the thermal stability of G* was changed, as shown using DSC analysis (Figure 29). The values of enthalpy (ΔH), the maximum heat capacity of the phase transition (T_{peak}), and the temperature at which the tangent in the inflection point crosses the baseline (T_{onset}) were calculated from each thermogram. As reported in the literature, the increase in ΔH value confirmed the increase in organisation and stability of the immobilised enzyme G* in comparison with the free enzyme G.[123] Another indication for the better organisation and stabilisation of the system is the decrease in peak width, which is usually calculated as the difference between T_{peak} and T_{onset}. In addition, the tailing of the endothermic peak shown in Figure 30 in the case of G* can also be considered an indication that cross-linking took place. Similar results were observed in the third cycle (not shown).

The hydrodynamic particle size or "size" of the enzymes G* (or G) in 0.1 M PBS pH 6.2 solution was measured with Zetasizer Nano ZS, at rt. The size of ca. 7.7 nm for the native glucose oxidase enzyme, which was reported by Talbert (2014) was used as a reference value.[124] According to the results shown in Table 12, the sample containing G* in PBS solution consisted of several distinct particle populations, with size of about ca. 850.9 nm (60.9 %I), 65.7 nm (9.6 %I), and 13.5 nm (29.5 %I), respectively. In contrast, the sample containing G in PBS solution seems to be predominantly composed of free enzymes with a size of ca. 8.8 nm (81.9 %I). The increase in the size of the particles occurred after the chemical reaction, suggesting that cross-linking took place. However, free enzymes are also present in the sample containing cross-linked enzymes, indicating that the cross-linking reaction was not complete or that aggregates were partially broken during sonication. It is necessary to state that, even though the results obtained with Zetasizer Nano ZS are in line with the results observed with DSC and discussed above, they should not be used as reference values, and

further studies will be needed to more precisely determine the size of G* (or G) in solution.

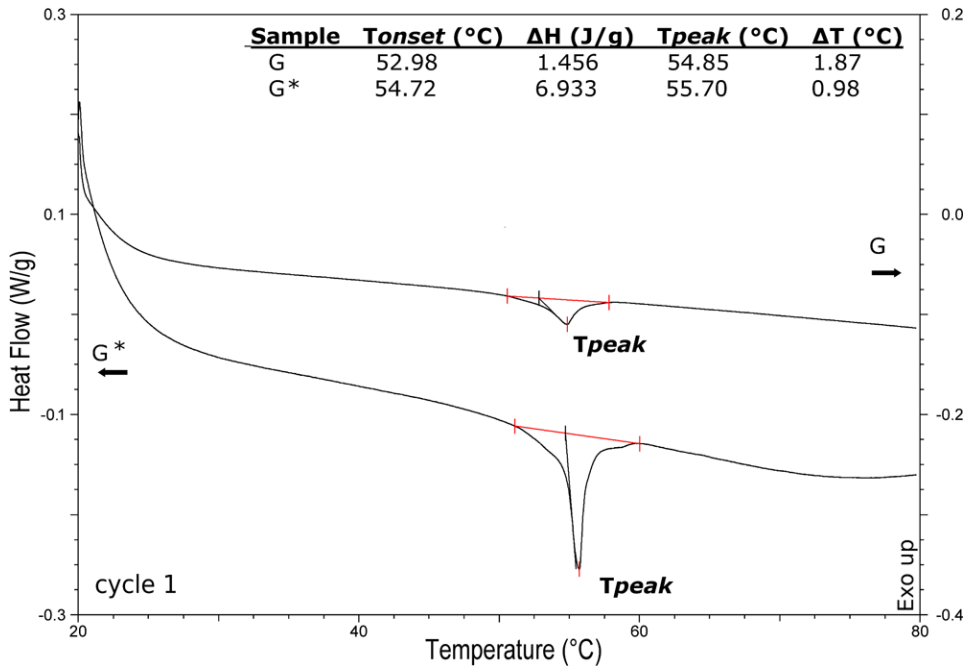

Figure 30. Differential scanning calorimetry (DSC) of the free enzyme (G) and the cross-linked enzyme (G*), showing the endothermic peaks after first heating named cycle 1. [Reproduced from Vega et al.[87]]

Table 12. Results obtained with Zetasizer Nano ZS.

	Size (S) and percentage of intensity (%I)							
	Peak 1		Peak 2		Peak 3		Av.	
sample	S (nm)	%I	S (nm)	%I	S (nm)	%I	S (nm)	PDI
G	8.8	81.9	300	15.8	5093	2.2	22.5	0.26
G*	850.9	60.9	13.5	29.5	65.7	9.6	51.1	1.00

G, commercial enzyme. **G***, immobilised enzyme. **Av.**, average. **PDI**, poly dispersity index.

The IR spectra of free glucose oxidase G and cross-linked glucose oxidase G* exhibited the expected characteristic absorption bands associated with the vibrational modes of the secondary amide groups of proteins (Figure 31).[125] The IR absorption bands observed at ca. 3300 $cm^{-1}$and ca. 3100 cm^{-1} (not shown in Figure 31) were assigned to Amide A and amide B, respectively. These characteristic bands are associated to the secondary amide N–H stretching vibrations and the secondary amide II overtone. The band at ca. 1642 cm^{-1} was assigned to amide I band, which is associated with C=O stretching coupled to C–N stretching and N–H bending vibrations. The band at ca. 1535 cm^{-1} was assigned to amide II, which is associated with N–H bending vibration coupled with C–N stretching vibrations. It is worth mentioning that the amide I and II bands observed in the spectra of proteins are the most important for analysis of the protein secondary structure, which plays a key role in enzyme activity. Particularly in the case of the amide I band, the exact wavenumber of the associated vibrations depends on the nature of hydrogen bonding involving amide groups, which is determined by the secondary structure adopted by the protein. Thus, the similarities between the amide I band of the free enzyme G and the amide I band of the immobilised enzyme G* observed in Figure 31 might evidence the similarities on the secondary structure of these enzymes. In fact, these similarities can be taken as an indication that the enzyme activity is preserved after the immobilisation.[126] The absorption band at 1300 cm^{-1} was assigned to the amide III band, which is due to C–N str., N–H bending, C=O stretching, O=C–N bending. The weak IR band in the range from 900 to 800 cm^{-1} was assigned to symmetrical C–N–C stretching vibrations. Despite the similarities between the G and G* IR spectra, some differences can be pointed out. For example, a small increase in the relative intensity of the bands at 2824 and 1465 cm^{-1} was assigned to CH_2 deformation vibration. At the same time, the bands in the range from 1342 to 1359 cm^{-1}, which was assigned to CH deformation vibrations, showed stronger absorbance in the case of G*. These absorption increments are in agreement with the hypothesis that the chemical reaction between G and GA render a compound with larger number of methylene groups as suggested by Migneault et al.[127] Unlike the spectrum of G*, the bands at 1144 cm^{-1}, 1105 cm^{-1}, 1062 cm^{-1}, 963 cm^{-1}, and 842 cm^{-1} are not observed in the spectrum of G. The intensity of these bands, which can be assigned to deformation vibrations from acetals and NH deformation vibrations, is evidently reduced after immobilisation.

At least 10 different spots from G and from G* were analysed using X-ray spectroscopy (XPS). According to the results, the atomic composition of G was uniform between the analysed spots, with carbon and oxygen being the most abundant elements (Table 13). On the contrary, the atomic composition of G* was not uniform among the different analysed spots, and the values can be pooled into two main groups referred to as G*A and G*B. In comparison with G, the group G*B showed a similar carbon atomic percentage, larger atomic percentage of oxygen, and lower atomic percentage of nitrogen. The differences between G*B and G become even more evident when the elemental ratios O/C, N/C, and O/N are compared. Thus, the group G*B shows lower N/C, and larger O/N ratios. These observations are congruent with the hypothesis that G* resulted enriched with carbon and oxygen in comparison with G, due to the chemical reaction between G and GA.[127]

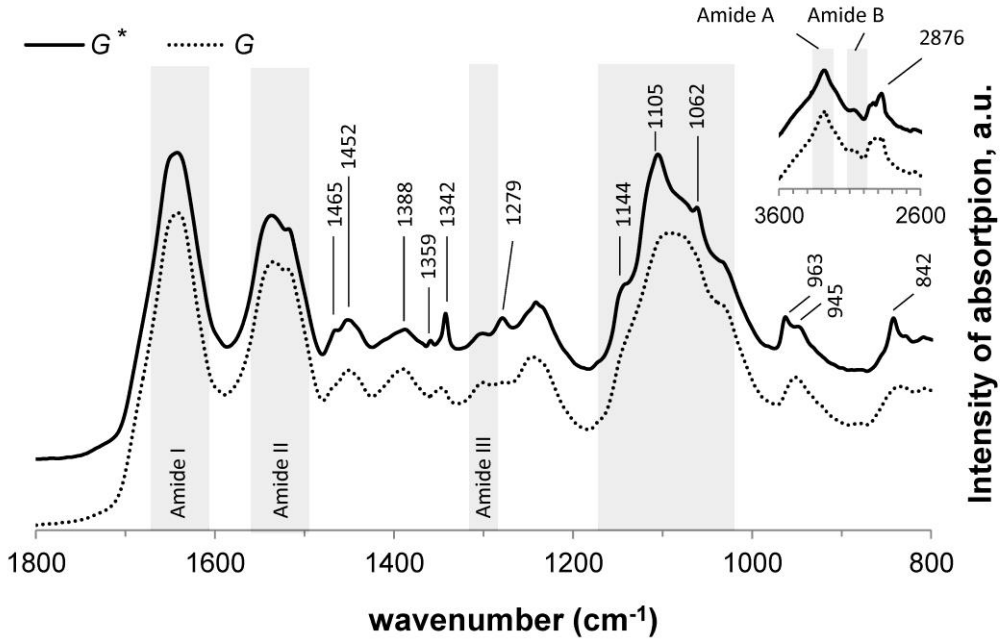

Figure 31. ATR-FTIR spectra of the glucose oxidase enzyme (G) and the cross-linked enzyme (G*). G* was obtained after reaction of G with glutaraldehyde followed by dialysis. [Reproduced from Vega et al.[87]]

Table 13. X-ray photoelectron spectroscopy (XPS) results.

#	Atomic percentage						Atomic percentage ratios					
	C (±σ)		**N** (±σ)		**O** (±σ)		**O/C** (±σ)		**N/C** (±σ)		**O/N** (±σ)	
G*A	**64.9**	*0.7*	**11**	*3*	**24**	*4*	**0.40**	*0.10*	**0.17**	*0.05*	**3**	*2*
G*B	**65.9**	*0.5*	**1.2**	*0.4*	**33**	*1*	**0.50**	*0.01*	**0.02**	*0.01*	**30**	*9*
G	**66.4**	*0.6*	**7**	*1*	**27**	*1*	**0.40**	*0.02*	**0.10**	*0.02*	**4**	*1*

#, sample. **G**, commercial enzyme. **G*A** and **G*B**, immobilised enzymes grouped in groups A and B, respectively, according to atomic percentage ratios.

Comparing the high-resolution spectra of G and G*B, the differences in chemical composition are also evident (Figure 32). Although an appropriate curve fitting of the C 1s spectra was not possible due to the complexity of the samples (i.e., multiplicity of the carbon chemical states), the C 1s spectrum of G*B shows the presence of a peak at about 287 eV, which is not present in the case of C 1s spectrum of G. On the other hand, the XPS results from G and the group G*A did not show any significant differences. The lack of uniformity in the XPS results in the case of G* opens a debate whether XPS analysis is suitable technique for the study of this sample, but there is still a clear difference between the chemical composition of G and G*. Moreover, the conclusions from XPS results and the results obtained from DSC and DLS are accordant.

The activity of G (and G*) in 0.1 M PBS pH 6.2 solution was measured at 37 °C using the two component ABTS-HRP system, and measuring the H_2O_2 that is produced over exact period of time with the help of the calibration curve (Supporting information, in Paper IV). As expected, the immobilisation leads to the loss of catalyst productivity (kg of product/kg of enzyme). Thus, the cross-linked enzymes G* in solution showed an enzyme activity of about 34% of the enzyme activity showed by the original enzymes G in solution.

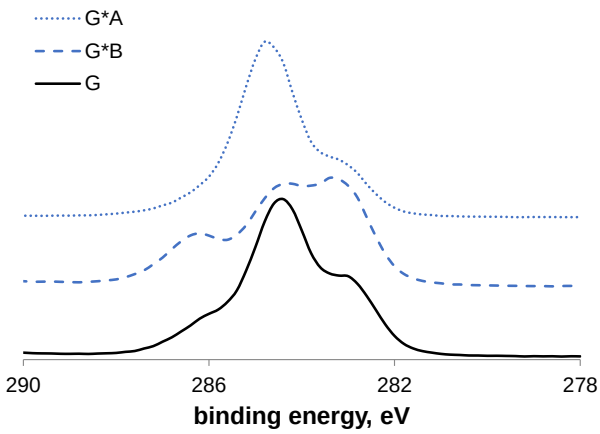

Figure 32. X-ray photoelectron spectroscopy (XPS) high-resolution C 1s spectra of the commercial glucose oxidase G, and the cross-linked enzyme G* (results from G* are grouped as G*A and G*B). [Reproduced from Vega et al.[87]]

3.4.2. Enzyme quantitation

The concentration of the enzyme in solution was plotted against the corresponding absorbance, yielding the Bradford enzyme concentration standard curve (Supporting information, in Paper IV). The enzyme standard curve was used for the determination of the enzyme concentration in unknown samples.

3.4.3. Characterisation of Fibres

- *Quantitation of the Enzyme in the Biocatalytic Fibres*. The QIE value, which represents the maximum amount of enzyme G* immobilised in the amino functional groups-containing fibres F, was calculated from Eq. 4:

$$QIE\ (mg/g) = (E_o - E_{losses}).(1/m) \qquad (Eq.\ 4)$$

According to the results, QIE value was equal to 11 $mg.g^{-1}$ (or 2.6 mg of G* per gram of wet F, dry content of 24%). No enzyme was detected in the supernatants S2 or in the washing solutions represented in Scheme 6. The amount of enzyme

G* that is bound to the Falcon tube is very small, about 1.2% of the original amount of enzyme utilised in the experiments.

- *Enzymatic Assay of Biocatalytic Fibres*. The enzyme activity was determined by a coupled enzyme array from enzyme assay kit MAK097, in which the target enzyme oxidizes D-glucose, generating H_2O_2 and D-glucono-δ-lactone. Because of the enzymatic reaction between H_2O_2 and the probe, which is catalysed by HRP provided with the kit, the formation of a colorimetric compound (λ_{max} = 570 nm) takes place. Then, the amount of H_2O_2 in glucose oxidase assay in buffer solution was plotted against the corresponding absorbance at 570 nm (A_{570}), yielding the H_2O_2 standard curve (supporting information in Paper IV). The amount of H_2O_2 (nmol) that was generated per gram of FG* was calculated from the H_2O_2 standard curve, and used for plotting the amount of H_2O_2 versus time (not shown). The glucose oxidase activity of the enzymes immobilised in the fibres F (nmol of H_2O_2 in 1min, per gram of FG*) was determined using Figure 33. According to the results and based on the definition of enzyme unit, the immobilised enzymes G* in the prepared fibres FG* showed an activity of 215 U/g of fibre (or 906 U/g of wet fibre, dry content of 24%). In other words, it was possible to convert 215 μmol of glucose into H_2O_2 per minute, per gram of dry biocatalytic fibres.

- *Effect of pH and Temperature on the Biocatalytic Fibres.* According to the results, the performance of the system FG* (expressed in terms of hydrogen peroxide per kg of fibre) was higher than in the case of FG, under all the tested conditions (Figure 34). Evidently, the enzyme cross-linking and subsequent immobilisation of the cross-linked enzymes on the cellulose fibres using glutaraldehyde is beneficial. As will be shown later in the fluorescence images, the retention of the enzyme on the solid carrier surface is very poor without the covalent bonds between fibres and enzymes. Therefore, the "dilution of activity" that is mentioned, for example in Sheldon (2007),[128] is observed, and because of that the system FG is less efficient than FG*.

Comparing the performance of the systems (FG* or FG) at the different tested conditions, the highest yield was observed at 32°C and pH of 5.5, whereas no significant enzyme activity was observed at 52°C. Surprisingly, the enzymes on FG* are very active under pH of 3.5, at 37°C. It is well-known that the stability of the enzymes is affected at high temperatures, and therefore, it is not a surprise that a drop in enzyme activity is observed at 52°C. However, further studies are needed in order to explain the observations at lower temperatures and will be important for optimising the performance of the system.

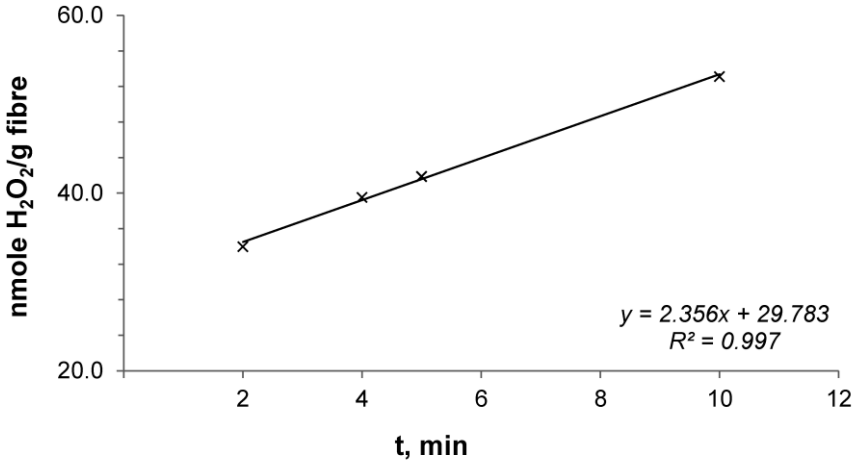

Figure 33. Enzyme activity showed by biocatalytic fibres FG*.[Reproduced from Vega et al.[87]]

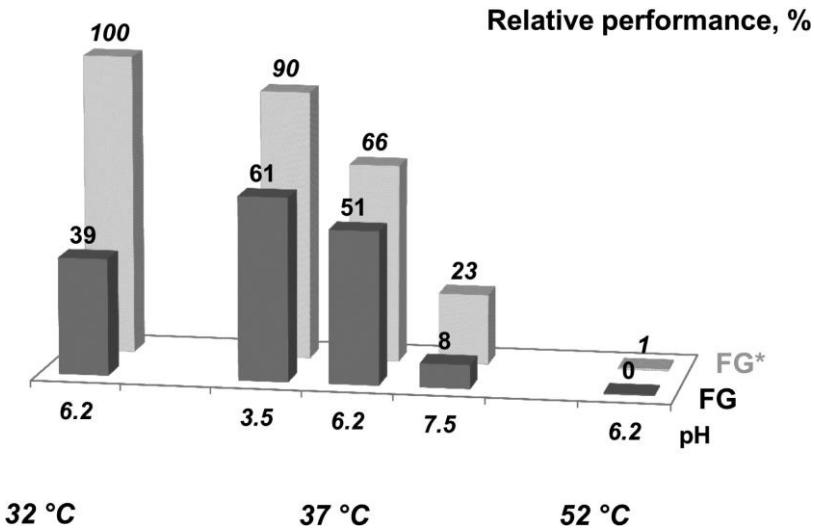

Figure 34. Relative performance of the biocatalytic fibres (in %), which is defined as the amount of hydrogen peroxide that is produced per kg of biocatalytic fibres, over the same period of time. For the comparison, the maximum value observed was considered equal to 100%. [Reproduced from Vega et al.[87]]

- *Imaging of Enzymes on Fibre Surfaces*. The cross-linked enzymes G* were labelled with the fluorescent dye Abberior STAR 635 (NHS ester), and immobilised in the amino functional groups-containing fibres F. The resulting material FLG* was studied with confocal microscopy and STED microscopy. The picture showing the orthogonal optical sections of a three-dimensional confocal image created from a z-stack of xy-scans of a fibre FLG*, revealed a dense and uniform distribution of the fluorophore groups on the surface of the fibres, but not to the interlayers of the fibres (Figure 35a). The used STED microscope has about 100 nm lateral resolution, which represents approximately a 5-fold increase of lateral resolution as compared to the used confocal microscopy (the comparison is valid in ideal case of transparent samples). Thus, the use of STED microscopy allowed an enhanced visualisation of the fluorophore groups on the surface of the treated fibres. Small fibre components with nanoscale dimensions, such as the fine cellulosic strands extending to the periphery of the pit chamber, can be more clearly distinguished on STED images in comparison with confocal images (Figure 35c and Figure 35b, respectively).

The FLG fibres, which contain dye-labelled G, were also studied using confocal- and STED microscopy (Figure 36). The STED figures and the set of pictures from confocal microscope that are compiled in a video (Supporting information, in Paper IV) permits one to distinguish the LG enzymes located only at the surface of the fibres FLG. In other words, as in the case of LG*, the LG enzymes cannot penetrate the inter layers of the cellulosic fibres even if the enzymes LG possess smaller size than the enzymes LG*. The images obtained with the confocal or STED microscope provide evidence of the large area available for the immobilisation of enzymes, and show the complex morphology of the solid carrier. Unlike FLG and FLG*, the fibres named BKPP-LG* did not show any significant fluorescence under a confocal or STED microscope (Supporting Information, in Paper IV). The remarkable difference demonstrates the benefits of amino-functionalisation of pulp fibre surface for the immobilisation of enzymes.

FE-SEM images from FG* clearly show the presence of the enzymes at the surface of the fibres (Figure 37). Evidently, the immobilised enzyme is not evenly distributed on the surface of biocatalytic fibres. Crystallisation occurs at the surface in many areas (Figure 37d), whereas smaller foreign structures are observed around the pits (Figure 37c). The heterogeneous distribution on particle size of the enzymes G* is evidenced by FE-SEM measurements in the case of the sample containing biocatalytic fibres FG*, and from the measurements

using Zetasizer Nano ZS in the case of the sample with G* in solution. However, the values for particle size obtained with these techniques are not comparable. In the case of FE-SEM results, the values are estimated from pictures obtained from solid samples under high-vacuum and after coating with carbon, whereas the hydrodynamic particle size obtained with Zetasizer Nano ZS is obtained from enzymes G* in solution.

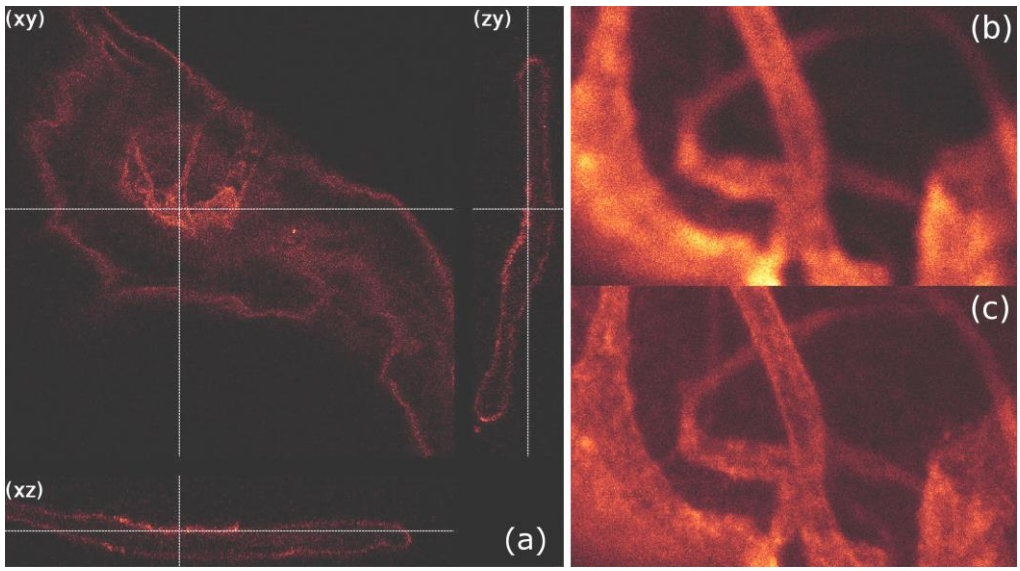

Figure 35. Orthogonal sectioning (xy, xz, and yz) from the confocal microscope pictures of a biocatalytic fibre FG* (a), confocal microscope picture with focus on the cellulosic strands of the same pit chamber exhibited in picture a (b), and the STED microscope picture of the same section than in picture b (c). The fluorescence observed in these pictures derived exclusively from the fluorophore Abberior® STAR 635 (NHS ester), which is covalently bonded to the enzymes (Dye/Enzyme ratio of 1.6). Picture dimensions: size-width and size height of 75 µm; step depth of 15.6 µm and step size of 0.25 µm (a); 10.73 µm × 6.62 µm (b,c). [Reproduced from Vega et al.[87]]

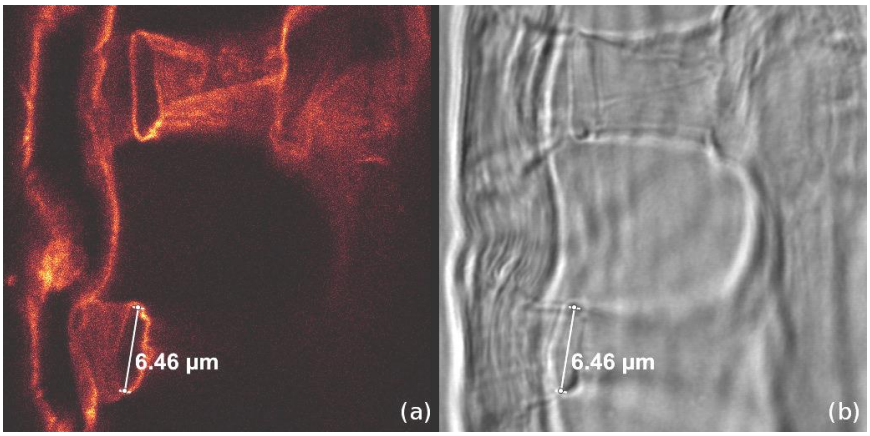

Figure 36. Stimulated emission depletion (STED) image of a biocatalytic fibre cross-section, bearing free enzymes labelled with Abberior® STAR 635 (a), and the corresponding transmission image (b). Dye/Enzyme ratio of 1.4. Picture dimensions: 32.53 µm × 32.53 µm (a,b). [Reproduced from Vega et al.[87]]

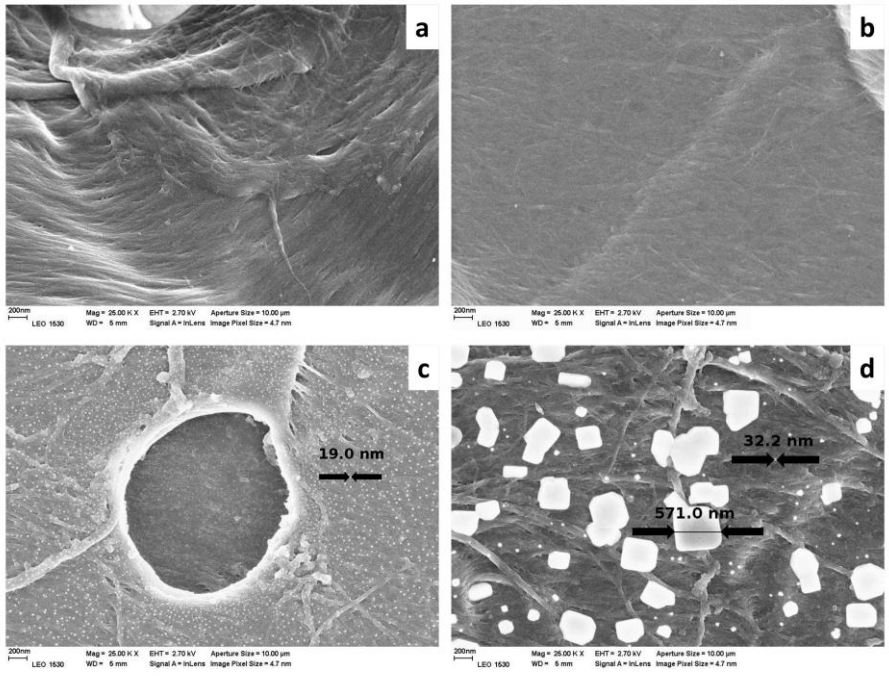

Figure 37. Field emission scanning electron microscope (FE SEM) pictures of the reference fibres (a,b), and the fibres obtained after chemical reaction between the functional fibres (F), the immobilised enzymes (G*), and GA (c,d), all pictures at 25000x magnification. [Reproduced from Vega et al.[87]]

4. Concluding remarks and future prospects

Pressurised hot water extraction (PHWE) has proved to be an excellent method for the recovery of pure hemicelluloses from wood chips. In the present thesis, short PHWE extraction times at relatively low temperatures (160°C) allowed for recovery of high molar mass acetylated-xylan from birch wood chips.

In the context of this thesis, three different xylan polyelectrolytes were synthesised from the isolated birch xylan: xylan sulphate (XS^-), carboxymethyl xylan (CMX^-), and 4-[*N,N,N*-xylan trimethylammonium] butyrate chloride ($XTMAB^+$). In addition, the synthesis of the following two cellulose derivatives was also carried out: (3-carboxypropyl) trimethylammonium chloride ester of 6-deoxyazidocellulose (N_3-$cell^+$), and (3-carboxypropyl) trimethylammonium chloride ester (CN^+).

Because of the ionic functional groups distributed within their polymeric chains, the five polyelectrolytes mentioned above resulted in being water-soluble to. Thanks to that, it was possible to test them for the first time as fibre-modifying agents in aqueous media. It has been shown that polysaccharide-derivatives (hence, the target functional groups) bearing cationic charge can be successfully incorporated onto the surface of cellulose fibres with this approach. The polyelectrolyte adsorption was performed in aqueous media under mild conditions over short reaction times, thus protecting the entire structure of the original fibres. Another perk of the described method, besides the remarkable simplicity, includes the possibility to control the amount of polyelectrolyte that is adsorbed onto the fibre surfaces. Hence, it is possible to adjust the concentration of the target function on the functional fibres. The challenge of introducing target functional groups onto cellulose fibre surfaces using tailor-made polysaccharide-based derivatives was faced. The results serve as proof of the concept that polysaccharide-based derivatives with cationic charge are excellent carriers of valuable functional groups, and can be self-assembled on the fibre surfaces in water suspension.

The fibres obtained from the sorption of N_3-$cell^+$ onto BKPP fibre surfaces (i.e., reactive fibres) were subjected to copper (I)-catalysed alkyne-azide cycloaddition (CuAAc) reaction. Propargyl amine and 1-ethynylpyrene were used in the CuAAc reaction with reactive fibres, yielding amino-fibres and photo-fibres. The positive results regarding the measurements involving amino- and photo-fibres, are proof of the concept that reactive fibres can be used in CuAAc

reactions. In view of the indisputable generality, selectivity and efficiency of CuAAc reactions, the same approach can be used for tagging pulp fibres with a broad variety of valuable probes.

In the search for applications for the amino-functional groups containing fibres (amino-fibres) described earlier, cross-linked glucose oxidase enzymes were covalently linked to the surface of the fibres using glutaraldehyde as a cross-linking agent. The cross-linked enzymes remained active after immobilisation, showing the highest activity at 32°C and pH 6.2. The results show the potential application of "biocatalytic fibres" in bioprocess engineering, were the correct enzyme for the target application can be immobilised to amino-functional groups containing fibres using glutaraldehyde.

5. Referenser/References

(1) Fengel, D.; Wegener, G. *Wood: chemistry, ultrastructure, reactions.*; 1989.

(2) FAO. *Pulp and Paper Capacities. Survey 2015-2020*; Food and Agriculture Organization of the United Nations (FAO): Rome, 2016.

(3) Westbye, P.; Köhnke, T.; Gatenholm, P. *Holzforschung* **2008**, *62* (1), 31–37.

(4) Koch, G. In *Handbook of Pulp, Vol 1*; Sixta, H., Ed.; WILEY-VCH Verlag GmbH &Co., 2006; pp 22–68.

(5) *J. Biol. Chem.* **1982**, *257* (7), 3352–3354.

(6) Payen, A. *Troisième mémoire sur le Dev. végétaux' Extr. des mémoires l'Academie R. des Sci. Tomes III des Savants Éntranges* **1842**.

(7) Sjöström, E. In *Wood Chemistry. Fundamentals and Appllications*; Academic Press, Inc.: California, 1983; pp 51–70.

(8) Ebringerová, A.; Hromádková, Z.; Heinze, T. In *Advances in Polymer Science*; Heinze, T., Ed.; Springer Berlin Heidelberg, 2005; pp 1–67.

(9) Boerjan, W.; Ralph, J.; Baucher, M. *Annu. Rev. Plant Biol.* **2003**, *54*, 519–546.

(10) Laine, C. Structures of hemicelluloses and pectins in wood and pulp, Helsinki University of Technology, 2005.

(11) Gellerstedt, G.; Henriksson, G. In *Monomers, Polymers and Composites from Renewable Resources*; Belgacem, M. N., Gandini, A., Eds.; Elsevier Ltd: Amsterdam, 2008; pp 201–224.

(12) Fahlén, J. The cell wall ultrastructure of wood fibres – effects of the chemical pulp fibre line, KTH Royal Institute of Technology, 2005.

(13) Stone, J. E.; Scallan, A. M. *Tappi* **1967**, *50* (10), 496–501.

(14) Mustoe, G.; Acosta, M. *Geosciences* **2016**, *6* (2), 1–25.

(15) Köhnke, T.; Lund, K.; Brelid, H.; Westman, G. *Carboh. Polym.* **2010**, *81* (2), 226–233.

(16) Fernandes Diniz, J. M. B.; GilJ, M. H.; Castro, A. A. M. *Wood Sci. Technol.* **2004**, *37* (6), 489–494.

(17) Dharm, D.; Tyagi, C. H. *Indian J. Chem. Technol.* **2011**, *18*, 145–151.

(18) Donaldson, L. *Int. Assoc. Wood Anat.* **2008**, *29* (4), 345–386.

(19) Harris, P. J. *New Zeal. J. For. Sci.* **2006**, *36* (1), 36–53.

(20) Sixta, H.; Potthast, A.; Krotschek, A. In *Handbook of Pulp, Vol 1*; Sixta, H., Ed.; WILEY-VCH Verlag GmBH & Co. KGaA, Weinheim: Lenzing, 2006; pp 109–482.

(21) Testova, L.; Chong, S.-L.; Tenkanen, M.; Sixta, H. *Holzforschung* **2011**, *65* (4), 535–542.

(22) Karlsson, P.; Roubroeks, J.; Glasser, W.; Gatenholm, P. In *Feedstocks for the Future*; Bozell, J., Patel, M. K., Eds.; ACS Symposium Series 921: Washington DC, 2006; pp 321–333.

(23) Johansson, M. H.; Samuelson, O. *Wood Sci. Technol.* **1977**, *11*, 251–263.

(24) Meier, H. *J. Polym. Sci.* **1961**, *51* (155), 11–18.

(25) Vega, B.; Grigoray, O.; Gustafsson, J.; Fardim, P. In *Biomass Sugars for Non-Fuel Applications*; Murzin, D., Simakova, O., Eds.; Royal Society of Chemistry, 2015; pp 134–158.

(26) Ebringerová, A.; Heinze, T. *Macromol. Rapid Commun.* **2000**, *21* (9), 542–556.

(27) Ebringerová, A.; Hromádková, Z. *Biotechnol. Genet. Eng. Rev.* **1999**, *16* (1), 325–346.

(28) Petzold-Welcke, K.; Schwikal, K.; Daus, S.; Heinze, T. *Carbohydr. Polym.* **2014**, *100*, 80–88.

(29) Ebringerová, A. *Macromol. Symp.* **2006**, *232* (1), 1–12.

(30) Hesse, S.; Liebert, T.; Heinze, T. *Macromol. Symp.* **2006**, *232* (1), 57–67.

(31) Sedlmeyer, F. B. *Food Hydrocoll.* **2011**, *25*, 1891–1898.

(32) Eduardo da Silva, A.; Rodrigues Marcelino, H.; Christine Salgado Gomes, M.; Eleamen Oliveira, E.; Nagashima Jr, T.; Sócrates Tabosa Egito, E. *Prod. Appl. Biopolym.* **2012**.

(33) Ebringerová, A.; Hromádková, Z. *Biotechnology & genetic engineering reviews*. 1999.

(34) Hamady, Z. *Ann. R. Coll. Surg. Engl.* **2013**, *95*, 235–240.

(35) Daus, S.; Heinze, T. *Macromol. Biosci.* **2010**, *10* (2), 211–220.

(36) da Silva, A. E.; Rodrigues Marcelino, H.; Salgado Gomes, M. C.; Eleamen Oliveira, E.; Nagashima Jr., T.; Sócrates, E.; Egito, T. In *Products and Applications of Biopolymers*; Verbeek, C. J. R., Ed.; InTech, 2012; pp 61–84.

(37) Von Schoultz, S. Method for extracting biomass. US 20150167234 A1, 2015.

(38) Malkov, S.; Tikka, P.; Gullichsen, J. *Pap. ja Puu* **2001**, *83* (8), 605–609.

(39) Malkov, S.; Tikka, P.; Gullichsen, J. *Pap. ja Puu* **2001**, *83* (6), 468–473.

(40) Nelson, R.; Schuerch, C. *J. Polym. Sci.* **1956**, *22* (102), 435–448.

(41) Jara, R. The Removal of Wood Components from Hardwood by Hot Water, The University of Maine, 2010.

(42) Aspinall, G. O. *Adv. Carbohydr. Chem.* **1959**, *14*, 429–468.

(43) Conner, A. H. *Wood Fiber Sci.* **1984**, *16* (2), 268–277.

(44) Teo, C. C.; Tan, S. N.; Yong, J. W. H.; Hew, C. S.; Ong, E. S. *J. Chromatogr. A* **2010**, *1217* (16), 2484–2494.

(45) Zumdahl, S. S.; Zumdahl, S. A. *Chemistry*, 7th ed.; Stratton, R., Schwartz, R. B., Brooks, C. L., Eds.; Houghton Mifflin Harcourt: New York, 2007.

(46) Kilpeläinen, P. Pressurized hot water flow-through extraction of birch wood, Åbo Akademi, 2015.

(47) Liu, S. *J. Biobased Mater. Bioenergy* **2008**, *2* (2), 135–147.

(48) Maloney, M. T.; Chapman, T. W.; Baker, A. J. *Biotechnol. Bioeng.* **1985**, *27* (3), 355–361.

(49) Liu, S. *Biotechnol. Adv.* **2010**, *28* (5), 563–582.

(50) Borrega, M.; Nieminen, K.; Sixta, H. *Bioresour. Technol.* **2011**, *102* (22), 10724–10732.

(51) ANDRITZ pre-hydrolysis cooking for dissolving pulp production http://www.andritz.com/products-and-services/pf-detail.htm?productid=15087 (accessed Mar 6, 2017).

(52) Chen, X.; Lawoko, M.; Heiningen, A. van. *Bioresour. Technol.* **2010**, *101* (20), 7812–7819.

(53) Amidon, T. E.; Bujanovic, B.; Liu, S.; Howard, J. R. *Forests* **2011**, *2*, 929–947.

(54) Peng, F.; Ren, J.-L.; Xu, F.; Bian, J.; Peng, P.; Sun, R.-C. *J. Agric. Food Chem.* **2009**, *57* (14), 6305–6317.

(55) Song, T.; Pranovich, A.; Holmbom, B. *Bioresour. Technol.* **2013**, *130*, 198–203.

(56) Koivula, E.; Kallioinen, M.; Sainio, T.; Antón, E.; Luque, S.; Mänttäri, M. *Bioresour. Technol.* **2013**, *143*, 275–281.

(57) Heinze, T.; Liebert, T.; Koschella, A. *Esterification of Polysaccharides*; Howard, G. B., Pasch, H., Eds.; Springer Berlin Heidelberg: Heidelberg, 2006.

(58) Heinze, T.; Petzcold-Welcke, K. In *Monomers, Polymers and Composites from Renewable Resources*; Belgacem, M. N., Gandini, A., Eds.; Elsevier Ltd: Amsterdam, The Netherlands, 2008; pp 343–368.

(59) ELEGIR, G.; KINDL, A.; SADOCCO, P.; ORLANDI, M. *Enzyme Microb. Technol.* **2008**, *43* (2), 84–92.

(60) Kim, S. Y.; Zille, A.; Murkovic, M.; Güebitz, G.; Cavaco-Paulo, A. *Enzyme Microb. Technol.* **2007**, *40* (7), 1782–1787.

(61) Persson, P. Strategies for cellulose fiber modification, The Royal Institute of Technology (Kun gliga Tekniska Högskolan), KTH, 2004.

(62) Li, X.; Tabil, L. G.; Panigrahi, S. **2007**, *15* (1), 25–33.

(63) Olaru, N.; Olaru, Li.; Vasile, C.; Ander, P. *Polimery* **2011**, *56* (11), 840–834.

(64) Fox, S. C.; Li, B.; Xu, D.; Edgar, K. J. *Biomacromolecules* **2011**, *12* (6), 1956–1972.

(65) Gruber, E.; Granzow, C.; Ott, T. In *Cellulose Derivatives*; Heinze, T. J., Glasser, W. G., Eds.; ACS Symposium Series eBooks, 1998; pp 94–106.

(66) Vuoti, S.; Laatikainen, E.; Heikkinen, H.; Johansson, L.-S.; Saharinen, E.; Retulainen, E. *Carbohydr. Polym.* **2013**, *96* (2), 549–559.

(67) Blomstedt, M.; Kontturi, E.; Vuorinen, T. *Nord. Pulp Pap. Res. J.* **2007**, *22* (3), 336–342.

(68) Aarne, N.; Laine, J.; Hänninen, T.; Rantanen, V.; Seitsonen, J.; Ruokolainen, J.; Kontturi, E. *ChemSusChem* **2013**, *6* (7), 1203–1208.

(69) Grigoray, O.; Wondraczek, H.; Heikkiläa, E.; Fardim, P.; Heinze, T. *Carbohydr. Polym.* **2014**, *111*, 280–287.

(70) Grigoray, O.; Wondraczek, H.; Fardim, P.; Heinze, T. *Macromol. Mater. Eng.* **2015**, *300*, 277–282.

(71) Köhnke, T. Adsorption of xylans on cellulosic fibres -Influence of xylan composition on adsorption characteristics and kraft pulp properties, CHALMERS UNIVERSITY OF TECHNOLOGY, 2010.

(72) Schwikal, K.; Heinze, T.; Saake, B.; Puls, J.; Kaya, A.; Esker, A. R. *Cellulose* **2011**, *18* (3), 727–737.

(73) Katrin Schwikal; Heinze, T. *Polym. Bull.* **2007**, *59* (2), 161–167.

(74) Köhnke, T.; Lund, K.; Brelid, H.; Westman, G. *Carbohydr. Polym.* **2010**, *81* (2), 226–233.

(75) Liebert, T.; Hänsch, C.; Heinze, T. *Macromol. Rapid Commun.* **2006**, *27* (3), 208–213.

(76) Xia, Y.; Wan, J. *Polym. Adv. Technol.* **2008**, *19* (4), 270–275.

(77) Briggs, D. *Surface Analysis of Polymers by XPS and Static SIMS*, 1st ed.; Clarke, P. D. R., Suresh, P. S., Ward FRS, P. I. M., Eds.; Cambridge University Press: Cambridge, 1998.

(78) Orelma, H.; Filpponen, I.; Johansson, L.-S.; Laine, J.; Rojas, O. J. *Biomacromolecules* **2011**, *12* (12), 4311–4318.

(79) Hannuksela, T.; Fardim, P.; Holmbom, B. *Cellulose* **2003**, *10* (4), 317–324.

(80) Fardim, P.; Moreno, T.; Holmbom, B. *J. Colloid Interface Sci.* **2005**, *290* (2), 383–391.

(81) Johansson, L.-S.; Campbell, J. M. *Surf. Interface Anal.* **2004**, *36* (8), 1018–1022.

(82) Hofmann, J. P.; Rohnke, M.; Weckhuysen, B. M. *Phys. Chem. Chem. Phys.* **2014**, *16*, 5465–5474.

(83) Bertaud, F.; Sundberg, A.; Holmbom, B. *Carbohydr. Polym.* **2002**, *48* (3), 319–324.

(84) Vega, B.; Petzold-Welcke, K.; Fardim, P.; Heinze, T. *Carbohydr. Polym.* **2012**, *89* (3), 768–776.

(85) Vega, B.; Wondraczek, H.; Bretschneider, L.; Näreoja, T.; Fardim, P.; Heinze, T. *Carboh. Polym.* **2015**, *132*, 261–273.

(86) Solomon B., Lotan N., K.-K. E. *Biopolymers* **1977**, *16* (9), 1837–1851.

(87) Vega Erramuspe, I. B.; Fazeli, E.; Näreoja, T.; Trygg, J.; Hänninen, P.; Heinze, T.; Fardim, P. *Biomacromolecules* **2016**, *17* (10), 3188–3197.

(88) Leskovac, V.; Trivić, S.; Wohlfahrt, G.; Kandrač, J.; Peričin, D. *Int. J. Biochem. Cell Biol.* **2005**, *37*, 731–750.

(89) *Recommended Labeling Protocols*; Abberior GmbH.

(90) Schöniger, W. *Mikrochim. Acta* **1956**, 1–6.

(91) Sano, S.; Kato, K.; Ikada, Y. *Biomaterials* **1993**, *14* (11), 817–822.

(92) Pohl, M.; Michaelis, N.; Meister, F.; Heinze, T. *Biomacromolecules* **2009**, *10* (2), 382–389.

(93) Schmid, B.; Schindelin, J.; Cardona, A.; Longair, M.; Heisenberg, M. *BMC Bioinformatics* **2010**, *11*, 274.

(94) Bradford, M. *Anal. Biochem.* **1976**, *72*, 248–254.

(95) Dybkaer, R. *Pure Appl. Chem.* **2002**, *73* (6), 927–931.

(96) Young, D. S. *Ann. Clin. Lab. Sci.* **1977**, *7* (2), 93–98.

(97) Kimura, K.; Kikuchi, S.; Yamasaki, S. *Plant Soil* **1999**, *216*, 117–127.

(98) Vega, B.; Petzold-Welcke, K.; Fardim, P.; Heinze, T. *Carbohydr. Polym.* **2012**, *89*, 768–776.

(99) Vega, B.; Wondraczek, H.; Salomão Pinto Zarth, C.; Heikkilä, E.; Fardim, P.; Heinze, T. *Langmuir* **2013**, *29* (44), 13388–13395.

(100) Kovac, J. *Mater. Tehnol.* **2011**, *45* (3), 191–197.

(101) Vega, B.; Wondraczek, H.; Salomão Pinto Zarth, C.; Heikkilä, E.; Fardim, P.; Heinze, T. In *6th International Colloquium on Eucalyptus Pulp*; Colonia (Uruguay), 2013; pp 1–15.

(102) Bock, V. D.; Hiemstra, H.; van Maarseveen, J. H. *European J. Org. Chem.* **2006**, No. 1, 51–68.

(103) Marsh, N. D.; Mikolajczak, C. J.; Wornat, M. J. *Spectrochim. Acta Part A* **2000**, *56*, 1499–1511.

(104) de Souza Bezerra, T. M.; Bassan, J. C.; Tabosa de Oliveira Santos, V.; Ferraz, A.; Monti, R. *Process Biochem.* **2015**, *50* (3), 417–423.

(105) Lakowicz, J. R. *Principles of Fluorescence Spectroscopy*, Third.; Springer Science+Business Media, LLC.: Baltimore, Maryland, USA, 2006.

(106) Lekha, P. K.; Prasad, E. *Chem. - A Eur. J.* **2011**, *17* (31), 8609–8617.

(107) Larkin, P. *Infrared and Raman Spectroscopy. Principles and Spectral Interpretation*, 1st ed.; Larkin, P., Ed.; Elsevier, 2011.

(108) Socrates, G. *Infrared and Raman Characteristic Group Frequencies*, 3rd ed.; John Wiley & Sons Ltd., 2004.

(109) Maddams, W. F.; Royaud, I. A. M. *Spectrochim. Acta Part A Mol. Spectrosc.* **1990**, *46* (2), 309–314.

(110) Pohl, M.; Michaelis, N.; Meister, F.; Heinze, T. *Biomacromolecules* **2009**, *10* (2), 382–389.

(111) Bettelheim, F. A.; Brown, W. H.; Campbell, M. K.; Farrell, S. O.; Torres, O. *Introduction to General, Organic and Biochemistry*, 10th ed.; Brooks/Cole, C. L., Ed.; Mary Finh: Belmont, USA, 2013.

(112) Daugaard, A. E.; Hvilsted, S.; Hansen, T. S.; Larsen, N. B. *Macromolecules* **2008**, *41* (12), 4321–4327.

(113) Anando Devadoss; Chidsey, C. E. D. *J. Am. Chem. Soc.* **2007**, *129* (17), 5370–5371.

(114) Liu, X.; Zheng, H.-N.; Ma, Y.-Z.; Yan, Q.; Xiao, S.-J. *J. Colloid Interface Sci.* **2011**, *358* (1), 116–122.

(115) Schmiers, H.; Friebel, J.; Streubel, P.; Hesse, R.; Köpsela, R. *Carbon N. Y.* **1999**, *37* (12), 1965–1978.

(116) Weng, L. T.; Poleunis, C.; Bertrand, P.; Carlier, V.; Sclavons, M.; Franquinet, P.; Legras, R. *J. Adhes. Sci. Technol.* **1995**, *9* (7), 859–871.

(117) Daugaard, A. E.; Hvilsted, S.; Hansen, T. S.; Larsen, N. B. *Macromolecules* **2008**, *41* (12), 4321–4327.

(118) Anando Devadoss; Chidsey, C. E. D. *J. Am. Chem. Soc.* **2007**, *129* (17), 5370–5371.

(119) Hein, J. E.; Fokin, V. V. *Chem. Soc. Rev.* **2010**, *39* (4), 1302–1315.

(120) Rostovtsev, V. V.; Green, L. G.; Fokin, V. V.; Sharpless, K. B. *Angewandte* **2002**, *41* (14), 2596–2599.

(121) Tornøe, C. W.; Christensen, C.; Meldal, M. *J. Org. Chem.* **2002**, *67* (9), 3057–3064.

(122) Rostovtsev, V. V.; Green, L. G.; Fokin, V. V.; Sharpless, K. B. *Angewandte* **2002**, *41* (14), 2596–2599.

(123) Mentink, C. J.; Hendriks, M.; Levels, A. A.; Wolffenbuttel, B. H. *Clin. Chim. Acta* **2002**, *321* (1–2), 69–76.

(124) Talbert, J. N.; He, F.; Seto, K.; Nugen, S. R.; Goddard, J. M. *Enzyme Microb. Technol.* **2014**, *55*, 21–25.

(125) Stuart, B. H. In *Infrared Spectroscopy: Fundamentals and Applications*; John Wiley & Sons Ltd.: Hoboken, NJ, 2004; pp 141–150.

(126) Zdarta, J.; Sałek, K.; Kołodziejczak-Radzimska, A.; Siwińska-Stefańska, K.; Szwarc-Rzepka, K.; Norman, M.; Klapiszewski, Ł.; Bartczak, P.; Kaczorek, E.; Jesionowski, T. *Open Chem.* **2015**, *13* (1), 138–148.

(127) Migneault, I.; Dartiguenave, C.; Bertrand, M. J.; Waldron, K. C. *Biotechniques* **2004**, *37* (5), 790–802.

(128) Sheldon, R. A. *Advanced Synthesis and Catalysis*. 2007, pp 1289–1307.

(129) West, G. *Biographia Britannica: or, the lives of the most eminen persons who have flourished in Britain and Ireland, from the earliest ages, down to the present times.*; John Adams Library: London, 1760; Vol. 5.

6. Acknowledgments

I would like to express my deepest gratitude to my supervisors Prof Pedro Fardim and Finnish Distinguished Professor (FiDiPro), PhD. Thomas Heinze. Your offer to start research in the field of pulp fibre modification has represented one of the greatest challenges and opportunities in my entire life. Thank you for your guidance and patience. All of the lessons learned from you during these years have helped to make this journey possible, and will definitely help me in the future in many ways.

I am grateful to the Finnish Funding Agency for Innovation (TEKES), which in the framework of the Advanced Polysaccharide-Based Biomaterials project (APOL project), provided the financial support during the largest portion of my research work. I also thank Åbo Akademi for providing the research grants which allowed me to complete the thesis.

I am also thankful to Professor Pekka Hanninen for enabling me to conduct experiments and take measurements in collaboration with researchers from his research group in Turun Yliopisto.

I would like to thank all of my colleagues from the Chemical Engineering Department in Åbo Akademi, especially those colleagues with whom I have shared precious moments along the years at the Laboratory of Fibre and Cellulose Technology (FCT): Anne Kotiaho, Asia Wojciechowska, Carl Lange, Christian Sieveking, Eduardo Iamasaki, Eduardo Keim Altamirano, Elina Heikkilä, Goran Kuzmanovski, Hong yan Mou, Jan Gustafsson, Jani Trygg, Jasmina Obradovic, Joakim Järnström, Konstantin Gabov, Leandro Blach, Liji Sobhanadhas, Linda Nisula, Malin Ekroos, Olga Gabov, Pablo Reyes Contreras, Paulina Saloranta, Peter Homlund, Piia Koskinen, Poonam Trivedi, Risto Korpinen, and Thomas Holmbom. Also, the co-authors and collaborators in the scientific publications, especially: Cíntia Salomão Pinto Zarth, Holger Wondraczek, Katrin Petzold-Welcke, Leonore Bretschneider, Martin Gericke (from Friedrich Schiller University, Jena), Elnaz Fazeli, Tuomas Näreoja (from Turun Yliopisto). Thanks for your support and interesting discussions; my research work improved a lot, and the complex process of learning and addressing the issues raised every day in the laboratory ran much more smoothly. I have learned something valuable from all of you, not only for my career but for use in my everyday life!

Likewise, my sincere thanks to Erja Ämmälahti (Tekes), Pirkko Liias (MetsäFibre), Pia Nilsson (UPM), Heidi Saxell (StoraEnso), Jonna Uggeldal (ViscoTeepak), Jonni Ahlgren (Kemira), Lars Gädda (FIBIC), and Hannu Koivikko (Danisco) for the interesting discussions and advice during steering group APOL meetings, which were celebrated regularly, in Turku-Finland and Jena-Germany.

My thanks go also to Agneta Hermansson and Marika Ginman (secretaries at FCT) for helping me with the tedious numbers.

I do not want to forget the authorities in the Comisión Sectorial de Investigación Científica (CSIC), Universidad de la República del Uruguay (UdelaR), Metsa-Fibre (ex Botnia), Academy of Finland and Conicyt-Chile with Polysmart Project, because they enable me to take the first steps from Uruguay towards Finland. Correspondingly, I want to express my gratitude to Carlos Mantero and Pilar Menéndez for the same reason.

Last but never least, I am very thankful to my family and all of my friends, from those who I have known during these years here in Finland to those living in the “exotic” (Finnish view point) little country called Uruguay. Your kind words, messages, and supportive actions are simply indescribable and helped me more than “a lot” during my doctoral studies. A big thank you to all of you!

Acknowledgments:

Tekes – the Finnish Funding Agency for Technology and Innovation

Finland Distinguished Professor Programme

Turun yliopisto
University of Turku

Laboratory of Biophysics, Cell Biology and Anatomy, Institute of Biomedicine

seit 1558

Friedrich-Schiller-Universität Jena

Åbo Akademi

ISBN 978-952-12-3630-3